KERNFORSCHUNGSANLAGE JÜLICH GmbH
Institut für Festkörperforschung
Projektstudiengruppe Spallations-Neutronenquelle

IKOR

An Isochronous Pulse Compressor Ring for Proton Beams

by

The IKOR - study group
G. Schaffer, editor

Jül - Spez - 114
Juni 1981
ISSN 0343-7639

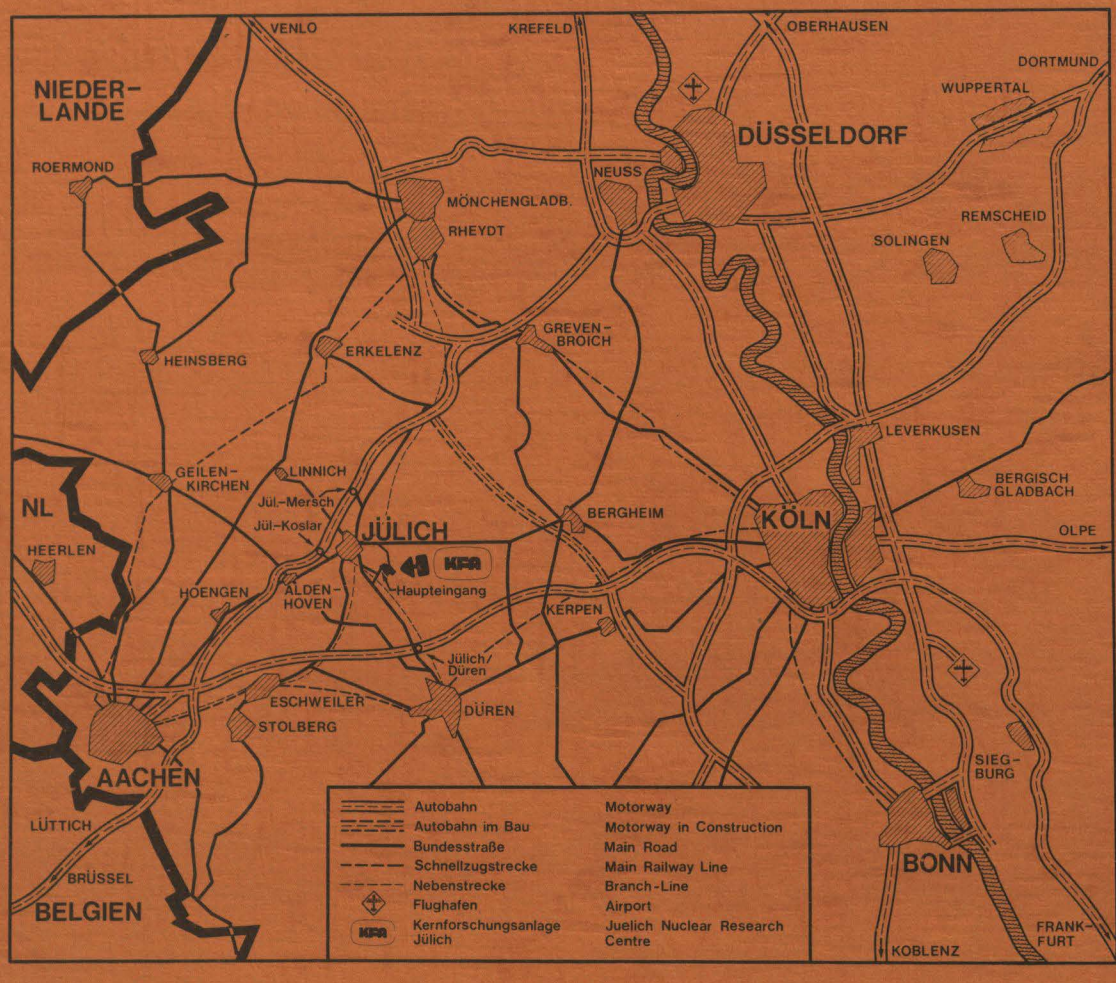

Als Manuskript gedruckt

Spezielle Berichte der Kernforschungsanlage Jülich - Nr. 114

Institut für Festkörperforschung
Projektstudiengruppe Spallations-Neutronenquelle

Jül - Spez - 114

Zu beziehen durch: ZENTRALBIBLIOTHEK der Kernforschungsanlage Jülich GmbH
Postfach 1913 · D-5170 Jülich (Bundesrepublik Deutschland)
Telefon: (02461) 61-0 · Telex: 833556 kfa d

IKOR

An Isochronous Pulse Compressor Ring for Proton Beams

by

The IKOR - study group
G. Schaffer, editor

Abstract

This report contains the results of a study carried out for an isochronous compressor ring IKOR which compresses the 500 μs linac macropulses into pulses of 0.68 μs length. Its basic component is a ring magnet with alternating gradient and separated functions. Due to the isochronous operation, an rf system can be avoided which otherwise would be necessary in order to maintain a void in the circulating beam for the purpose of ejection. Injection is performed by charge exchange. The H^- beam of the accelerator is first converted into a H^0 beam by stripping off one electron by a high gradient magnet placed in the transfer channel. Subsequently, the beam is converted into a proton beam by removing the remaining electron through a stripping foil in the ring. IKOR will be filled in 658 turns. Immediately after filling, the beam is ejected in a single turn via a kicker and a septum magnet and is transported to the spallation target. Because of the high intensity of 2.7×10^{14} protons per pulse and, secondly, due to the high repetition rate of 100 Hz, beam dynamics and radiation protection aspects dominate the design and are, for this reason, treated in detail.

Foreword

The IKOR Study Group was set up and guided by Hans Willax, during 1979 and 1980, until a severe illness interfered with his plans to promote the development of an important new instrument for basic research. By his death, on 17 April 1981, the family of accelerator designers lost a member whose friendly attitude and creative power have led to significant achievements.

This report, written under the reference designation 'chapter D2', is part of the SNQ Study Report. It describes preliminary ideas for an optional device to be added to the linear accelerator of the neutron spallation source. Comments on these ideas, by our readers, are very welcome.

Many thanks are due to those who helped to issue this report as a result of an international collaboration.

G. Schaffer
KFA, June 1981

Members of the IKOR Study Group

J. Ahlbäck, Scanditronix, Uppsala

W. Busse, c/o CERN, Geneva (HMI, Berlin)

R. Cappi, CERN, Geneva

C.J.A. Corsten, TH Eindhoven

J.S. Colonias, c/o Scanditronix, Uppsala (LBL, Berkeley, USA)

W. Davies, c/o Scanditronix, Uppsala (CRNL, Chalk River, Canada)

J.P. Delahaye, CERN, Geneva

H. Fischer, Grand Saconnex, Geneva

K. Goebel, CERN, Geneva

H.L. Hagedoorn, TH Eindhoven

M. Höfert, CERN, Geneva

W. van Kampen, Univ. Delft

H. Lindqvist, Scanditronix, Uppsala

P.F. Meads, c/o Scanditronix, Uppsala (Oakland, Calif., USA)

I. Palumbo, c/o Scanditronix, Uppsala (Univ. Neapel)

K.H. Reich, CERN, Geneva

G. Schaffer, KfK, Karlsruhe

V. Vaccaro, c/o Scanditronix, Uppsala (Univ. Neapel)

H. Willax, c/o KFA (SIN Villigen)

R. Wolgast, c/o Scanditronix, Uppsala (LBL, Berkeley, USA)

G. Wüstefeld, KFA

(addresses as of December 1980)

Content

References at the end of each section

D2.1 General aspects

2.1.1 Synopsis

This report contains the results of a study carried out for an isochronous compressor ring IKOR which compresses the 500 μs linac macropulses into pulses of 0.68 μs length. Its basic component is a ring magnet with alternating gradient and separated functions. Due to the isochronous operation, an rf system can be avoided which otherwise would be necessary in order to maintain a gap in the circulating beam for the purpose of ejection. Injection is performed by charge exchange. The H^- beam of the accelerator is first converted into a H^0 beam by stripping off one electron by a high gradient magnet placed in the transfer channel. Subsequently, the beam is converted into a proton beam by removing the remaining electron through a stripping foil in the ring. IKOR will be filled in 658 turns. Immediately after filling, the beam is ejected in a single turn via a kicker and a septum magnet and is transported to the spallation target. Because of the high intensity of 2.7×10^{14} protons per pulse and, secondly, due to the high repetition rate of 100 Hz, beam dynamics and radiation protection aspects dominate the design and are, for this reason, treated in detail.

No arguments could be found which throw doubts on the feasibility of the ring. The study, however, cannot be considered as fully completed. The total construction cost of IKOR were estimated to be 126 million DM, and the construction period seven years after completion of the preliminary design study.

2.1.2 Design concept and reasons for choice

Introduction

The purpose of the compressor ring is to compress the 0.5 ms linac pulses into pulses of < 1 μs duration so as to increase the peak neutron flux from the target without a significant decrease of the mean

flux (see chapter 1 of part I). Pulses shorter than 200 ns are specified for neutrino experiments /1/.

While one can imagine novel tailor-made machines for achieving this purpose, the present proposal relies on the proven principle of an alternating gradient ring (AG), as used in modern synchrotrons. After accumulation over 658 turns, the beam is ejected in a single turn (Fig. D2.1-1).

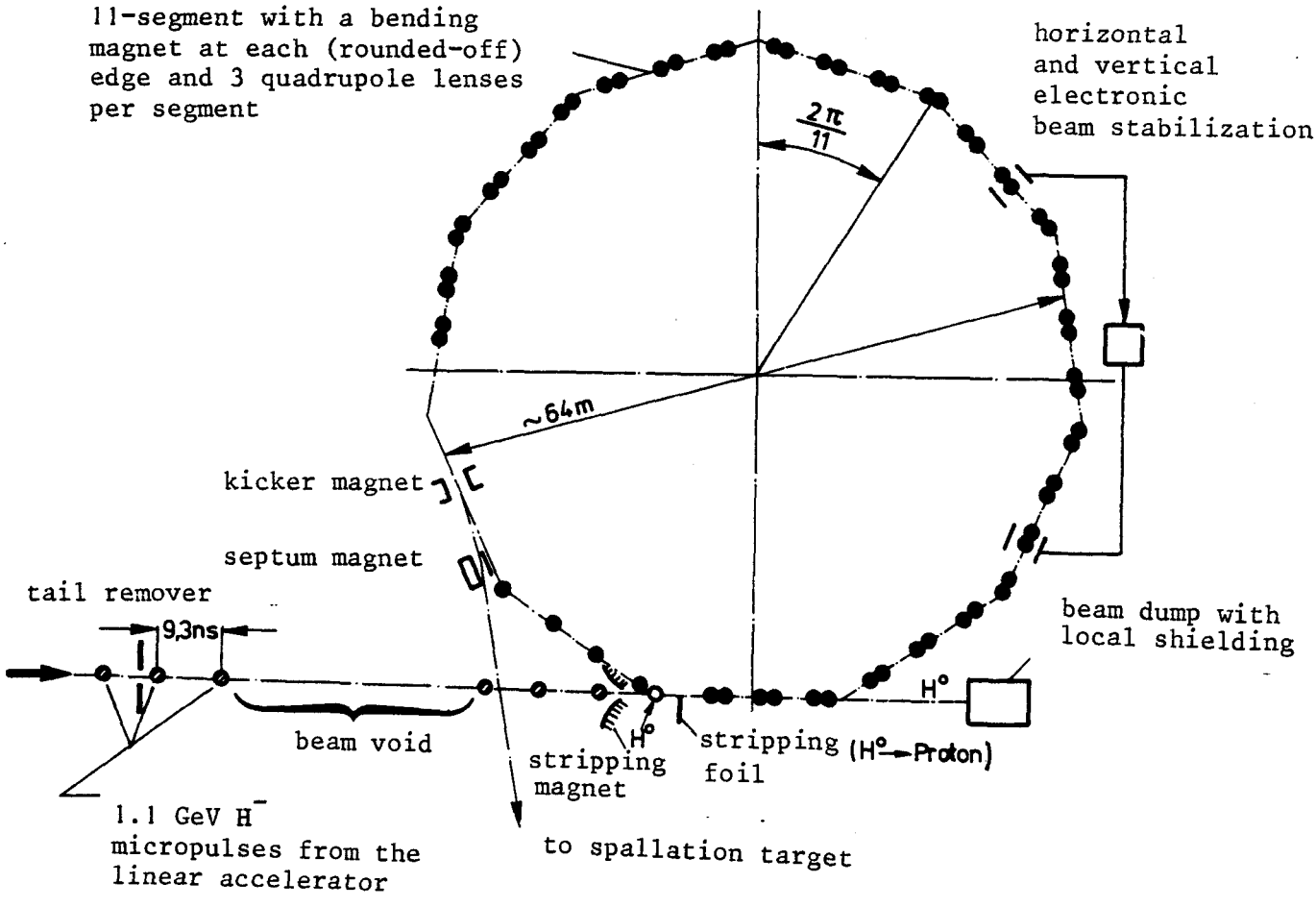

Fig. D2.1-1. IKOR concept, schematically

IKOR is designed for filling it, by means of charge-exchange injection, with about 87% of the nominal linac macropulse intensity. Of the other 13%, 12% are dumped in the linac preinjector by means of a fast chopper /2/ so as to leave an azimuthal void in the compressor beam, and 1% of the beam is scraped off during the controlled tail-trimming in the injection line. The void is required for avoiding beam loss while the deflecting field of the ejection kicker magnet is being built up. In order to minimize possible beam blow-up or loss due to instabilities (which take some time to develop), the beam is ejected as soon as the filling is completed. The whole process can be repeated with the 100 Hz linac macropulse repetition frequency.

Beam dynamics considerations

With a proton intensity of 2.7×10^{14} p/filling and a flux of 2.7×10^{16} p/s the SNQ compressor ring would have five times the intensity and at least forty-three times the flux of the LASL high-current proton storage ring /3/. With respect to the Rutherford SNS /4/, proton intensities would be ten times higher and proton fluxes twenty times higher.

Under these conditions beam dynamics considerations practically dominate almost all aspects of the ring design /5/. On the one hand, this design must ensure that beams of such very high intensities can be injected (sub-section 2.2.4) and kept stable (sub-section 2.2.5) in the ring. On the other hand, relative beam losses must be kept far below what is currently admissible, which further emphasises the need to understand fully the beam dynamics (irrespective of the indispensable engineering considerations concerning equipment radiation hardening, remote handling, etc.). For instance, a transverse active damping system is planned to avoid beam loss due to lower order instabilities.

On the whole, the existing body of single particle and collective beam dynamics theory /6,7/ is, in principle, sufficient to tackle the problems on hand. However, some extension is required (sub-section 2.2.5) for an isochronous ring, i.e. one working close to transition energy /8,9/.

Machine radius and apertures

The volume-cost relationship basically advocates a ring of modest dimensions. However, beam dynamics introduces some overriding constraints into the optimization.

To ensure various advantages discussed further below, it appears interesting to design an isochronous ring /8,9/. The basic ingredient for this is a lattice which yields for the normalized transition energy $\gamma_{tr} \approx 2.2$ ($\approx \gamma_p = 2.17$ = total proton energy at 1100 MeV/proton rest energy).

In a classical A.G. (alternating gradient) lattice one has $\gamma_{tr} \approx Q_H$ (= number of horizontal betatron oscillations per turn). With a 90^o betatron phase advance per cell, one then needs about nine cells as a minimum to meet the condition $\gamma_{tr} \approx 2.2$.

For identical magnets, stopbands (= resonances of betatron oscillations) are narrowest in a fully symmetrical design (= identical cells).

For fast beam ejection one needs about a 4m straight section space for the kicker magnet and about twice that amount for drift spaces and the septum magnet. As the cross-section of the ejected beam is comparable to that of the machine acceptance, it is very attractive (and possible /10/) to eject over a short distance (in order to avoid doubling the machine acceptance in the ejection region). Putting these considerations together, and adding six meters for the main magnet and quadrupoles in a cell, one arrives at a minimum cell length of about $4 + 8 + 6 = 18$ m. Hence, the minimum circumference is $18 \times 9 = 162$ m or $\bar{R} \approx 26$ m. Optimization studies eventually showed that a more favourable situation and a safer design is obtained with $R \approx 32$ m (sub-section 2.2.2); a larger radius is also favoured because it decreases the magnitude of the circulating current and the number of turns to be injected.

Provided the injection process does not require a larger aperture, the minimum machine aperture is very largely determined by the need to increase the beam cross-section in order to keep the space-charge fields at tolerable levels (sub-section 2.2.5). For 2.7×10^{14} p/filling this leads, at 1.1 GeV, to beam emittances of $\varepsilon_H = 150\pi \cdot 10^{-6}$ rad m and $\varepsilon_V = 50\ \pi \cdot 10^{-6}$ rad m. Working at lower energy would require and increase of these emittances as $\beta^{-2}\ \bar{\gamma}^{3}$, all other parameters staying constant.

Starting from these emittances, appropriate margins are added for accommodating closed orbit amplitudes and some beam halo (tails of the distribution) to arrive at machine apertures. At this stage of the study, the numbers given represent the best risk/cost compromise available. Further refined studies may reveal that an optimum design calls for slightly different apertures.

Reasons for choosing an isochronous ring

In a non-isochronous ring, the azimuthal void in the beam will close with time because of the different revolution frequencies of protons with different momenta. A (pulsed) RF system is then required to keep this void open /9/ unless a different ejection scheme is adopted (sub-section 2.7.1). Choice of an isochronous ring /8,9/ means saving of effort and cost for such an RF system. Furthermore, the absence of such a system leads to smaller minimum beam emittances, and more favourable beam stability conditions (sub-section 2.2.5).

In contrast to isochronous cyclotrons or ring accelerators, synchrotrons during most of the acceleration cycle have a non-vanishing dependence of the revolution frequency on machine radius. In AG synchrotrons this dependence can have either sign. The normalized energy where the sign change occurs is called the transition energy, γ_{tr}. Hence for isochronism, the ring has to be operated close to γ_{tr}.

For the present capacitive beam coupling impedance, γ_{tr} should, in all cases, be sufficiently high so that no protons have γ values (γ_p)

above γ_{tr} and hence none experience the negative mass instability. However, the exact value of γ_{tr} which was chosen results from a compromise (sub-section 2.2.5): on the one hand a significantly higher value than γ_p is favourable for the rapid debunching of the linac micropulses in the ring, as well as for ensuring that non-linearities and space-charge effects will not lower γ_{tr} below γ_p in part of the beam. On the other hand a value of γ_{tr} closer to γ_p better ensures that the void is kept free of protons, and increases the rise times of longitudinal instabilities. It is planned to work with dynamic γ_{tr} values, i.e., γ_{tr} is programmed during the filling so as to ensure that it stays correctly above γ_p despite the increasing space-charge effects (which change the local value of γ_{tr}). Should unexpected difficulties arise with isochronous operation, in contrast with promising experiments on the PS of CERN /11/, other possibilities of operation exist (sub-section 2.7.1).

Beam losses

Tolerated beam losses in existing machines are easily a few percent, and up to 50% or more not uncommon. A 1% loss in the present ring, as the only user of the linac beam, would mean 44 μA × 1.1 GV ≈ 50 kW of dissipated power. Clearly, such a loss level, if continuous and uncontrolled would lead to severe problems, both in terms of damage to the ring and of induced radioactivity rendering repairs and maintenance difficult.

The following remedial measures are planned:

i) minimum-loss designs throughout,
ii) provision of beam scrapers/catchers where appropriate (scraping off the halo before injection and ejection, catching the residual H^o beam, etc.),
iii) appropriate beam monitoring instrumentation,
iv) radiation resistant design of components, use of appropriate material,
v) adequate radiation shielding, and
vi) component design compatible with remote handling and provision of such handling.

References on section D2.1 (*) this study, annex D

/1/ H. Fischer, Neutrinoflüsse aus dem Pionen- und Myonenzerfall bei verschiedenen Pionen-Pulslängen, KFA Jülich 1.2.HF.2 and references quoted (*)

/2/ G. Schaffer, HF-Einrichtungen zur Dunkeltastung des Linacstrahls einer Spallationsneutronenquelle, KfK Primärbericht 11.04.02 P12E, März 1980 (*)

/3/ G.P. Lawrence et al., LASL high-current proton storage ring, LA-UR 80-1946, Proceedings XIth Int. Conf. on High Energy Accelerators, CERN 1980

/4/ L.C.W. Hobbis, G.H. Rees and G.C. Stirling, A pulsed neutron facilitiy for condensed matter research, RL-77-064/C, June 1977, and updated parameter list (November 1980)

/5/ K.H. Reich, Proton beam dynamics in the SNQ compressor ring including collective effects and implications for the reference design, KFA Jülich 1.2.KHR.1 (*)

/6/ See for instance:
C. Bovet, R. Gouiran, I. Gumowski, K.H. Reich, A selection of formulae and data useful for the design of A.G. Synchrotrons, CERN/MPS-SI/Int. DL/70-4

/7/ See for instance:
M.H. Blewett (Editor), Theoretical aspects of the behaviour of beams in accelerators and storage rings, CERN 77-13

/8/ H. Fischer, K.H. Reich, Notes on the meeting with H.G. Hereward on 5th February 1980, at the KfK Karlsruhe, KFA Jülich 1.2.HF/KHR.1, (*)

/9/ H. Fischer, Formung des SNQ Kompressorstrahls im Längsphasenraum mittels gepulster HF-Spannungen, KFA Jülich 1.2.HF.1 vom 26.2.1980 , (*)

/10/ K.H. Reich, Some comments on the lattice design for the compressor ring, CERN/PS/BR Note/80-8, KFA Jülich 2.2.KHR.1 (*)

/11/ R. Cappi, J.P. Delahaye, K.H. Reich, PS beam measurements at flat-top fields near transition energy, Proc. Washington Particle Acc. Conf. 1981, IEEE Trans.Nucl.Sci., Vol. 28, No. 3, June 1981

D2.2 Parameters and beam dynamics

2.2.1 IKOR main parameters

The main parameters of the compressor system, main ring components and injection/ejection components are listed below and are discussed in the individual sub-sections.

General machine parameters

Proton kinetic energy	E_{kin} = 1.1 GeV ($\gamma = 2.172$)
Proton momentum	p_p = 1.81 GeV/c
Proton design intensity	N_p = 2.7×10^{14} p/filling
Proton current	I_p = 66 A
Proton pulse duration	T_p = 0.68 µs
Repetition rate (max)	f_{rep} = 100 Hz
Orbit circumference	C = 202.175 m
Revolution period	T_{rev} = 0.76 µs
Mean ring radius	$\bar{R}$ = 32.18 m
Lattice structure (separate functions)	FO DOO DOOB
Number of lattice cells	N = 11
Approximate horizontal betatron tune	Q_H = 3.25
Approximate vertical betatron tune	Q_V = 4.40
Maxima of Twiss parameters (nominal values)	
in the whole ring	β_H = 31.3 m
	β_V = 41.0 m
in bending magnet	β_H = 31.4 m
	β_V = 6.3 m
Momentum compaction factor	α_p = 6.9 m
Nominal transition energy/rest energy	γ_{tr} = 2.226 (η = 0.01)
Nominal beam emittances	ε_H = 150 π 10^{-6} rad m
(not normalized)	ε_V = 50 π 10^{-6} rad m
Injection (charge exchange)	$H^- \rightarrow H^o \rightarrow p$
Duration of injection	T_F = 500 µs (658 turns)
Ejection (as soon as injection completed)	single turn, in hor. plane
Operational vacuum pressure	P = 10^{-7} Torr
Maximum tolerable operational beam loss	$\Delta N_p/N_p = 5 \cdot 10^{-3}$

Parameters of main lattice components

Bending magnets (11 sector magnets)

field	B	= 1.3 T
magnetic length (mean orbit)	L_B	= 2.65 m
bending radius	ρ	= 4.64 m
gap height	h_B	= 100 mm
width of useful field	w_B	= 200 mm

Quadrupole lenses (33)

gradient	G_Q	= up to 3.5 T/m
magnetic length	L_Q	= 0.4 m
bore diameter	d_Q	= 210 mm

Parameters of injection and ejection components

Injection bump magnets (4):

max. orbit displacement	d_i	= 5.8 cm
field	B_i	= 0.6 T
magnetic length	L_i	= 0.6 m
apertures	h_i	= 100 mm, w_i = 200 mm

Ejection kicker magnet:

deflection angle	α_K	= 11 mrad
bending strength	$\int Bdl$	= 0.066 Tm
aperture	h_K	= 90 mm, w_K = 180 mm
rise time	τ_K	= 50 ns (10% to 90%)

Septum magnet:

deflection angle	α_S	= 7.48^o (=130.6 mrad)
field	B_S	= 0.985 T
gradient (F)	G_S	= 0.5 T/m
magnetic length	L_S	= 0.8 m
useful aperture	h_S	= 70 mm, w_s = 160 mm

2.2.2 Lattice structure

Criteria for the lattice

For the design of the lattice, the following aspects were taken into account:

Working region in Q_H/Q_V-diagram (Fig. D2.2-1) /1/: In order to avoid coupling resonances, the horizontal and vertical betatron frequencies should differ, but not by too much lest the Twiss parameters become too unfavourable. Because vertical aperture implies more power than horizontal aperture, the vertical focussing should be stronger than the horizontal. Thus $Q_V \approx Q_H + 1$ was chosen (Q being again the number of betatron oscillations per turn). The tunes must be chosen so that the Laslett tune shifts do not drive particles into adjacent stop bands (/2,3/ and sub-section 2.2.5).

Number of cells N /1/: Transverse stability considerations prevent betatron frequencies that are near multiples of N/2. Extraction considerations suggest frequencies near N/4, and cost considerations usually result in frequencies near N/5 to N/4. Also, the working point plus any spread in frequencies due to nonlinearities must be chosen to avoid resonances of the type $m \cdot Q = k \cdot N$ (structural stop bands for integers m, k, see sub-section 2.2.3).

Ejection /4/: In order to preserve the symmetry of the ring, no special ring elements should be incorporated in the extraction cell. If possible, the kicker magnet should be placed in front of a horizontally defocusing lens so as to reinforce the action of the kicker. The phase advance between the kicker and the septum magnet should be in the range $50^\circ < \mu < 130^\circ$, and the Twiss parameter β_H should be as large as possible in the kicker magnet in order to maximize its effectiveness. Then, the space provided for the ejection cell is also sufficient for the injection cell.

Isochronism and adjustment of γ_{tr}: IKOR should also be able to work at a slightly lower energy ($\approx$ 1 GeV). The adjustment range required for this is estimated to be $2.07 < \gamma_{tr} < 2.37$, and this should preferably be independent of the betatron frequencies.

In sub-sections 2.1.2 and 2.2.5, the interest in changing γ_{tr} during filling is pointed out. In order to increase γ_{tr} the change in orbit length ΔC with momentum must be decreased. One way of doing this is to use the method developed for the γ_{tr}-jump at the CERN PS /5/. A simpler approach has been explored in this study. The change in γ_{tr} essentially arises from the difference of path length in the bending magnets, so the problem is to adjust $\alpha_p(s)$ (and hence β_H (s)) in these magnets.

Bending magnets: Because of manufacturing considerations, the field should be of the order of 1T. For similar reasons, a seperated-function design with no gradients or edge angles in the bending magnets is preferred. To minimize the gap height, β_V should be small in the bending magnets.

Quadrupole lenses: There must be a minimum of three quadrupoles per cell in order that γ_{tr}, Q_H, and Q_V be independently adjustable. The gradient G_Q should not exceed 5.5 T/m to avoid excessive pole-tip fields.

Beam ring radius $\bar{R}$: Basic considerations were already explained in sub-section 2.1.2, as well as above under 'ejection'. The following more specific arguments are added: For ejection the kicker magnet needs a 4 m long straight section; about 8 m is required for the drift space and septum magnet if extraction is to take place entirely within one cell and thus avoid special magnets. The bending magnets occupy a total azimuthal length of 38 m for 1T fields. In order to provide space for three quadrupoles per cell with reasonable minimum intermagnet spacing, the mean radius of the ring for N = 11 is 32 m.

Comparison of different lattices

Using the computer program LATTICE /62/, lattices of periodicity 8, 10, 11, and 14 /1,4,6-14/ and also some lattices with the π-2π insertion /15-17/ have been examined.

The more conventional lattices are favoured over those with insertions because a reduction in periodicity increases the number of structure-driven (systematic) resonances. For the N = 8 and N = 10 configurations, the possible working points will be too close to dangerous stop-bands at some point in the accumulation process, whereas for N = 11, the only adjacent structural resonance is not dangerous /18, 19/ (Fig. D2.2-1).

For N = 14 an isochronous lattice at 1.1 GeV can only be constructed with great technical difficulties, such as high fields and gradients or edge angles in the bending magnets. One disadvantage of the 11-fold periodicity is that correction elements must be placed in every cell. Among the lattices studied for N = 11, the "Distributed Triplet" (FODOODOOB) (Fig. D2.2-2) is superior, allowing independent adjustment of the main parameters. It is also suitable for horizontal extraction.

The distributed triplett for N = 11 /9/

This structure is shown in fig. D2.2-2, the related Twiss parameter in D2.2.-3 and the beam envelopes in D2.2-4. For other parameters see sub-sections 2.2.1 and 2.3.1.

With the constraint that the distance between the bending magnet and the radially focusing quadrupole lens, QF be 0.5 m, a combination of $\bar{R}$ = 32.18 m and a distance of 0.8 m between QF and QD1 yields a minimum γ_{tr} = 2.07. The mean radius of 32.18 m corresponds to a harmonic number of 82 of the linac frequency (108 MHz) with 10 cm added to the circumference. For h = 81 the minimum γ_{tr} is not sufficiently low and for h = 83 the circumference is unneccessarily long. The 0.8 m drift space between QF and QD1 can be used for correction elements.

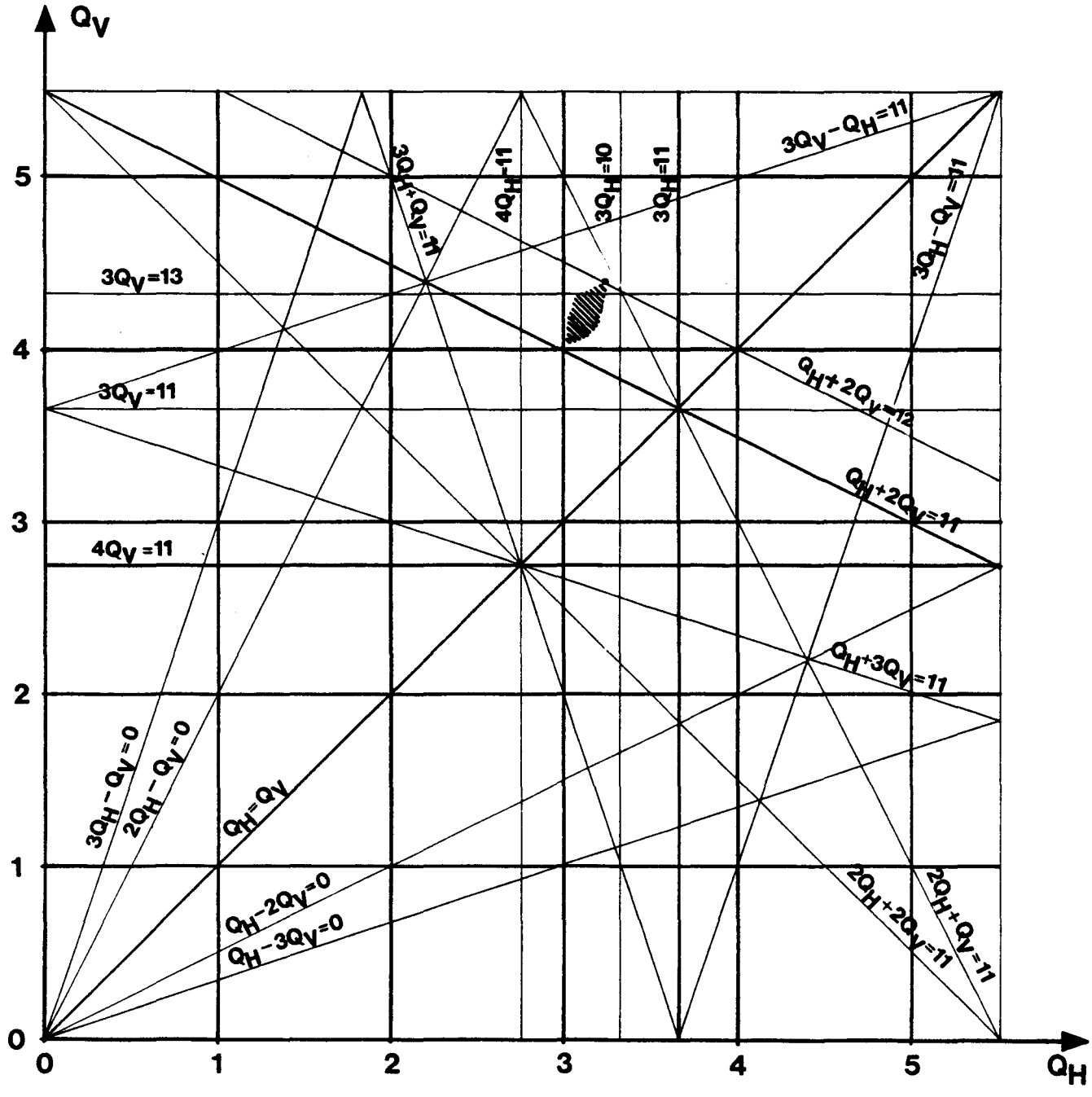

Fig. D2.2-1. Stop bands including higher order stop bands, and working region for nominal values Q_H = 3.25 and Q_V = 4.4, with maximum shifts ΔQ_H = -0.21 and ΔQ_V = -0.37 (hatched region). For N = 11 the structural stop bands are outside the working region.

The adjustment range for γ_{tr} is from 2.07 to in excess of 2.35 (fig. D2.2-5). The Q-values are adjustable over a wide range, but for γ_{tr} close to 2.07 there are some limitations. The tuning is mainly done by changing the gradients in QF and QD1. The Q-values should decrease during accumulation /20/.

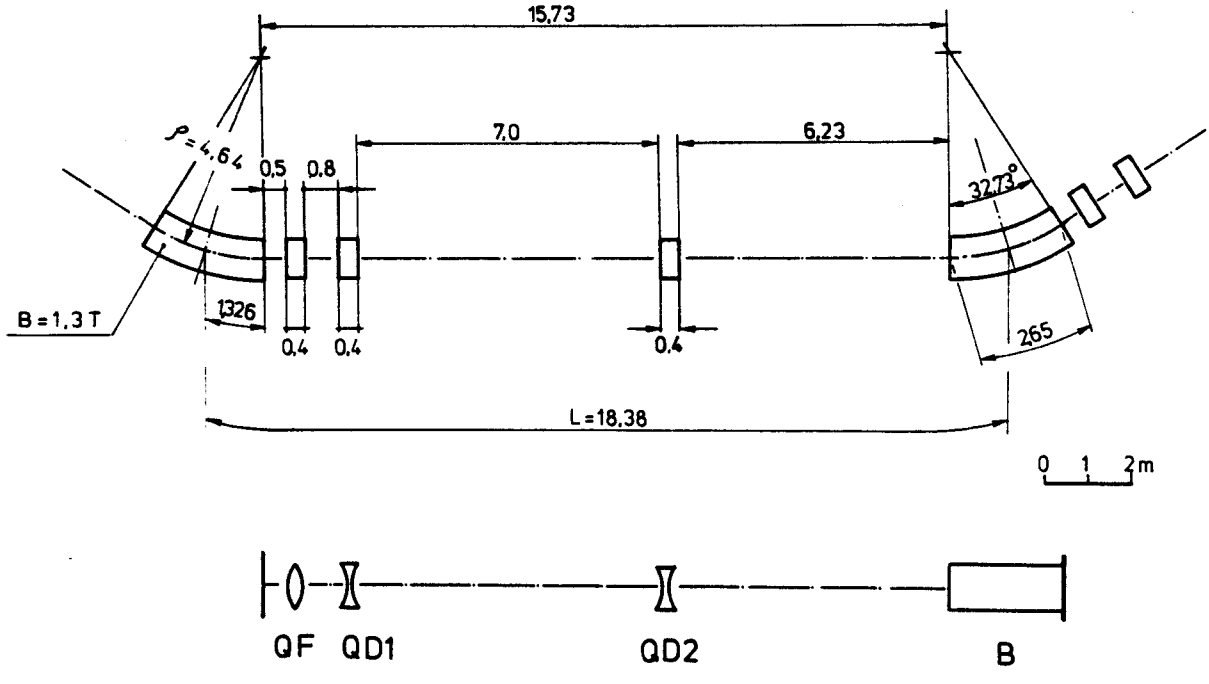

Fig. D2.2-2. Distributed triplet for N = 11

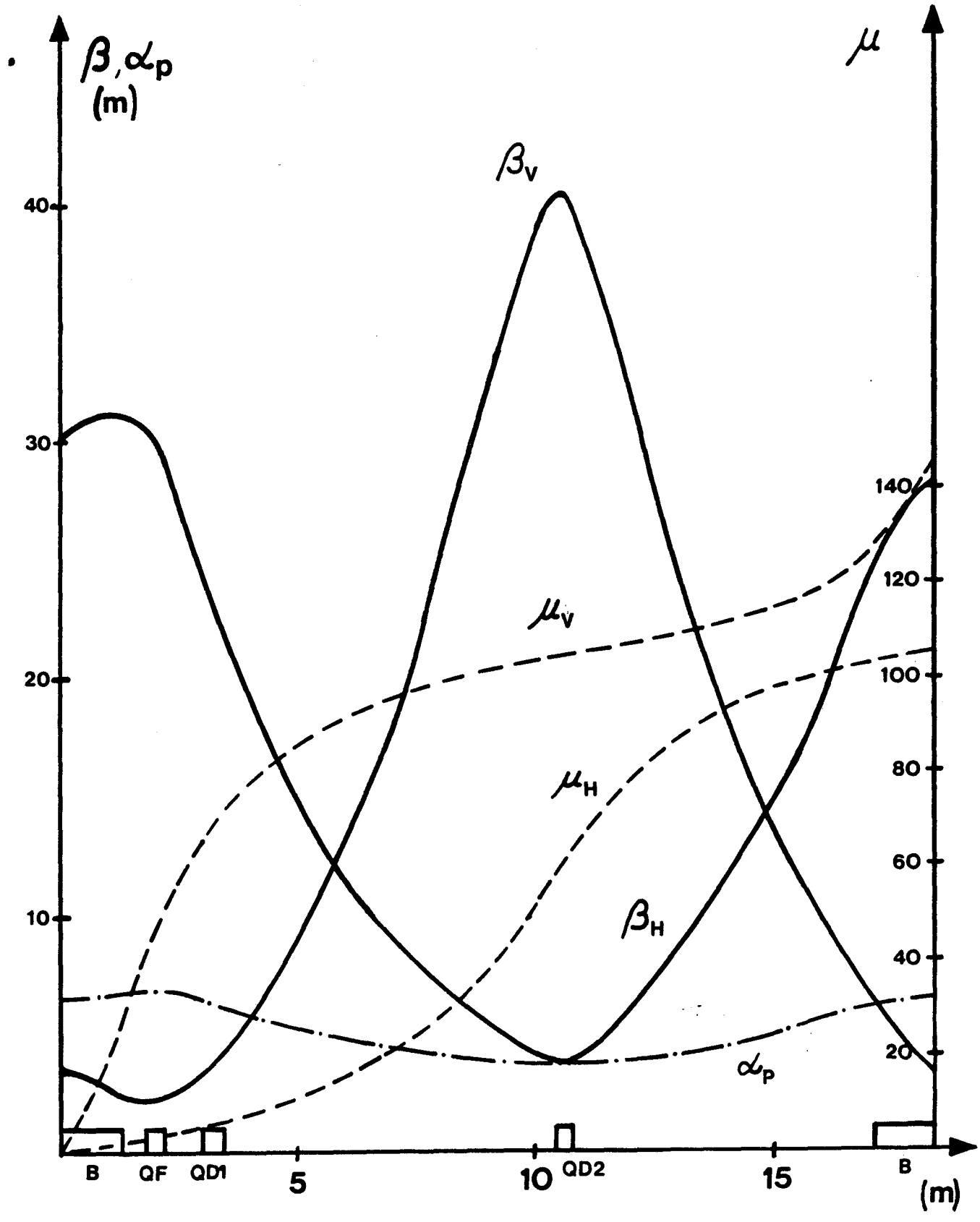

Fig. D2.2-3. Twiss parameter β, phase advance μ and momentum compaction factor α_p for distributed triplet (N = 11)
Q_H = 3.25, Q_V = 4.4, γ_{tr} = 2.226.

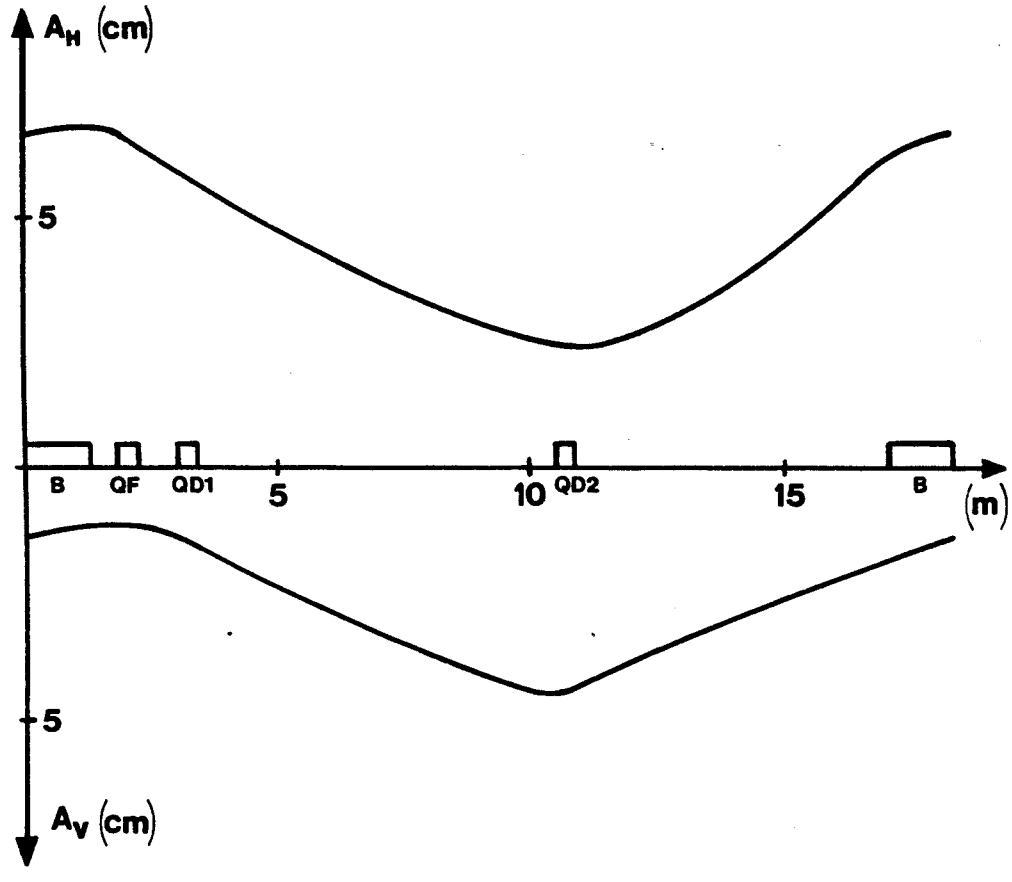

Fig. D2.2-4. Beam envelope for distributed triplet (N = 11)
Q_H = 3.25, Q_V = 4.4, γ_{tr} = 2.226, ε_H = 150 π mm mrad,
ε_V = 50 π mm mrad, Δp_p = 0.

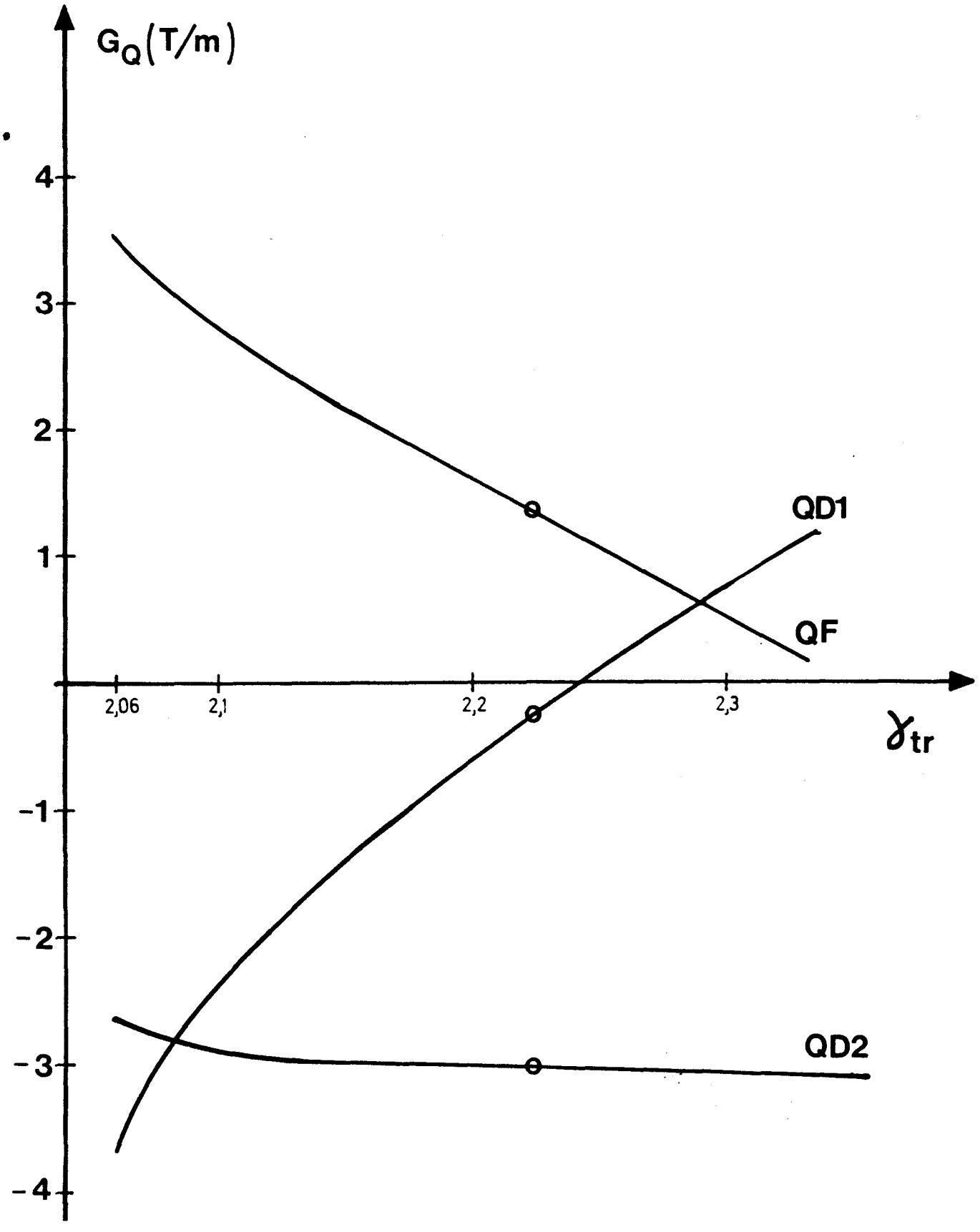

Fig. D2.2-5. γ_{tr} tuning by the quadrupole lenses for distributed triplet (N = 11), Q_H = 3.25, Q_V = 4.4.

2.2.3 Tolerances and corrections

Closed orbit deviations

Errors in the magnetic field and misalignment of the bending magnets will cause a distortion of the closed orbit. If an imperfection occurs at an azimuthal position s_k, the maximum closed orbit distortion occurs at the azimuthal position s_o and is given by

$$\hat{y}(s_o) = \frac{\sqrt{\beta_y(s_k)\beta_y(s_o)}}{2|\sin \pi Q_y|} \cdot \overline{\delta(B(s_k)L)/B\rho}$$

with the Twiss parameter β_y, the Q-value Q_y, and the error $\delta(B(s_k)L)$ at s_k (B = magnetic induction and L = length of the dipole). The position s_o is given by the relation

$$|\mu_y(s_o)-\mu_y(s_k)| = \Delta\mu = (Q_y-m)\pi \qquad m = 1,2,3,\ldots < Q_y$$

where μ is again the phase of the betatron oscillation. With $Q_H = 3{,}25$, $\Delta\mu = 45^o$, $\sqrt{\beta_H(S_k)\beta_H(s_o)} \simeq 11.5$ m, $L_B = 2.65$ m, and $\rho = 4.64$ m the closed orbit distortion in the horizontal plane due to magnetic field errors is given by

$$\hat{y}_H = 4.6\ \overline{\delta B_z/B}\ \text{(m)} \quad .$$

In the vertical plane ($Q_V = 4.4$, $\Delta\mu = 72^o$, $\sqrt{\beta_V(s_k)\beta_V(s_o)} \simeq 9$ m) a field error $\overline{\delta B_x/B}$ causes a maximum orbit deviation

$$\hat{y}_H = 4.6\ \overline{\delta r/\rho}\ \text{(m)} \quad .$$

So, for a relative error of 10^{-4} ($\delta B_x/B = \delta B_z/B = 10^{-4}$) in one bending magnet the closed orbit errors are $\hat{y}_H = 0.46$ mm and $\hat{y}_V = 0.27$ mm. A radial position error of 1 mm in one bending magnet gives $\hat{y}_H \simeq 1$ mm.

Also, positioning errors of quadrupole lenses introduce closed orbit deviations. A positioning error of 1 mm (rms) of a lens introduces a maximum horizontal (vertical) deviation of 1 mm (1.9 mm). If all 11 lenses of the same type are positioned with this error, the maximum deviation increases to 3.3 mm (vertically 6.3 mm). These approximate values are based on $Q_H = 3.25$ and $Q_V = 4.4$.

Closed orbit deviations can be corrected by additional dipole windings (see 'correction elements' at the end of this sub-section).

Gradient errors

Random errors in the field gradient introduce a modulation of beam envelopes and shifts in the Q-values Q_H and Q_V. The tune shifts $\Delta Q_{H,V}$ depend linearly on the Twiss parameters $\beta_{H,V}$. Therefore the quadrupoles QF and QD1, where β_H is large (see fig. D2.2-3), will mainly influence Q_H. The quadrupole lens QD2, where β_V is large, will mainly influence Q_V. The tune shifts for a relative gradient error of 10^{-3} in the quadrupoles lie between 10^{-4} and $6 \cdot 10^{-4}$, and are therefore negligible.

Nonlinear resonances

Principle: Resonant build up of transverse oscillations due to imperfections of the azimuthal distribution of the bending fields or of the gradient fields is avoided by avoiding integral and half-integral values of the Q-values Q_H and Q_V. In general imperfections of the azimuthal contributions of the sextupole, octupole and higher multipole components of the focussing field can produce build up of betatron-oscillations by nonlinear resonances, characterized by the relation $\ell Q_H + m Q_H = k$ with ℓ, m and k integers. $|\ell| + |m|$ is the order of the resonance. In general, the lower the order the more dangerous the resonance and the faster the growth. Those terms for which k is a multiple of N (periodicity of the machine), $k = n \cdot N$, are the most dangerous ones. Other terms can occur only as the result of error fields and are thus expected to be of smaller amplitude.

ℓ	m	k	resonances	
3	0	11	$3Q_H = 11$	correction sextupoles
3	0	11	$3Q_H = 11$	sextupole errors in bending magnet
3	0	10	$3Q_H = 10$	sextupole error in bending magnet
1	2	11	$Q_H + 2Q_V \approx 11$	correction sextupoles
2	1	11	$2Q_H + Q_V = 11$	rotation error of correction sextupoles
1	2	12	$Q_H + 2Q_V = 12$	sextupole error in bending magnet
4	0	11	$4Q_H = 11$	correction octupoles

Table D2.2-1. Important nonlinear resonances for N = 11

Onedimensional resonances, so-called sum resonances (ℓ and m of same sign) can lead to beam blow-up and beam loss. In order to avoid these effects the working point must be chosen such that $|\ell Q_H + mQ_V| > \delta Q$. The value δQ increases with the amplitude of the driving harmonic and decreases with increasing ordinal number. Here we have to consider third order resonances due to sextupoles placed in the lattice for γ_{tr} control or chromaticity control, sextupole errors in the bending magnets and fourth order resonances due to octupoles included for Landau damping. From the quantitiy δQ, tolerances can be computed. Table D2.2-1 gives a summary of the considered resonances, also with the fields which excite these resonances.

Detailed results concerning these resonances can be found in /18/ and /21/. The essential conclusions are:

Excitation by correction sextupoles: Putting two sextupoles in each cell as indicated in fig. D2.2-6 the resonance $3Q_H = 11$ can be excited. In order to keep the related stop band sufficiently thin, the integrated sextupole strength must stay below 3.4 T/m. For the coupling resonance $Q_H + 2Q_V = 11$ the corresponding value is 4.5 T/m (K1).

Excitation by sextupole errors in the bending magnets: Under the assumption of a sextupole error in the bending magnet, the resonance $3Q_H = 11$ is excited again. Under the same conditions as above the error must stay below 1.2 T/m. This means that

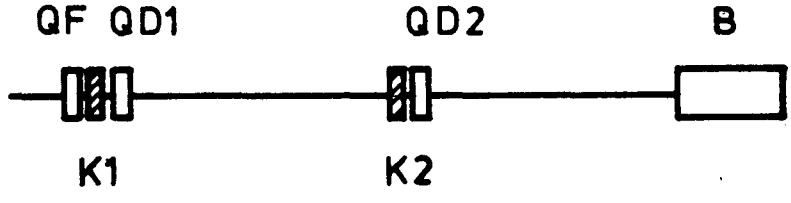

Fig. D2.2-6. Grouping of correction elements K1 and, if necessary, K2, in a magnet cell (each corr. element containing a correction dipole, a sextupole and an octupole lens).

the horizontal magnetic induction in the bending magnets must satisfy the condition B_x (x = 5 cm, z = 1 cm) < 6 Gauss. The 10^{th} azimuthal harmonic of the sextupole fields excites the resonance $3Q_H = 10$. Here, the required distance leads to the condition B_x (x = 5 cm, z = 1 cm) < 4 Gauss (for B" < 2.8 T/m^2). By fulfilment of this condition, the sum resonance $Q_H + 2Q_V = 12$ also looses significance. We may conclude that sextupole errors in bending magnets are rather critical which follows from the high values of β_H in these magnets. A very good field quality is necessary in order to avoid beam blow-up. In case sextupole errors cannot be kept small enough, harmonic correction sextupoles must be provided (K2 in fig. D2.2-6).

Correction elements /22,23/

One correction element (K1) per cell is firmly planned. An additional one (K2) can be added if required (fig. D2.2-6). Dipole fields up to 0.01 Tm can thus be generated for vertical correction of the equili-

brium orbit. Sextupole fields of 0.5 T/m are useful to diminish the dependance of γ_{tr} from orbit radius (proton momentum) or for chromaticity adjustment. Octupole fields up to 250 T/m^2 can be used for Landau damping of transverse oscillations of higher order.

For horizontal correction of the equilibrium orbit, supplementary windings on the bending magnets are provided.

2.2.4 Injection

Synopsis

For the preparation of the injection, the 100 mA, 1100 MeV H^- ion beam from the linear accelerator is passed through a section where the extreme tails are stripped to protons for subsequent removal and is then transported to a localized gradient magnet where the beam is converted to neutral ions. The neutral ion beam passes through a carbon foil in the ring where the remaining electron is removed. During the injection process, the equilibrium orbit is displaced by a set of programmed bending magnets so that ions pass through the foil only a few times. A programmed tune shift, together with the space-charge-induced tune shift, yields a uniform filling of the two two-dimensional betatron phase spaces as shown in fig. D2.2-7. The layout of the IKOR injection section is shown in fig. D2.2-8.

Injected beam characteristics

The rms emittance in each of the two transverse planes at 1100 MeV is 1.56 π mm mrad (not normalized). However, there are large tails to the distribution; the emittance for 100% of the beam is estimated to be ten times the rms emittance. The energy spread of the beam is $\pm$ 0.145%. The microstructure of the beam has a 1% duty cycle; thus 2.5 cm bunches of an instantaneous current of 10 A are separated by 2.5 m. By an adjustment of the linac parameters, this spread can be increased by up to five times at the IKOR input. The spread may be further increased by operating the injection line in a dispersive mode (see sub-section 2.4.1). The bunch length entering the ring must exceed 12 cm (see sub-section 2.2.5).

A fast chopper at the injection end of the linac will remove approximately 100 nsec of beam every 760 nsec in order to create the azimuthal void in the beam. The timing of the chopped section will vary with turn number in order that the longitudinal charge density not change too abruptly at the edges of the azimuthal void.

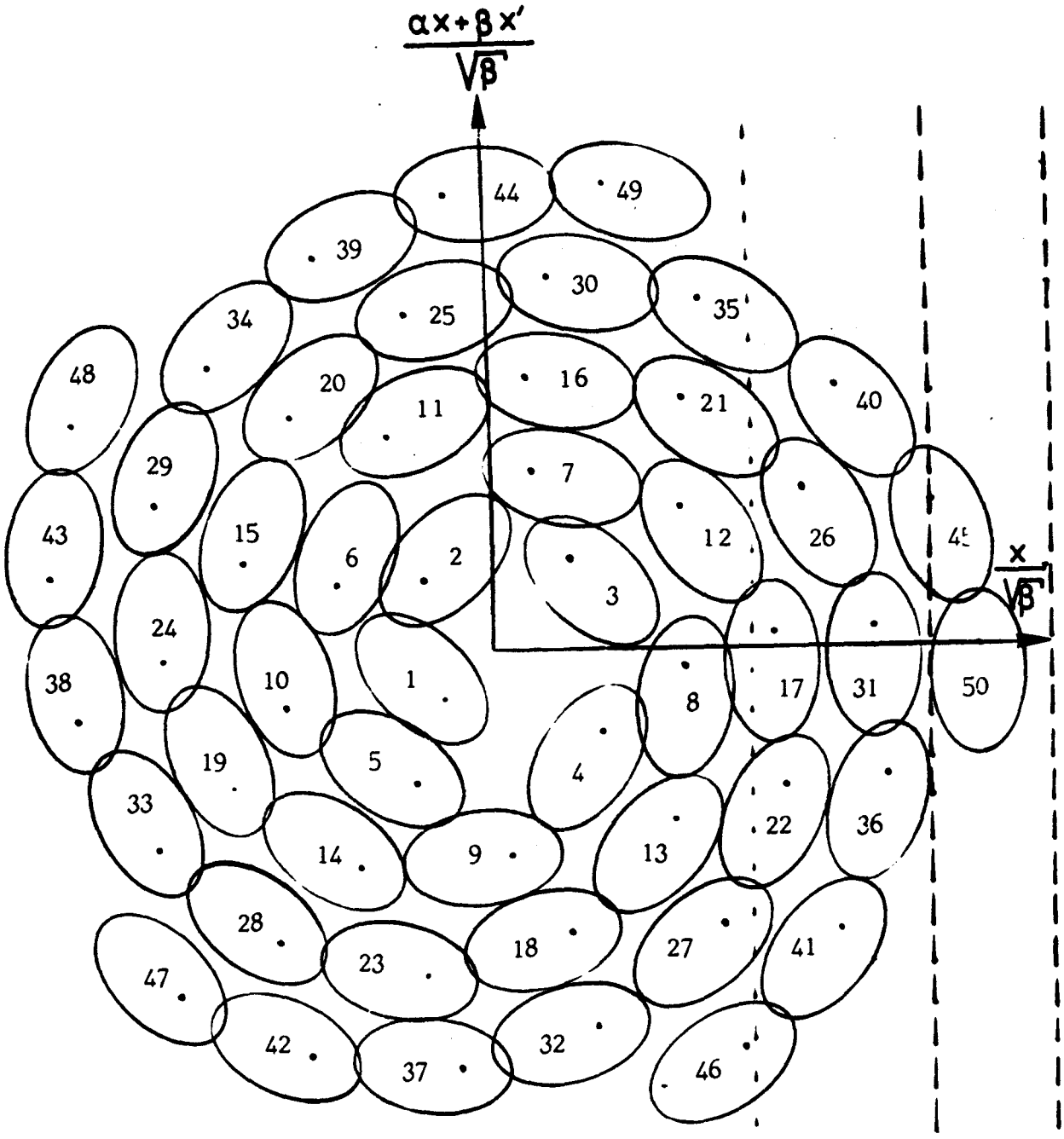

Fig. D2.2-7. Spiral injection, principle: Injection of 50 turns in normalized radial phase space is shown with the 50th turn passing through the stripping foil. The center of the pattern is the equlibrium orbit, about which the entire patterns rotates from turn to turn. The dense portion of the foil is that between the heavy dashed vertical lines; a thinner portion extends to the left of the dense portion as indicated by the light dashed line. As shown, a portion of turn 45 appears to pass through the foil a second time; this can be prevented by using a coherent betatron displacement in the vertical plane. However, clearly several turns pass through the thin portion of the foil.

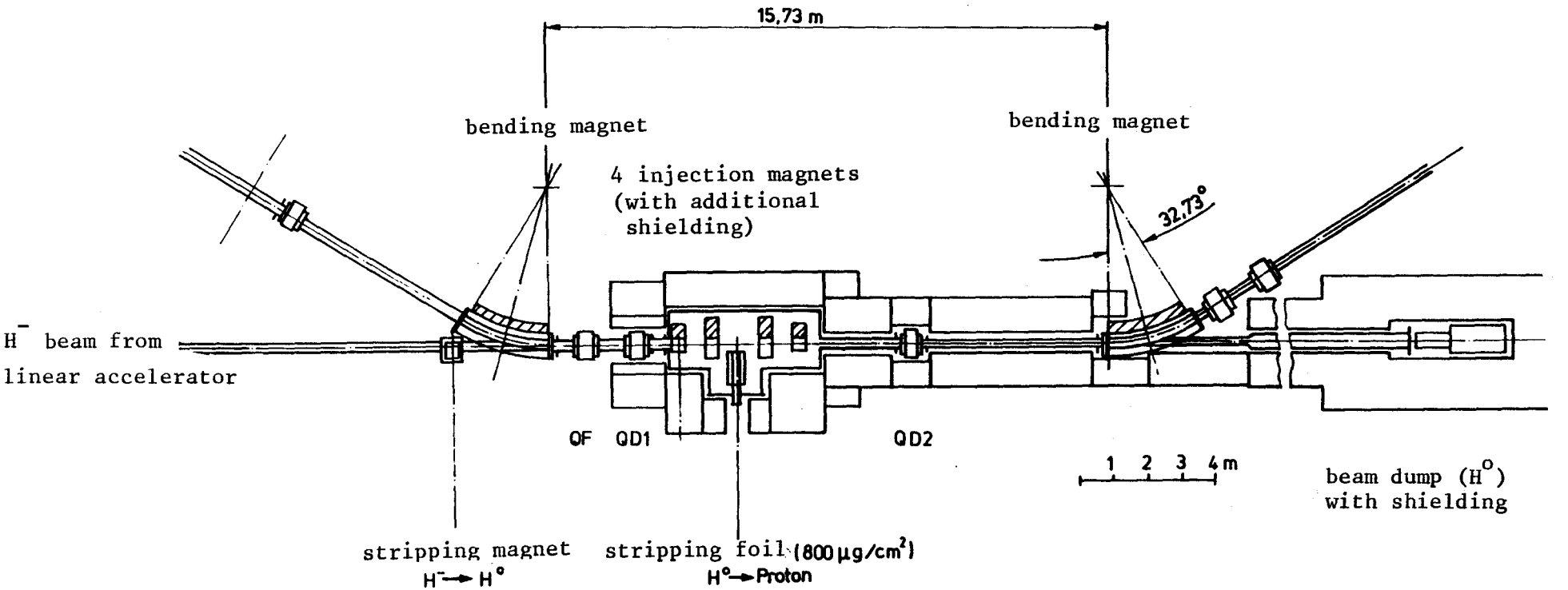

Fig. D2.2-8. IKOR-injection section

Tail remover

It is important that the stripping magnet have a rapidly rising magnetic field to minimize the distribution in longitudinal position where stripping occurs. This distribution induces an additional spread in angle in the plane normal to the magnetic field. It is thus important to minimize the gap in this magnet. Elimination of a fraction of the large tails in the plane of the gap allows this gap to be reduced with the loss of just a small fraction of the beam. The method used to remove the tails is to place thick stripping foils at the edges of the beam at a location that is an optical image of the stripping magnet as suggested by the Los Alamos group /25/.

Gradient stripping magnet

The cross sections for the Lorentz stripping of one electron from H^- is now well known over ten decades of magnetic fields /26/. The magnet should be designed so the fringing field is as sharp as possible. Essentially no stripping occurs for fields below 0.4 T whereas stripping is immediate for fields around 2 T. The designs at Los Alamos for a magnet with a peak field of 1.8 T indicate that the longitudinal distribution in stripping location associated with a gap of n cm results in an additional angular spread for 800 MeV ions of n mrad in the plane normal to the field /27,28/. At 1100 MeV, the spread is 30% of that at 800 MeV /26,29/. This additional spread in angle causes an increase in the beam size at the stripping foil and also causes an increase in the exit width of the (unstripped) neutral beam that must be taken from the foil to an external beam dump.

Pulsed injection magnets

The function of the pulsed injection magnets is to displace the equilibrium orbit as a function of time in order that there be a uniform filling of the betatron phase spaces. This is desirable as the number of passes of an ion through the stripping medium is minimized.

The most direct and economic way of achieving this function is to place a pulsed magnet at positions that are 1/4 betatron wavelength ahead and behind the foil. If this is to be done in both planes then four such magnets would be required. It is difficult to find free locations satisfying this criterion in both planes. Also, because of the planned tune shifts, the position will change, and thus an additional pair of correction bending magnets is required if the betatron amplitudes are not to be increased. We have chosen to place pairs of pulsed bending magnets immediately on both sides of the foil with no other optical elements between /30/. In this way, the orbit displacement becomes independent of the betatron tunes. By rotating the magnet array, the equilibrium orbit can be moved simultaneously in both planes.

In order that the equilibrium orbit can be displaced so as to pass through the foil as is planned for the first injected turn, four magnets of 0.6 meters length and 0.6 T peak field are required /31/.

Spiral injection

In order to minimize the number of times each injected ion passes through the stripping foil (and thus minimize the heat deposition and multiple scattering), the filling will be done in a manner similar to that necessary for proton injection. A total of 658 turns will be injected along a multiarmed logarithmic spiral (see fig. D2.2-7) in both transverse phase planes /32,33/. To achieve this loading, the stripping foil is located just beyond the periphery of the full beam in both planes. The equilibrium orbit is moved by pulsed injection magnets so it passes through the foil at the start of the injection process. The fields in these magnets are then reduced in proportion to the square root of the injected turn number. Simultaneously, the tunes in both planes are shifted in proportion to the reciprocal of the equilibrium orbit deflection. Much of this shift will come from the Laslett tune shift, and the balance will come from changing the quadrupole fields. Unlike the case for proton injection, failure to meet these criteria exactly merely results in a slight irregularity

in the number of passes through the foil that the injected ions make. The program of the pulsed magnets may be changed to vary the loading of the phase spaces. Achieving this, control of the ring parameters should be much easier than for injection into a synchrotron because the ring runs at a constant field, and that field is much higher than that for synchrotron injection.

The method here outlined yields a uniform charge density in both the radial and the vertical phase spaces. This yields the "waterbag distribution" of Ehrman /34/ and dePackh /35/. Sacherer shows that the tune shifts with this distribution are slightly nonlinear: 8% greater than those for a uniform distribution at the edge of the beam and 27.3% greater at the center of the beam /36/. The tune spreads for a Gaussian distribution are 150% greater than for the waterbag distribution.

Stripping foil

Stripping efficiency: At 1100 MeV, the cross section for stripping on carbon of incoming H^- ions is 8.04×10^{-19} cm^2, whereas that for stripping 1100 MeV neutrals to protons is 2.77×10^{-19} /37,38/. As the injection method prevents the beam from passing through the foil more than a few times, a thick foil that yields very high stripping efficiency is recommended. For example, a 800 $\mu g/cm^2$ foil will let no negative ions through, and only fifteen in a million incoming ions will not be stripped to protons.

Because of the spread due to the gradient magnet and that due to the residual tail in the intensity distribution, there will be a fraction of the incoming beam that lies nearer the equilibrium orbit than the thick foil (which is sized to intercept only the bright portion of the beam plus the outer tails). A thin foil placed to intercept this fraction of the beam will strip with acceptable efficiency. This foil will intercept a substantial number of previous turns and thus must be kept thin to avoid excessive heating. A thickness of 50 $\mu g/cm^2$ will

strip one half of the incoming tail to protons with roughly 5% of the heat deposition per particle of the thick foil.

Heat deposition: The 500 μsec of beam represents essentially an impulse heating of the foil whose temperature then diminishes somewhat by thermal radiation during the 9.5 msec interval to the next burst /39/. For the IKOR parameters, assuming acceptable temperature cycling, the mean temperature of the foil is given by $T = (Q/A)^{0.25} \times 1816$ (^{o}K) where Q/A is the heating intensity in Joules/cm^2 /40/. The temperature difference immediately before and after the burst is just the heating intensity divided by the product of the foil thickness (g/cm^2) and mean specific heat. With the thick foil, each proton passage yields 1521 eV to the foil whereas the stripped electron yields 1266 eV to the foil. Assuming there are, on the average, 4 foil traversals for each entering ion, and assuming that 100 nsec of beam is chopped in the linac for each injected turn, the total heating per burst is 0.32 Joules. If the beam spot is 1 cm^2 then the median temperature is 1099 ^{o}C, and the cycling range is about 207^{o} (max. temp. is 1202^{o}).

Foil fabrication: Stripping foils are made commercially. It is planned to have the foils made with varying thickness so that the density of heat deposition will be constant over the surface of the foil. This is desirable to eliminate the thermal stress caused by temperature gradients within the foil.

Foil lifetime: Little experience exists for lifetime of carbon foils at the energy and intensity of IKOR. However, the stripper foil used at the TRIUMF cyclotron lasts for months (indefinitely) where it is subjected to continuous bombardment of 550 MeV H^- ions at currents of 100 μAmps or more /41/. It is generally accepted that the foil lifetime is a function only of the total deposited energy, and thus one would expect the lifetime of the foil in the accumulator to be of the order of 1% of that in TRIUMF. The planned minimal temperature cycling and lack of temperature gradients should minimize mechanical damage.

Activation: At the injection energy, the total cross section is about the geometric cross section, 0.280 barns /42/. For a thickness of 800 $\mu g/cm^2$, the fraction loss per foil traversal is 1 part in 89000; if we assume an average of four traversals per entering ion, the beam spilled is 4.5 μA which is 1.4×10^{12} nuclear events per second. This is slightly more than the production assumed in the LASL report /39/; after two hours, about 4 Curies of C^{11} will have been produced. Scaling this result, we expect 64 mCi of H^3 to accumulate in the ring in a year.

Stripping by laser beam

The charge exchange mechanism $H^- \rightarrow H^o \rightarrow$ proton by application of laser beams has been considered /60/. However, with present technology, this method seems to be not applicable.

2.2.5 Effect of space charge and image fields, countermeasures:

Emittance and incoherent tune shift

For establishing the beam emittance and the tolerable tune shift we will use the results of /42/. According to Laslett /43/ the minimum emittance for a given number and energy of protons and for a given lattice structure is essentially determined by the tolerable shift ΔQ of the number Q of betatron oscillations per turn. The geometry of the vacuum chamber comes in via the image fields. Definite requirements concerning the cross-section of the chamber are also found out by coherent stability considerations. The geometry chosen in table D2.2-2 fulfils both requirements.

chamber section	chamber length m	beam width max. cm	beam width min. cm	beam height max. cm	beam height min. cm	chamber dimensions width cm	chamber dimensions height cm *)
I	4.60	6.9	5.8	1.7	1.0	9.00	2.65
II	4.60	5.8	3.0	3.6	1.7	8.85	4.60
III	4.60	3.2	2.3	4.3	3.1	6.15	5.25
IV	4.60	5.6	3.2	3.1	1.4	8.60	4.10

*) without regard to closed orbit distortion

Table D2.2-2. Half diameters of the elliptic cross-section of the beam and of the vacuum chamber of a ring period. The ring period is divided in four equal sections I to IV.

The tune shifts ΔQ_H and ΔQ_V cannot be chosen independently since a minimum distance of the working point to the adjacent stop band must be maintained (see fig, D2.2-1). Based on experience /44/ $\Delta Q_H = 0.21$ and $\Delta Q_V = 0.37$ were taken as upper limits. A ratio $\varepsilon_H/\varepsilon_V = 3$ was taken for horizontal and vertical emittances in order to achieve reasonable values for the apertures in bending magnets and in lenses.

The emittance after Laslett is calculated from these initial conditions but with the following refinements: The local horizontal and vertical half diameters of the beam are selected by emittance and local betafunction. In addition, a weight factor G is introduced which takes the transverse particle density into account, f.i. G = 1.55 if the density decreases quadratically from the center to the edge or G = 1.0, respectively, if the density is constant. Thus, for the vertical emittance, we obtain

$$\varepsilon_V = \frac{\overline{\pi\gamma^2}}{1+\sqrt{\frac{\beta_H}{\beta_V}\frac{\varepsilon_H}{\varepsilon_V}}} \left\{ \frac{\Delta Q_V B \pi \beta^2 \gamma}{N r_o G} - (B\beta^2+1/\gamma^2)\varepsilon_1 \overline{\beta_V/h^2} - \frac{\varepsilon_2 B \beta^2 \rho}{\bar{R} h_B^2} \cdot \overline{\beta_V} \right\}^{-1}$$

with the ratio B average over peak longitudinal proton density = 0.89, chamber height h and gap height h_B of the bending magnet. The bending radius ρ of the magnet determines the weight of the last term inside the bracket, according to the length of the magnets related to the circumference of the ring. The values ε_1 and ε_2 are geometrical parameters according to Laslett. The betafunctions follow from computations concerning the lattice structure (see fig. D2.2-3). Fig. D2.2-9 shows the emittances calculated in this way. Under the assumption that the transverse density during filling is time dependent but not dependent from position we choose ε_V = 50 π mm mrad as vertical emittance (G $\approx$ 1.2).

The horizontal and vertical tune shifts are calculated with the so determined emittance. In addition, the influence of the momentum spread $\Delta p/p$ is taken into account. The momentum spread increases the horizontal beam radius a by $\Delta a = \alpha_p \Delta p/p$. Supplying a by a + Δa in the formula given by Laslett and taking into account the changes described above we obtain the results listed in table D2.2-3.

The expected values of momentum spread and weight factor shift the Q-value by an acceptable amount. Within the frame of our considerations, the momentum spread leads to a more stable behaviour of the beam. Additional tune shifts which are produced by correction sextupoles and octupoles should stay below 0.10.

$\Delta p/p$	ΔQ_H	ΔQ_V	ΔQ_H	ΔQ_V
o/oo	G = 1		G = 1.55	
0	0.104	0.223	0.162	0.345
2	0.081	0.206	0.126	0.319
4	0.067	0.193	0.104	0.299

Table D2.2-3. Tune shift with momentum spread $\Delta p/p$

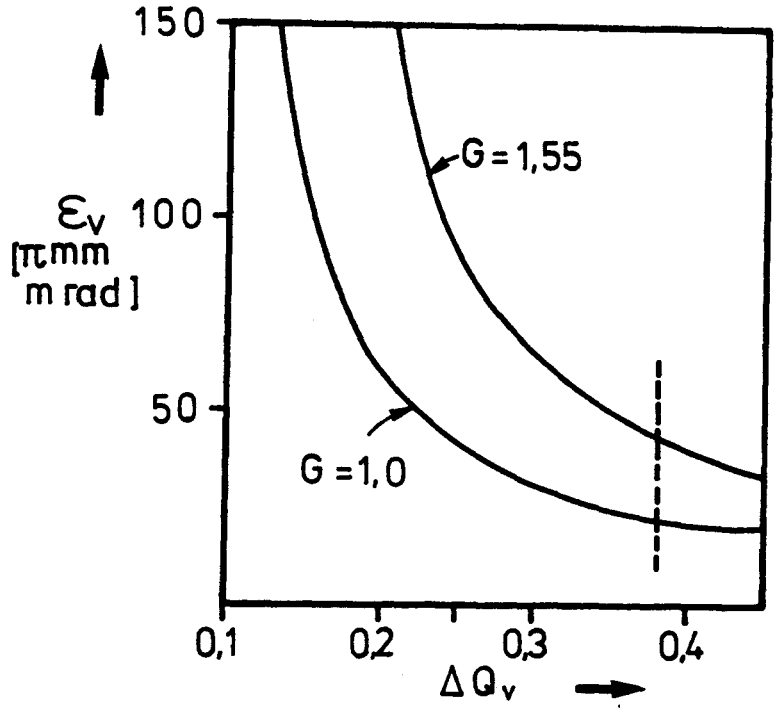

Fig. D2.2-9. Dependance of emittance (ε_V) on incoherent tune shift for two typical weight factors ($\varepsilon_H/\varepsilon_V = 3$).

Transverse stabilization

Through coupling by the vacuum chamber or the kicker magnet transverse forces may act upon the beam leading to instabilities. Under the given conditions, the beam cannot be sufficiently stabilized by Landau-damping /45/ because the required tune spread (horizontal and vertical) would shift the working point into stop bands. Therefore, the rise times of instabilities must be sufficiently slow ($\tau_T \geqq 1$ ms) in order to keep the beam stable during filling.

The rise time τ_T /45,46/

$$\tau_T = \frac{k \pi Q \gamma}{R_T I_p c}$$

with $k = 4m_o c^2/e = 3.75 \times 10^9$ V, R_T = transverse resistance, and
Q = number of betatron oscillations per turn

is calculated without considering the beam gap or the filling mechanism. The beam gap adds to the attenuation of possible instabilities. The beam current I_p shows full intensity at the end of the filling only, thus also the rise time reaches its smallest value only at the end. In this way, both effects are estimated to the safe side. Their exact calculation, together with the determination of the shortest acceptable rise time, could essentially contribute to a more precise result of the following considerations.

Vertical stabilization: Vertical instabilities are not excited by the kicker magnet /47/ but only by the vacuum chamber. The rise times follow from the resistance R_{TW} of the chamber /52/:

$$R_{TW} = \bar{R} \cdot \overline{h^{-3}} \cdot \sqrt{\frac{2 \bar{R} Z_o}{\beta \sigma (n-Q_V)}}$$

(h = height of chamber, σ = conductivity of chamber wall).

Fig. D2.2-10 shows the rise time for a steel and a copper chamber, respectively. With a copper chamber these values remain sufficently long for the higher modes. For the lower modes with rise times below 1 ms an active damping system /48/ must be provided. By this, the first 8 modes (until 4.8 MHz) are stabilized.

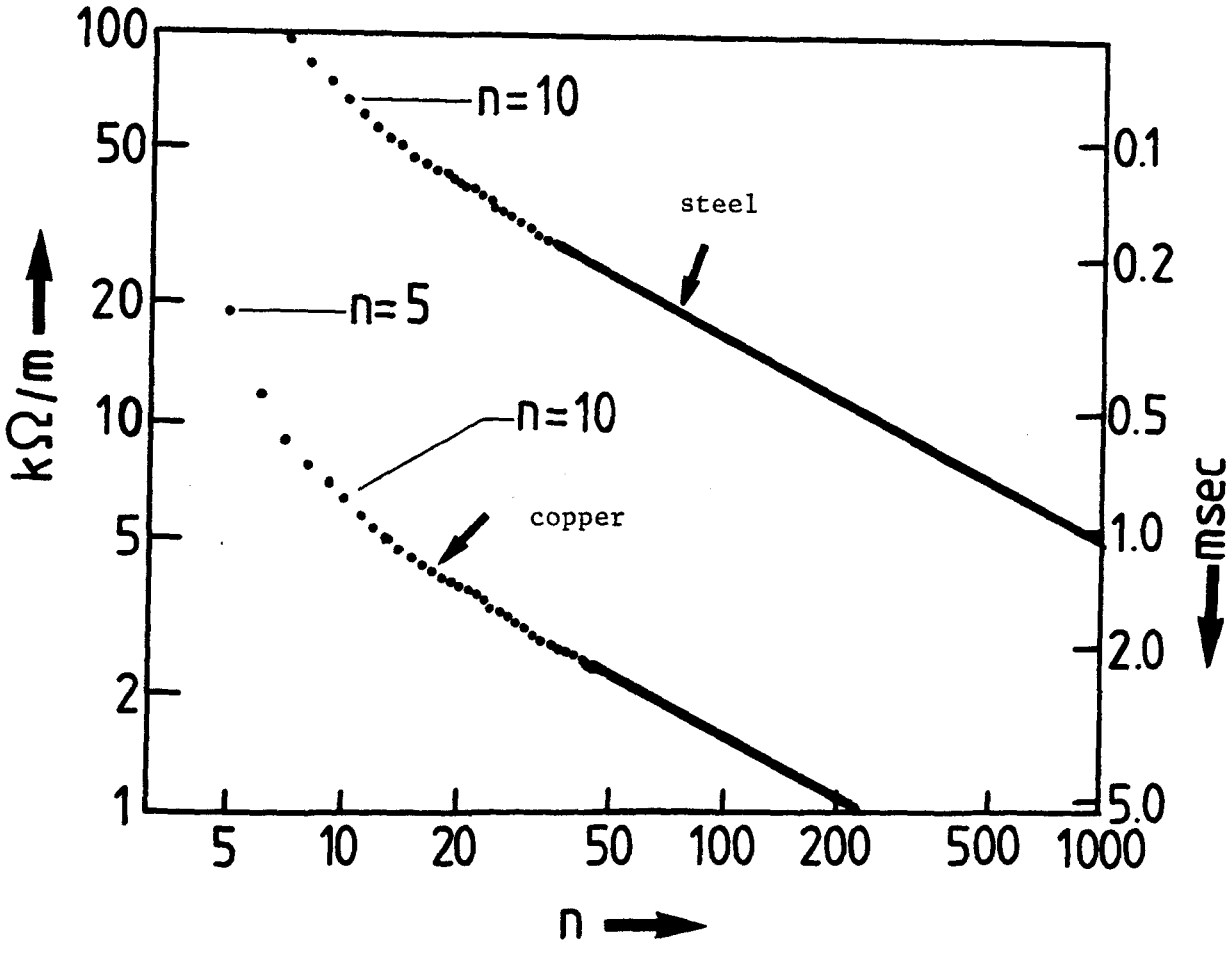

Fig. D2.2-10. Rise time of vertical instability and related chamber resistance R_{TW} (n = mode number).

Horizontal stabilization: Here, in addition to the chamber, the kicker magnet is destabilizing. For calculations of the transverse resistance R_{TK} of the kicker magnet we use the method proposed in /49/. In addition, permeability and conductivity of the ferrite material are taken into account /45,46/. For the resistance R_{TK} we obtain /51/

$$R_{TK} = 8 \frac{Z_o^2}{Z_K} \cdot \frac{4\bar{R}}{h_K^2} \cdot \frac{\sin^2((n-Q_H)\ell/2\bar{R})}{(n-Q_H)} \cdot \frac{e^{\frac{-h_k}{s}}}{\left[1 + \frac{R_F}{2R_L}\right]^2}$$

(s = frequency dependent effective ferrite thickness; R_F and R_L = reluctance of the gap or yoke, respectively).

Fig. D2.2-11 shows the rise times calculated by this way, with attention to the transverse horizontal resistance of a copper chamber. For reasons of safety, horizontal instabilities with rise times below 1 ms should also be attenuated. Mode numbers n = 1 until n = 15 are concerned among these, which corresponds to a maximum frequency of 15.5 MHz. A damping system is feasible for these frequencies /48/.

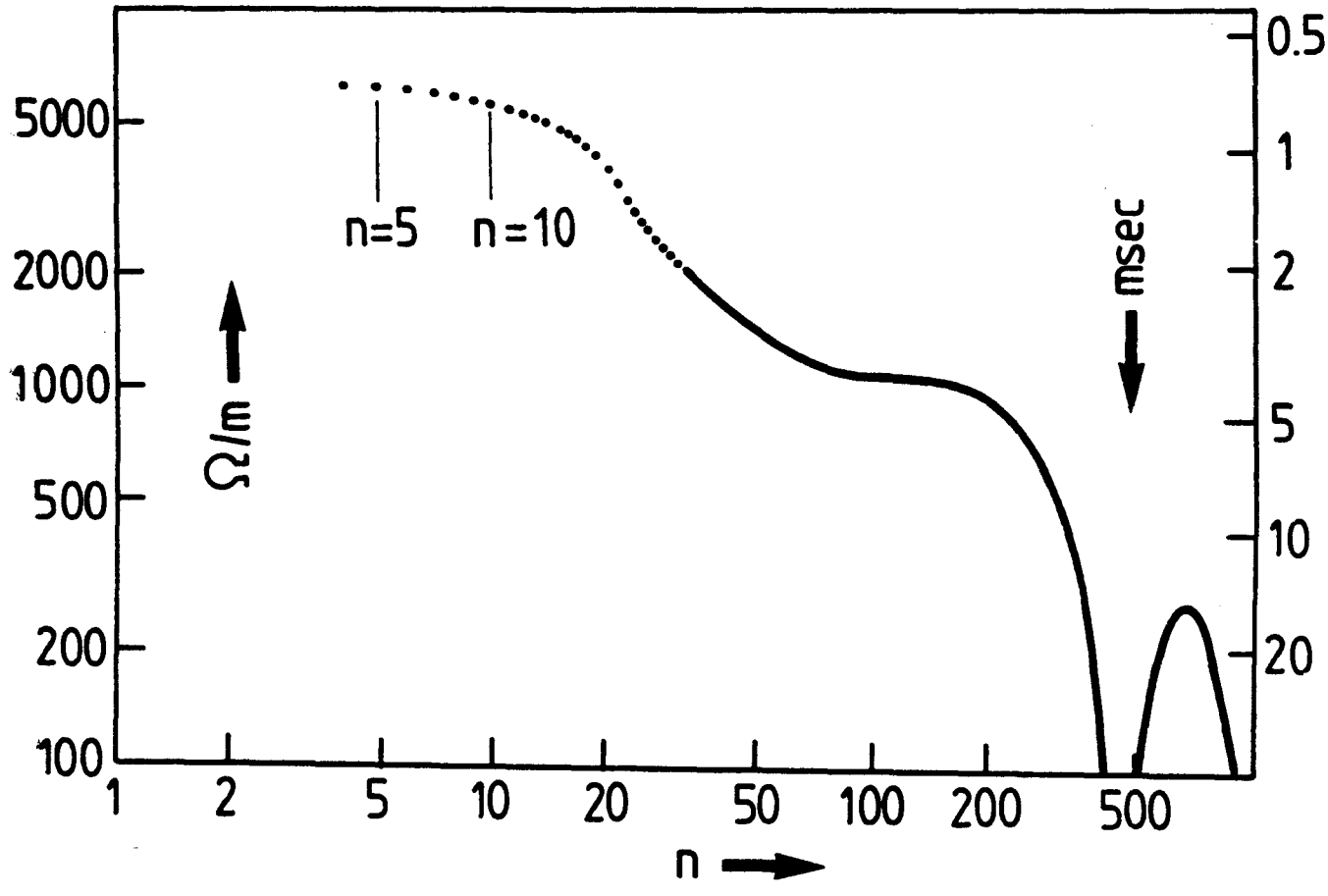

Fig. D2.2-11. Rise time for horizontal instability and related resistance R_{TK} of the kicker magnet.

Longitudinal stabilization

For machines which operate with small momentum spread and heavy currents it is not possible to maintain longitudinal stability (without electronic damping system) /45/. However, it is possible to achieve sufficiently long rise times for the instabilities. With capacitive

beam equipment interaction, the particle energies must be below the transition energy and the resistances which act upon the beam must be sufficiently small /45/. Beam equipment interaction of capacitive behaviour is to be expected for the smooth vacuum chamber in the present case.

The rise time of instabilities is given by the following equation /50,64/:

$$\tau_L = \frac{2\bar{R}}{cR} \cdot \sqrt{\frac{k}{I_p} \cdot \frac{\pi}{2} \cdot \gamma \left| \frac{X_L}{n \cdot \eta} + \frac{\pi}{2} \frac{k}{I_p} (\Delta p/p)^2 \gamma\beta^2 \right|}$$

with the values $R = R_W + R_K$ (see below), $k = 4m_o c^2/e = 4 \cdot 938$ MV, the proton current $I_p = 66$ A and mode number n.

The most important parameters which influence the rise time are:

a) the longitudinal reactance X_L, defined by the vacuum chamber and the smallest half diameter a of the beam /52/

$$X_L = n \frac{Z_o}{\beta\gamma^2} \left(\frac{1}{4} + \ln \frac{b_e}{a}\right) .$$

For exact results with elliptic walls an appropriate equivalent radius b_e instead of the ordinary radius for circular geometry is introduced /51/;

b) the longitudinal resistance R_W due to finite conductivity σ of the wall /52/

$$R_W = \frac{1}{b} \sqrt{\frac{\bar{R} Z_o \beta n}{2\sigma}} .$$

For a conservative estimate b = h = the half height of the chamber is chosen.

c) The longitudinal resistance of the kicker magnet /49,51/ given by

$$R_K = 8\,\beta^2\,\frac{Z_o^2}{Z_K}\cdot\frac{x^2}{(h_K/2)^2}\,\sin^2(n\ell/2\bar{R})$$

where h_K = 0.09 m is the kicker aperture, ℓ = 0.45 m the magnetic length and Z = 50 Ω the characteristic impedance of the kicker magnet. 8 equal kicker modules are assumed with matched output (see sub-section 2.3.2). The longitudinal resistance depends on the lateral displacement x of the beam for which a maximum value x = ±1 mm is chosen. Fig. D2.2-12 shows the resistance and the rise times calculated for the example of a steel chamber including kicker magnet. The rise times of these instabilities are not dangerous. A copper chamber would increase the rise times by a factor of about 8.

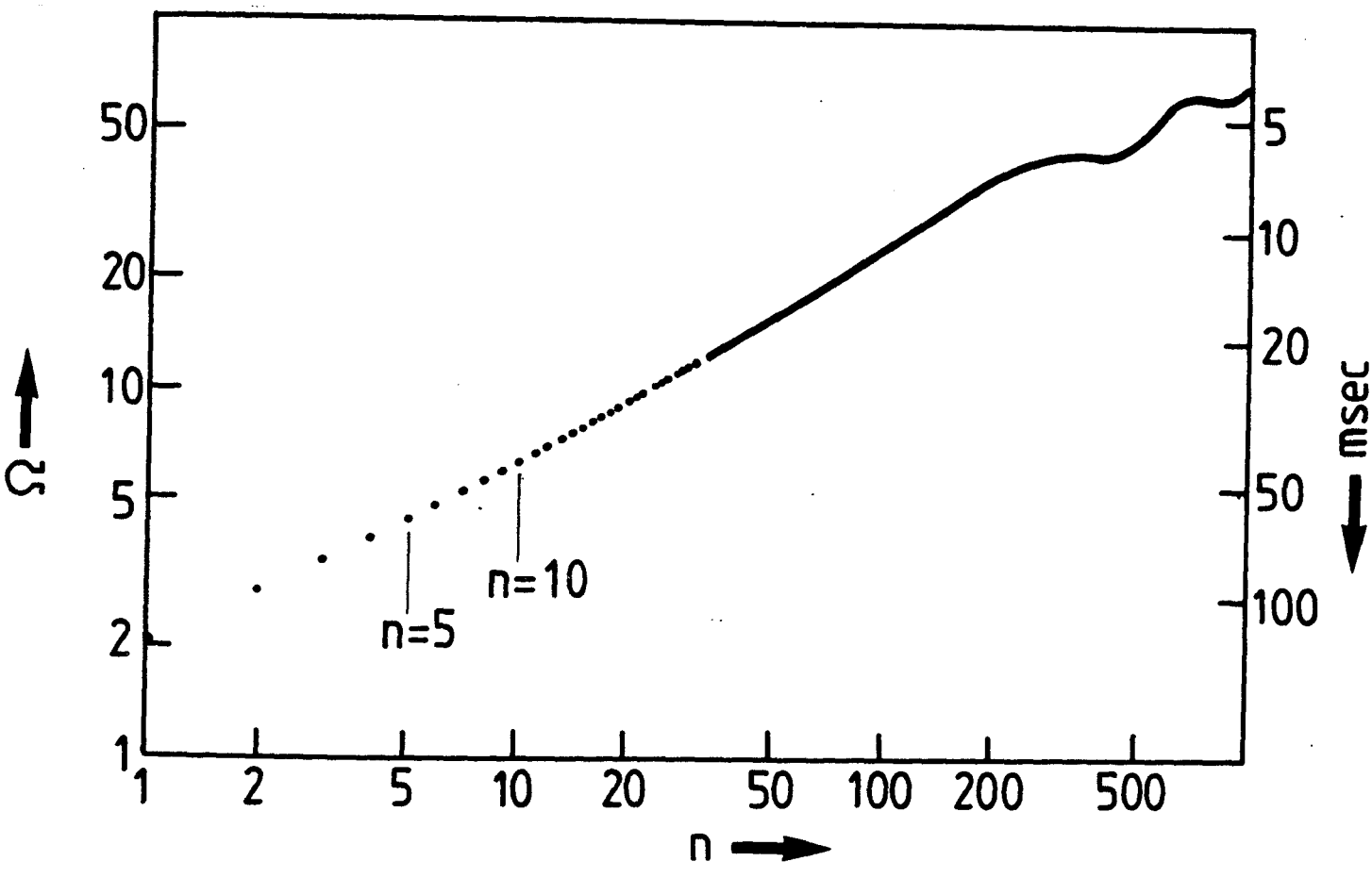

Fig. D2.2-12. Rise time for longitudinal instability and related resistance of vacuum chamber and kicker magnet.

Increase of momentum spread and consequences

Momentum change: The results of investigations concerning coherent effects /53/ are summarized in the following sections (changes of the cross section of the particle beam as a whole due to self-excited electromagnetic forces). Common to all these effects is a gradient in longitudinal particle density distribution which in proportion generates an electric field. This field changes the momentum of the particles which in turn influences the radial and longitudinal position of particles. The bunch of particles becomes elongated and skewed (fig. D2.2-13).

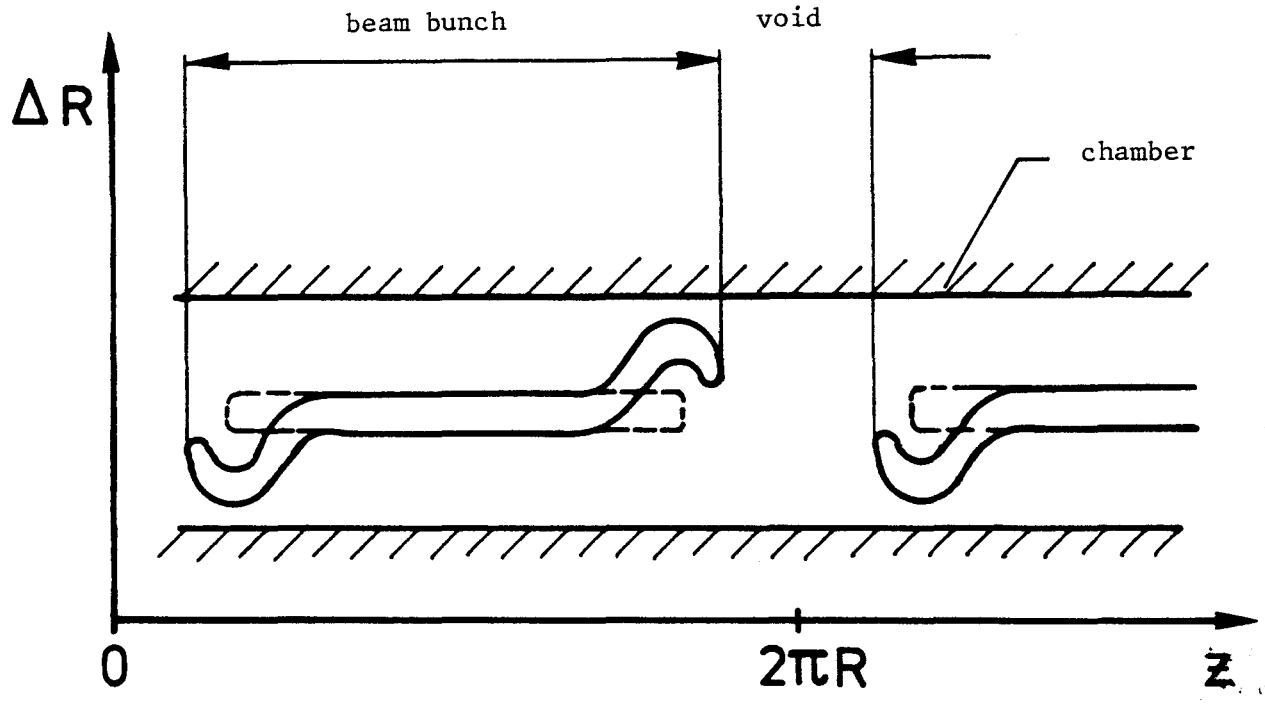

Fig. D2.2-13. Radial and longitudinal distortions of the particle bunch by the gradient of the longitudinal density (qualitative presentation).

The longitudinal electric field at position P, generated by the longitudinal density gradient

$$E_z(t,P) = -\frac{c\,X(t,P)}{2\,\pi\,\gamma^2}\,\frac{\partial\lambda}{\partial z}$$

is indicated here as function of the position and time dependent reactance $X(t,P) = \beta\,\gamma^2\,X_L(t,P)/n$ and charge density $\lambda(z,t)$. The momentum change with time, proportional to the force

$$\frac{\partial}{\partial t}\,\frac{\Delta p}{p} = \frac{eE_z}{\beta\gamma m_o c} = -\frac{2\,X(t,P)\,c^2}{\beta\,\gamma^3\,k\,\pi}\,\frac{\partial\lambda}{\partial z}$$

can be calculated in this way. From this follows a radial particle velocity v_y of

$$v_y = \partial\bar{R}/\partial t = \alpha_p \frac{\partial}{\partial t} \Delta p/p$$

with the momentum compaction factor α_p (= orbit displacement related to $\Delta p/p = 1$).

The change Δv of the longitudinal velocity v follows from the calculation

$$\frac{\partial}{\partial t} \Delta v = \beta c \eta \frac{\partial}{\partial t} \frac{\Delta p}{p} \quad ,$$

where $\eta = \frac{1}{\gamma^2} - \frac{1}{\gamma_{tr}^2}$.
The momentum change thus influences the bunch structure.

Considering first the case $\eta = 0$ (particle energy = transition energy) where also particles of small momentum deviation maintain their revolution frequency one sees that here also the longitudinal density distribution remains contant. Changes of particle momentum by the density gradient result only in a radial orbit displacement i.e. the bunch is only skewed.

In the case of deviation from the isochronous condition the length of the bunch changes in addition. If the interaction between beam and equipment is of capacitive nature and if the particle energy is below the transition energy then the behaviour of the particle bunches is mainly determined by Coulomb forces. In this case an increasing momentum leads to an increasing revolution frequency and the bunch of particles becomes longer.
Above the transition energy an increasing momentum leads to a smaller revolution frequency and the particles of a bunch approach each other. The particles show reverse behaviour with respect to the transition energy if the beam equipment interaction is mainly of inductive nature.

Landau damping by large momentum spread could prevent self-bunching of the particles. However, the momentum spread in our case is not sufficient to reach a sufficient amount of attenuation. There are two possibilities to avoid this selfbunching:

i) capacitive beam equipment interaction below transition energy

ii) inductive interaction above transition energy.

Since a smooth vacuum chamber acts in the capacitive sense we have chosen this first possibility. In this case additional components of inductive behaviour in the system must not prevail the capacitive part.

Momentum change within the microbunch: Because of the very high charge density in the microbunch the momentum range within a particle bunch changes relatively much. For an estimate of the increase in momentum the gradient is expressed by a form factor F and by the length T_μ, a measure for the length of the bunch:

$$\frac{\partial \lambda}{\partial z} = q \cdot \frac{F}{T_\mu^2} \qquad (q = \text{charge of the bunch}) \quad .$$

Our investigations have brought results for the assumption that the form factor $F(z/T_\mu)$ is time independent and that the bunch is only lengthened but maintains its characteristic shape*). In this case the development of T_μ with time can be calculated in a simple manner. Due to the increasing momentum spread the particle bunch shows rapid dilatation and the space charge forces diminish. Thus there is an upper limit for the momentum spread /53/ (T_{μ_o} = initial width of the bunch, in this case $4T_{\mu_o}$ = 0.125 m):

$$\left(\frac{\Delta p}{p}\right)_{\text{final}} = \sqrt{\frac{4cX(t,P)qF}{\pi\gamma^3 k\eta\beta^2}} \quad \frac{1}{\sqrt{T_{\mu_o}}} \quad .$$

*) However, the validity of this assumption is limited (see latest comments in /53/, p. 17).

If the charge of the bunch is described by a Gaussian, with time dependent width T_μ, a particle in the region of the maximum gradient receives a momentum change of 3 °/oo (see fig. D2.2-14). For this case $\eta = 0.01$ has been chosen. In order to limit the increase of momentum spread this should at the same time be the lower limit of η. A radial displacement of $\Delta R = \alpha_{max} \cdot \Delta p/p = 0.023$ m which does not lead to particle losses with the chosen geometry, results from the momentum spread of 3.3 °/oo. The investigation of this phenomenon is continued. First results indicate that the approximation has given a momentum spread which is somewhat too large. As shown by the results obtained so far, high local charge densities are rapidly spread out, in any case, by the space charge effect.

Momentum change in the macrobunch: The following assumptions which are discussed in more detail in /53/ were made for the calculation of the momentum change of the end of the filling:

The charge density $\lambda(z,t)$ is split into a position dependent and a time dependent part, $\lambda(z,t) = q(t) \cdot f(t)$. The time dependent part grows proportionally during filling. The position dependent part remains constant over a large range, both tails are approximated by Gaussian distribution or by a cosine distribution. The reactance has been calculated for an elliptic chamber /51/ with a beam radius $a = a(t)$ growing as the square root of time /20/. Then, for the momentum at the end of the filling time T_F follows

$$\frac{\Delta p}{p} = -\frac{2c^2}{\beta\gamma^3 k\pi} \int_0^{T_F} X(t,P) \frac{\partial \lambda}{\partial z}\, dt \quad .$$

The integration has been carried out with the assumptions mentioned above, leading to the result

$$\left(\frac{\Delta p}{p}\right)_{max} = \begin{cases} 4.2 \cdot 10^{-3} & \text{for Gaussian distribution} \\ 5.5 \cdot 10^{-3} & \text{for } \cos^2 \text{ distribution} \end{cases}$$

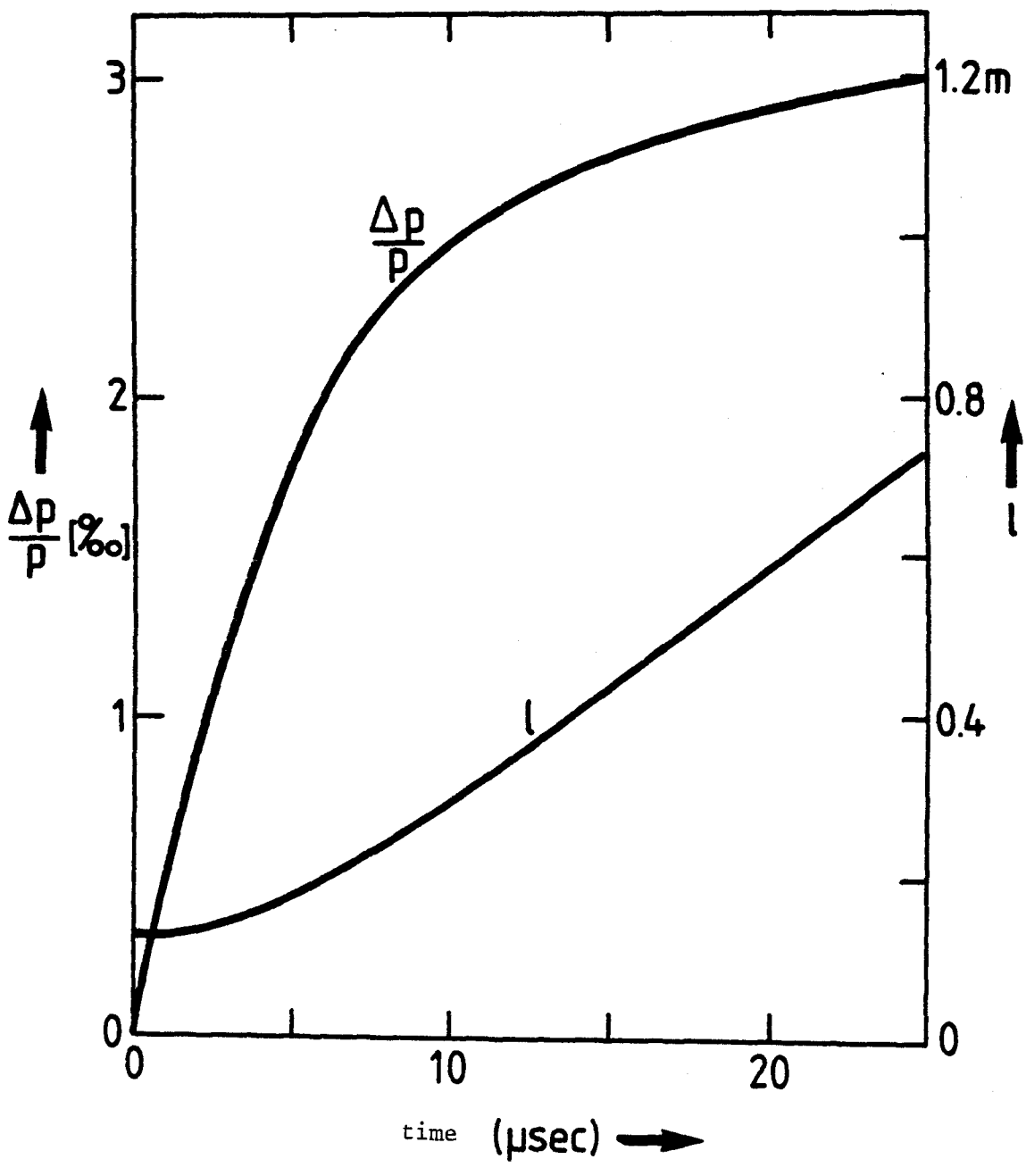

Fig. D2.2-14. Momentum spread $\Delta p/p$ and length ℓ of a microbunch as a function of time, due to space charge forces.

in the region of the maximum gradient of the distribution. With this increase of momentum one obtains a radial displacement of $\Delta\bar{R} = \alpha_{max} \cdot \Delta p/p = 2.9$ cm, which is still just acceptable for the vacuum chamber.

Longitudinal displacement: The CERN experiment /54/ has shown that it is possible to maintain a stable bunch structure near γ_{tr}. In section 'momentum change in the microbunch' a value of $\eta = 0.01$ has been chosen as minimum distance. On the other hand, this distance should not be increased either, since the longitudinal void for ejection would close too rapidly. As an upper limit, a maximum particle displacement at each end of $\Delta z = 6.9$ m follows from the rise time of the ejection kick of 50 ns (equivalent to 13.3 m) and from the beam void of 27.1 m. The value of Δz follows from beam dynamics calculations as $\Delta z = \beta c \int_0^{T_F} \eta \, \Delta p/p \, dt$, where η and $\Delta p/p$ are time dependent. The time dependence of $\Delta p/p$ follows from integration /53/. For $\eta = \gamma^{-2} - \gamma_{tr}^{-2}$ and nominal values η_o, γ_o, γ_{tro} we have

$$\gamma = \gamma_o + \Delta\gamma_o = \gamma_o(1 + \beta^2 \, \Delta p/p)$$

$$\gamma_{tr}(t) = \gamma_{tro} + \Delta\gamma_{tro} \frac{t}{T_F} \left(1 - \frac{f(z)}{f_{max}}\right) \pm A \, \gamma_{tro} \frac{\Delta\gamma_o}{\gamma_o}$$

Here, $\Delta\gamma_{tro}$ signifies a shift of the transition energy (for $t = T_F$), resulting from space charge (see fig. D2.2-15). This shift is proportional to time and is chosen such that the value for $\gamma_{tr} = \gamma_{tro}$ remains unchanged for particles in the region of maximum space charge ($f(z) = F_{max}$). The shift has to be compensated by rapidly varying quadrupole fields (see sub-sections 2.2.2 and 2.3.1).

As maximum shift $\Delta\gamma_{tro} = 0.1$ has been assumed, an estimated value which has to be checked /55/. The ratio $A = (\Delta\gamma_{tr}/\gamma_{tro})/(\Delta\gamma/\gamma_o)$ is approximated by the natural chromaticity $\xi = -1$ ($\xi \approx A$, the influence of A has been neglected in fig. D2.2-15 for reasons of simplicity).

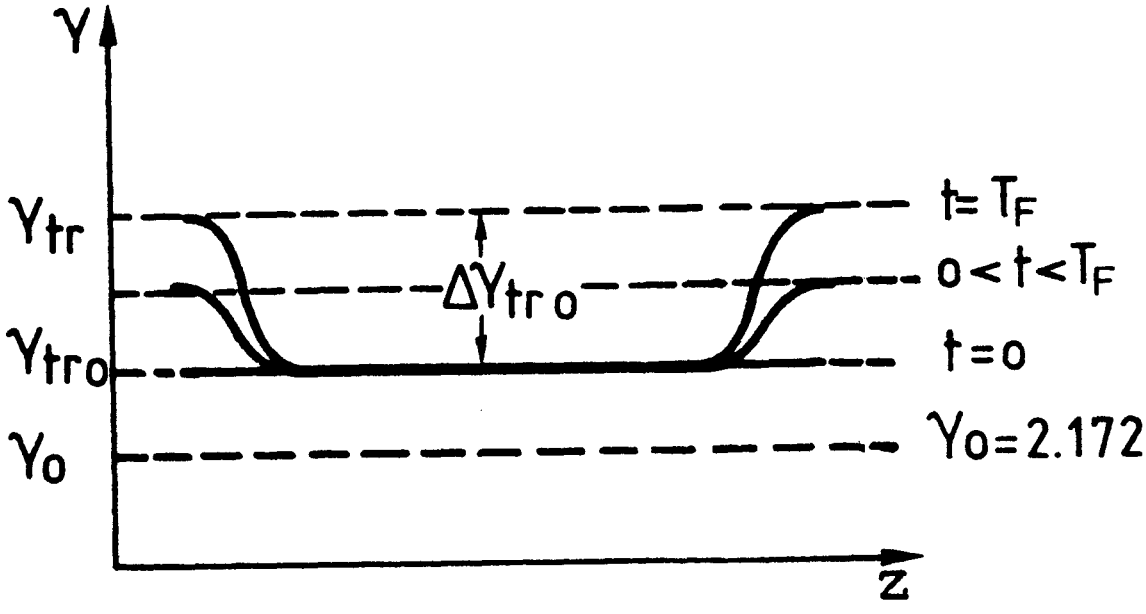

Fig. D2.2-15. Shift of the transition energy γ_{tr} during filling. The transition energy $\gamma_{tr}(t)$ is increased in a programmed way during filling (dashed lines) in order to compensate the shift of γ_{tr} caused by space charge. The continuous lines show $\gamma_{tr}(z)$ along the circumference for 3 different times ($t = 0$, $0 < t < T_F$ and $t = T_F$). The distance $\gamma_{tro}-\gamma_o$ is kept constant, $\gamma_{tr}-\gamma_{tro}$ shifts with increasing accumulated charge ($\gamma_{tro} = 2.226$, $\Delta\gamma_{tro} = 0.1$).

The longitudinal displacement Δz can be calculated from the values selected in this manner.

Particles in the region of the inflection point of the density distribution experience maximum shift in momentum. If only the macrobunch is considered, one obtains $\Delta z = 2.5$ m. This displacement is not critical because the inflection point is located at 10 m distance from the end of the charge distribution. If the displacement in the microbunch is calculated as a consequence of the momentum increase $\Delta p/p = 3.3\ ^{o}/_{oo}$, we obtain $\Delta z = 8.3$ m with conservative assumptions.

2.2.6 Ejection

The ejection concept provides in principle an extraction efficiency of 100%. This is made possible by a void in the circulating beam which allows time for the extraction kicker magnet to rise to full field strength without disturbing the circulating beam. The void is provided by the time structure of the current pulses received from the linac and maintained by the isochronism of the ring.

As mentioned in sub-section 2.2.2, one reason for choosing the distributed triplet lattice is its suitability for extraction which can be made within one cell without any special ring elements.

The IKOR ejection section, with its most important components, is shown in fig. D2.2-16. The kicker magnet, with an effective length of 4 m, is placed with its center 3 m downstream from quadrupole lens QD1. It creates a horizontal kick of 11 mrad which is enhanced by the horizontally defocussing quadrupole lens QD2 to 20.6 mrad (see fig. D2.2-17). In QD2 the center line displacement of the extracted beam from the circulating is 4.5 cm. The Twiss parameter β_H, in the middle of the kicker magnet, is about 10 m.

A septum magnet, with an effective length of 0.8 m, is placed with its center 1.6 m upstream from the bending magnet. At the entrance of the septum magnet the beam center line is displaced about 13.5 cm and the separation between the extracted and circulating beams is 3.8 cm. This allows space for a substantial septum magnet coil of 2.2 cm width and a clearance to the beams on each side of about 0.8 cm. With a field of 0.985 T in the septum magnet an extraction angle of 8.66^{o} is achieved. As the extracted beam is strongly horizontally defocussing, a horizontally focussing gradient of 0.5 T/m in the septum magnet is needed. The beam envelopes for different gradients are shown in fig. D2.2-18.

After leaving the septum magnet, the ejected beam passes partially under the coils of the open side of the ring bending magnet (which has

a "C" magnet configuration). In this region, some local magnetic shielding of the extracted beam and some field shimming of the bending magnet will be required. Kicker and septum magnets are described in subsection 2.3.2.

Space charge effects are expected to cause some radial deflection of the head and tail of the circulating beam bunch, which could cause some beam loss on the septum. A narrow beam-stopper shield will be provided ahead of the septum coil.

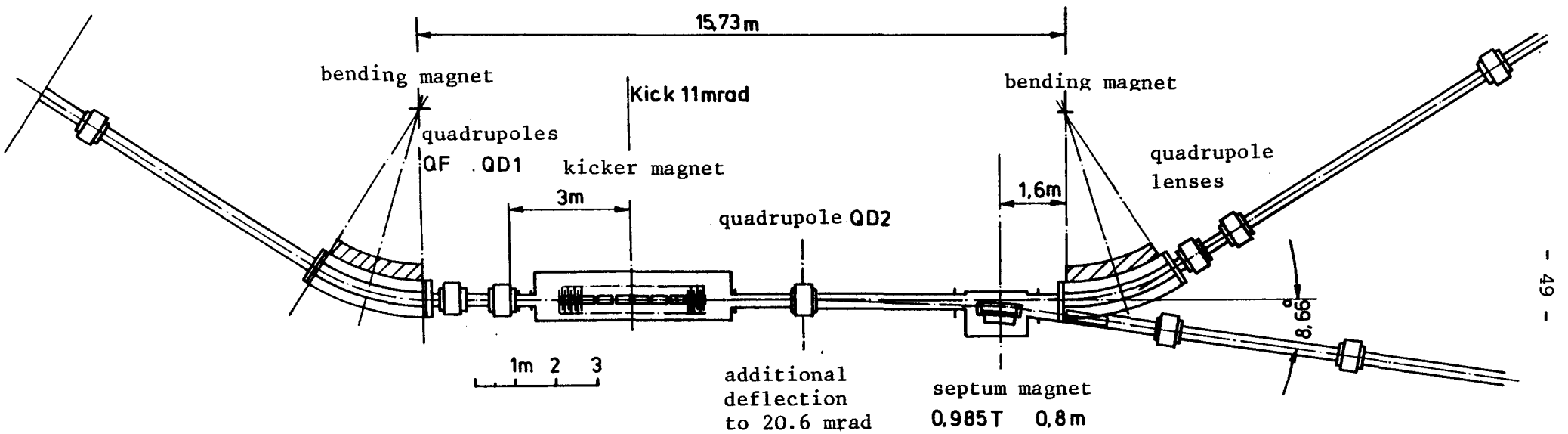

Fig. D2.2-16. IKOR ejection section

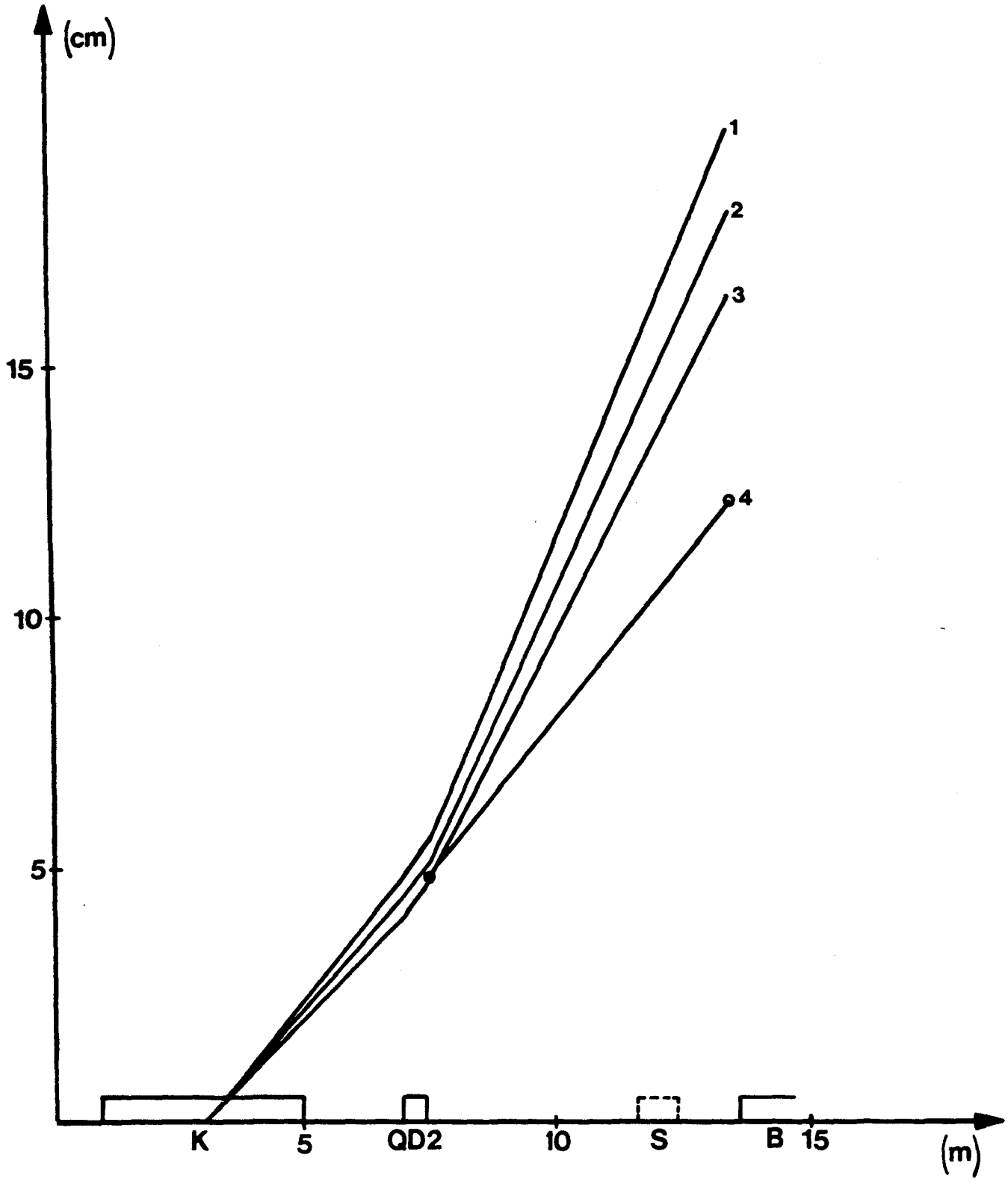

Fig. D2.2-17. Influence of the kicker magnet for a 10, 11, and 12 mrad kick (curve 3, 2, and 1). The kick is enhanced by QD2 to 18.7, 20.6, and 22.5 mrad. The distance between curve 4 and any of the others is the distance between the extracted and circulating beam. For an 11 mrad kick it is 3.8 cm.

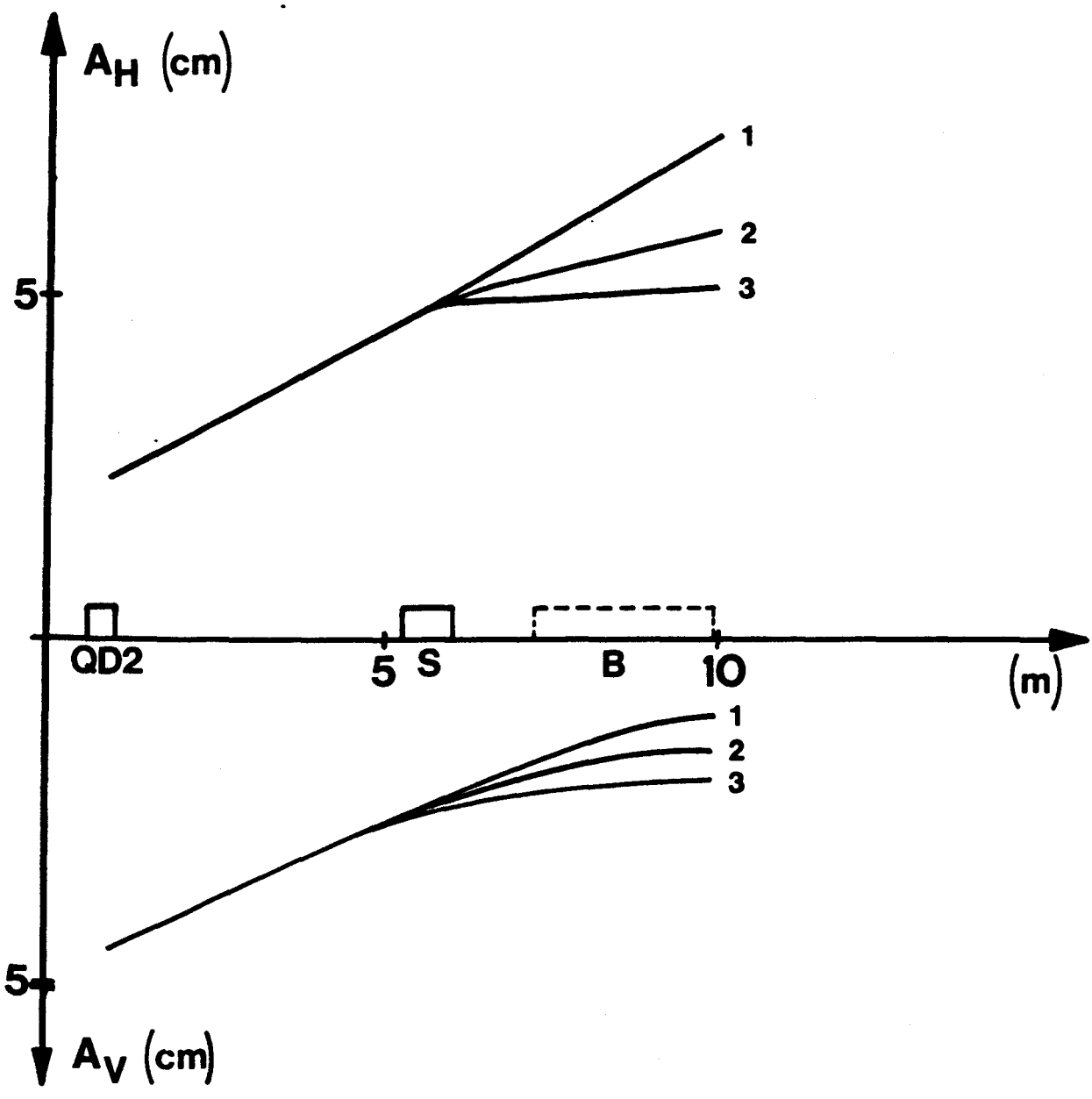

Fig. D2.2-18. Horizontal and vertical amplitudes A_H and A_V of the beam for a horizontally focussing gradient of 0, 0.50, and 0.83 T/m, (curve 1, 2, and 3) in the septum magnet.

References on Section D2.2 (*) this study, annex D

/1/ J.P. Delahaye, Contribution to the study of a proton accumulator ring: comparison of FODO, triplet and quadruplet lattices, KFA Jülich, 2.2.JPD.1 (*) and CERN-PS/BR Note 80-4

/2/ H. Lindqvist and P.F. Meads jun., Comparison of Laslett space-charge-induced tune shift, KFA Jülich, 2.5.HL/PFM.1 (*)

/3/ H. Lindqvist, Tune-shift due to space charge effects in free space, KFA Jülich, 2.5.HL.1 (*)

/4/ s. ref. /10/ on Section D2.1

/5/ W. Hardt, Gamma-transition-jump scheme of CPS, Prov. IXth Int. Conf. on High-Energy Acc., Stanford 1974, p. 434-438

/6/ H. Lindqvist, Lattice calculations for a proton accumulator ring, KFA Jülich, 2.2.HL.1 (*)

/7/ H. Lindqvist, Comments on lattice calculation for a proton accumulator ring (N = 14, N = 11), KFA Jülich, 2.2.HL.2 (*)

/8/ H. Lindqvist, Lattice study for the Jülich accumulator ring: a comparison between "FODO with corrections", "Special FODO" and "Asymmetric triplet" for N = 11, Q_H = 3.25, Q_V = 4.4 at 1.1 GeV, KFA Jülich, 2.2.HL.3 (*)

/9/ H. Lindqvist, The distributed triplet N = 11 and a Summary of other lattices studied for IKOR, KFA Jülich, 2.2.HL.4 (*)

/10/ C.J.A. Corsten, Lattice calculations for the SNQ compressor ring, KFA Jülich, 2.2.CC.1 (*)

/11/ P.F. Meads jun., Some N = 11 lattices for 1200 MeV protons for the accumulator ring, KFA Jülich, 2.2.PFM.1 (*)

/12/ P.F. Meads jun., More N = 11 one microsecond lattices - type ODFBBFDO - stronger vertical focusing, KFA Jülich, 2.2.PFM.3 (*)

/13/ H. Willax, A symmetric ODOFBFODO lattice for N = 11 and N = 14 to achieve $\gamma_{tr} = \gamma$ and acceptable values of Q_H and Q_V, KFA Jülich, 2.2.HW.1 (*)

/14/ H. Willax, R = 30.2 in Ring N = 10 "Adjustable lattice types", KFA Jülich, 2.2.HW.2 (*)

/15/ P.F. Meads jun., A π-2π insertion with zero dispersion in the long drift, KFA Jülich, 2.2.PFM.2 (*)

/16/ P.F. Meads jun., Some compact racetrack isochronous lattices, KFA Jülich, 2.2.PFM.4 (*)

/17/ P.F. Meads jun., A compact accumulator ring with long insertions, KFA Jülich, 2.2.PFM.6 (*)

/18/ C.J.A. Corsten, Betatron-resonances of interest for the Jülich Proton Accumulator Ring. Internal Report VDF:NK 80-46, Eindhoven University of Technology, and KFA Jülich, 2.3.CC.1 (*)

/19/ C.J.A. Corsten, Resonances for the lattices "special FODO" and "quadruplet + correction quad.", KFA Jülich, 2.3.CC.2 (*)

/20/ P.F. Meads jun., Scheme for loss-free, low-dilution multiturn injection into radial and vertical betatron phase space, KFA Jülich, 2.4.PFM.9 (*)

/21/ C.J.A. Corsten, The effect of sextupole fields on the operation of the SNQ Compressor Ring, KFA Jülich, 2.3.CC.4 (*)

/22/ K.H. Reich, Some considerations on the correction elements for the SNQ Compressor Ring, KFA Jülich, 2.3.KHR.1 (*)

/23/ C.J.A. Corsten, Natural chromaticity and its correction for the Jülich Proton Accumulator Ring, KFA Jülich, 2.3.CC.2 (*)

/24/ s. ref. /2/ on section D2.1

/25/ D.W. Hudgings and A.J. Jason, Injection system for the Proton Storage Ring at LASL, Prov. XIth Int. Conf. on High-Energy Acc., CERN, Geneva 1980

/26/ L. Scherk, An improved value for the electron affinity of the negative hydrogen ion, Canadian Journal of Physics 57, o. 558 (1979)

/27/ A. Jason, LASL, private communication

/28/ D.W. Hudgings, Neutral beam injection for a proton storage ring, IEEE Trans. Nucl. Sci. NS-26, p. 3556 (1979)

/29/ R.R. Fullwood, ed., Design study for a medium-energy, intense proton storage ring (WNR Ring), Los Alamos Report LA-4946, p. 11 (1972)

/30/ P.F. Meads jun., On implementing H^- injection, KFA Jülich, 2.4.PFM.11 (*)

/31/ H. Lindqvist, Injection study for the Jülich accumulator ring for "FODO with corrections" N = 11, KFA Jülich, 2.4.HL.1 (*)

/32/ P.F. Meads jun., New methods for multiturn injection into synchrotrons, IEEE Trans. Nucl. Sci. NS-20, p. 401 (1973)

/33/ s. ref. /20/

/34/ Ehrman, Longitudinal oscillations in unbounded one-dimensional non-uniform plasmas, Phys. Fluids 8, p. 1846 (1965)

/35/ de Packh, Water-bag model of a sheet electron beam, J. Electron. Control. 13, p. 417 (1962)

/36/ F. Sacherer, Transverse space-charge effects in circular accelerators (thesis), UCRL-18454, pp 86-90 (1968)

/37/ G. Gillespie, Physical Dynamics, La Jolla, Calif., private communication

/38/ G. Gillespie, High-energy cross section for H^- ions incident on intermediate and high-Z atoms, Phys.Rev. A16, p. 943 (1971)

/39/ A.J. Jason, Foil stripper design considerations, LASL PSR Tech. Note 29 (1980)

/40/ P.F. Meads jun., Heat-bàlance considerations for the stripping foil foil, KFA Jülich, 2.4.PFM.5 (*)

/41/ G. Mackenzie, TRIUMF, private communication

/42/ G. Wüstefeld, Emittanz und inkohärente Q-Wertänderung, KFA-KFA Jülich, 2.5.GW.1 (*)

/43/ L.J. Laslett, Acc. Summer Study, Bróokhaven BNL 7534, p. 324 (1963)

/44/ K.H. Reich, private communication

/45/ L. Palumbo, V. Vaccaro, G. Wüstefeld, Coherent instabilities in IKOR, KFA Jülich, 2.5.LP/VV/GW.2 (*)

/46/ L.J. Laslett, V.K. Neil. A.M. Sessler, Transverse resistive instabilities of intense coasting beams in particle accelerators, Rev.Sci.Instr. 36 (1965), p. 436

/47/ G. Schaffer, Ejection kicker and high voltage system design for IKOR, KFA Jülich, 3.2.GS.1 (*)

/48/ H. Fischer, Betatron-Dämpfung durch transversale Rückkopplung, KFA Jülich, 2.5.HF.1 (*)

/49/ G. Nassibian, F. Sacherer, A method for measuring transverse coupling impedance, CERN/PS/BR 77-40, Oct. 1977

/50/ V.K. Neil, A.M. Sessler, Longitudinal resitive instabilities of intense coasting beams in particle accelerators, Rev.Sci.Instr. 36 (1965), p. 429

/51/ L. Palumbo, V. Vaccaro, G. Wüstefeld, Beam coupling impendance in IKOR, KFA Jülich, 2.5.LP/VV/GW.1 (*)

/52/ G. Guignard, Selection of formulae concerning proton storage rings, CERN 77-10 (1977)

/53/ L. Palumbo, V. Vaccaro, G. Wüstefeld, Coherent space charge phenomena, KFA Jülich, 2.5.LP/VV/GW.2 (*)

/54/ s. ref. /11/ on section D2.1

/55/ H. Lindqvist, Q-shift and γ_{tr} change due to space charge effects for the "distributed triplet" N = 11 for IKOR, KFA Jülich, 2.5.HL.2 (*)

/56/ H. Lindqvist, Some extraction studies for the accumulator ring for N = 10, N = 11 "special FODO" lattices, KFA Jülich, 2.6.HL.1 (*)

/57/ H. Lindqvist, Extraction study for the Jülich accumulator ring for "FODO" with corrections" N = 11, KFA Jülich, 2.6.HL.2 (*)

/58/ H. Lindqvist, Extraction distributed triplet N = 11 for IKOR, KFA Jülich, 2.6.HL.3 (*)

/59/ P.F. Meads jun., Extraction of the accumulator beam, KFA Jülich, 2.6.PFM.1 (*)

/60/ G. Wüstefeld, Laserstrippen bei der Injection in IKOR?, KFA Jülich, 2.4.GW.1 (*)

/61/ G. Schaffer, V. Vaccaro, G. Wüstefeld, Ferrite losses and implications to beam stability in IKOR, KFA Jülich, 2.3.GS/VV/GW.1 (*)

/62/ J.S. Colonias, LATTICE, an interactive lattice computer code for the IBM 360/178 computer system of KFA Jülich, KFA Jülich, 2.2.JSC.1 (*)

D2.3 Machine components

2.3.1 Bending magnets, quadrupole lenses, correction elements, and injection magnets

General

As a general rule, the design of machine components to be located in the ring will be as simple and reliable as possible consistent with the machine requirements. A minimum amount of equipment will be located in the ring tunnel. The components will be constructed of materials resistant to an accumulated radiation dose greater thean 10^{10} rads (see sub-section 2.5.2). This generally limits materials to metals and ceramics. All ring components will be designed to be removable by a remotely controlled crane (see sub-section 2.5.3). Utilities connections can be withdrawn and intalled through protected passages through the shielding.

There are three proven techniques for mineral insulated coil windings now in use at accelerator laboratories: mineral powder in a thin copper jacket (e.g. Pyrotenax used in SIN quadrupoles), plasma sprayed alumina (used on the SPS quadrupoles at CERN). These techniques are adequate for the ring components, but new developments may permit an improvement in cost and performance.

It is likely that more than half the circumference of the ring, those sectors that do not include injection, extraction, nor collimators, will experience a lower radiation dose significantly below that estimated in sub-section 2.5.2. However, consideration of the economics of design, fabrication, provision of spare units, and reliability indicates that all components of one type should be identical. An attempt to reduce costs by making some components not radiation resistant does not appear to be justified. This is especially true of the quadrupoles whose fields must change according to program within the 0.5 ms accumulation time. They may be series connected and must have identical field characteristics as a function of excitation current varying with time.

Bending magnets

The bending magnets have to produce a steady dipole field of 1.3 Tesla. Although the field is constant, the yokes will be coarsely laminated to allow prompt field stabilization at start-up. The laminations will be assembled on a curved fixture and welded to steel straps on the outer yoke surfaces. The laminations will be embossed near the outer radius sides so the fanning effect will keep the laminations and the magnet ends normal to the proton beam. Because the field level is substantially below the steel saturation level, the flux will spread from the lamination and produce a uniform field in spite of the tapered gaps in the pole face. No field gradient is planned. The yoke will separate at the magnet midplane to permit assembly to the coils.

The coil cross-sectional area provides for a moderate current density and power consumption. Extra space has been allowed for insulation by cement impregnation.

The front view of the IKOR bending magnet with main coil is schematically shown by fig. D2.3-1. Table D2.3-1 contains data referring to windings, power requirements and weight. The main parameters of the 11 bending magnets are listed in sub-section 2.2.1 (parameter list).

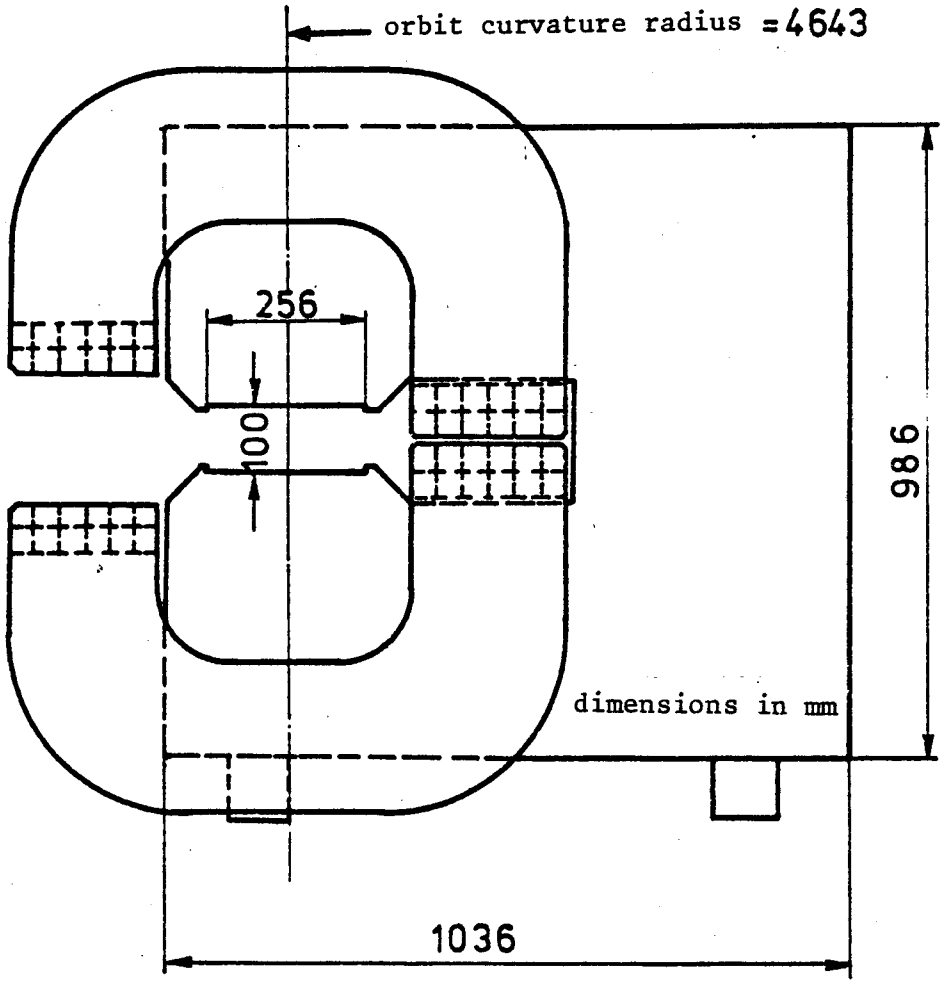

Fig. D2.3-1. Front view of an IKOR bending magnet, schematically (dimensions in mm)

Table D2.3-1. Supplementary data on IKOR bending magnets

number of turns	2 × 12	
current	4710 A	
conductor size	33.5 × 33.5 mm^2	
conductor cooling hole	11.5 mm dia.	
conductor current density	4.6 A/mm^2	
mean turn length	7.95 m	
	per magnet	11, each in series
resistance (80°C)	4.33 mΩ	47.6 mΩ
dissipated power	96 kW	1.056 MW
weight copper	1.75 Mp	19.25 Mp
steel	8.62 Mp	94.8 Mp

Quadrupole lenses QF, QD1 and QD2

For the reasons already mentioned, all quadrupole lenses will be made identical. Generation of a (maximum) field gradient $G_Q = 3.5$ T/m (see fig. D2.2-5) with a distance $2r = 210$ mm of the pole pieces requires 31000 ampere turns ($= r^2 G_Q/\mu_o$). The inductance L with w windings and with the length $\ell_E \approx 0.3$ m of the iron yoke, effective length $\ell_{eff} = 0.4$ m is approximately $\mu_o \ell_{eff} w^2 a^2/r^2$, where a is the distance of the head of the coil from the axis of the quadrupole. For $a \approx 1.4$ r and w = 1 we obtain $L \approx 1$ µH. With a rapid variation ΔG_Q of the gradient during the IKOR filling procedure, for instance $\Delta G_Q = 1$ T/m in 0.5 ms, the induced voltage for w = 1 ist about 18 V. In order to make the cross section of the conductor and thus the losses and cost, respectively, of connecting cables small, about 100 windings would be desirable. Then, with the same same number of ampere turns and ΔG_Q the induced voltage per lens rises to 1800 volts, for 11 lenses in series to 20 kV. This must be considered as much too high for the insulation even with the middle of the quadrupole chain at ground level (10 kV conductor against yoke).

Therefore, a decision is to be made concerning the feeding circuits with a rapidly varying gradient, between series connection of all (or several) quadrupole lenses (of a type) with small number of windings (and thick connecting lines) or individual feeding of quadrupole lenses, each having a larger number of windings. Under the aspects mentioned, at least for the types QF and QD1, it seems indicated to prefer individual feeding- The equality of quadrupole excitation currents with individual feeding can be secured within the required tolerances of about 10^{-3} (see sub-section 2.2.3). With individual feeding circuits there will also be smaller stray fields of the feeding and ground connections and more favourable solutions for the design of the plug-in contacts situated in the ring tunnel.

The main demensions of an IKOR quadrupole lens are about 0.6 m length including coils, and 0.9 m outer diameter for the laminated iron yoke. The lens is composed of 4 essentially equal parts each carrying a coil

of, for instance, 42 turns (= w/2). Ideas for the detailed design, which is still open, may come from existing quadrupole types with large accelerators (e.g. DESY and CERN).

The dc power requirement per lens is around 10 kW for a stationary field of 3 T/m (e.g. QD2, estimated coil resistance about 0.1 Ω, current intensity 310 A, conductor cross section ≈ 60 mm^2'. With the superposition of a pulsed gradient of ΔG_Q = 1 T/m the stored energy in a lens varies between 600 J maximum and 300 J minimum (at 3 T/m average value). Thus, during the pulse duration of 0.5 ms, 600 kW of pulse power are required. Cycling losses of a few percent and a duty factor of 5% give, as an order of magnitude, 1 kW additional average losses.

Within given initial and final values, the shape of magnet current pulses is specified with an approximation, however, the relative field deviations of individual magnets must be kept very small. It is proposed, as a solution to the problem, to excite the quadrupole lenses, and injection magnets in resonant circuits of a harmonic frequency of the pulse repetition frequency of 100 Hz (for instance at 300, 400 or 500 Hz /1/). By adjustment of the amplitude and phase, a section of the sin curve matched to a desired function may be used, adding a dc component if necessary (see fig. D2.3-2 and D2.3-3). This mode of pulsed magnet power supply is comparable to the magnet power supplies of circular accelerators operating with high repetition rate. Eventually, by insertion of suitable switches, idle oscillation periods or half periods may be suppresses, thus reducing average power and cooling requirements. More detailed investigations of the matter should be planned.

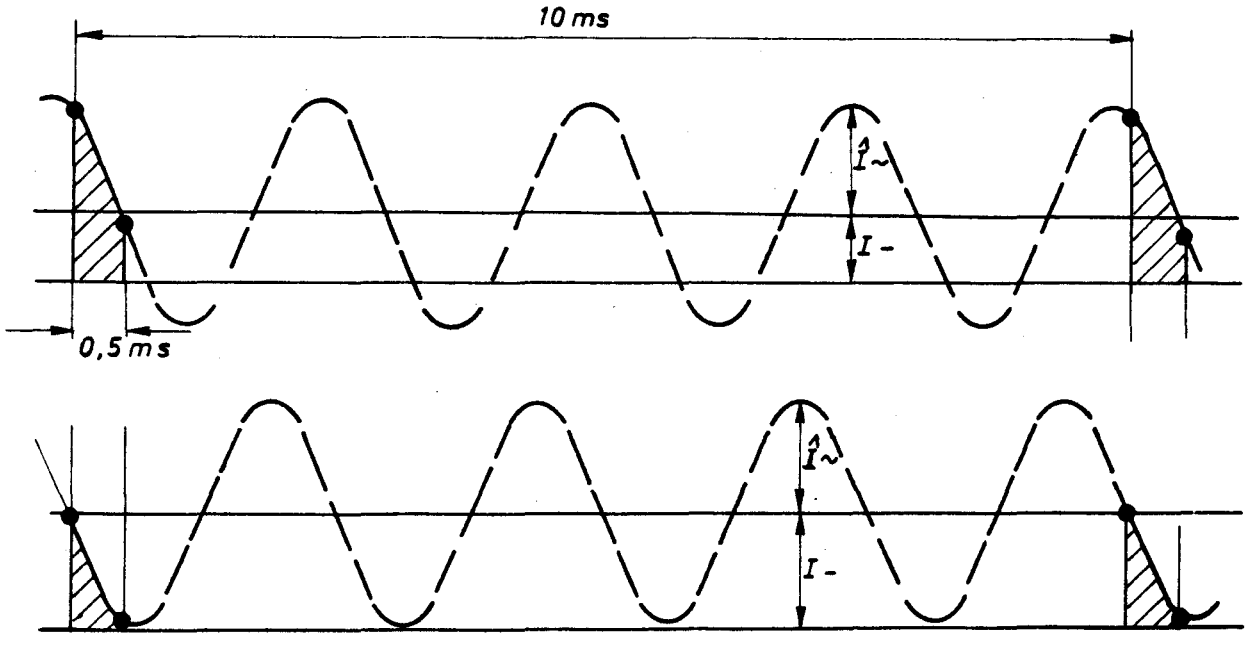

Fig. D2.3-2. Typical example of a current pulse generated by a 400 Hz sinusoidal oscillation and a DC component.

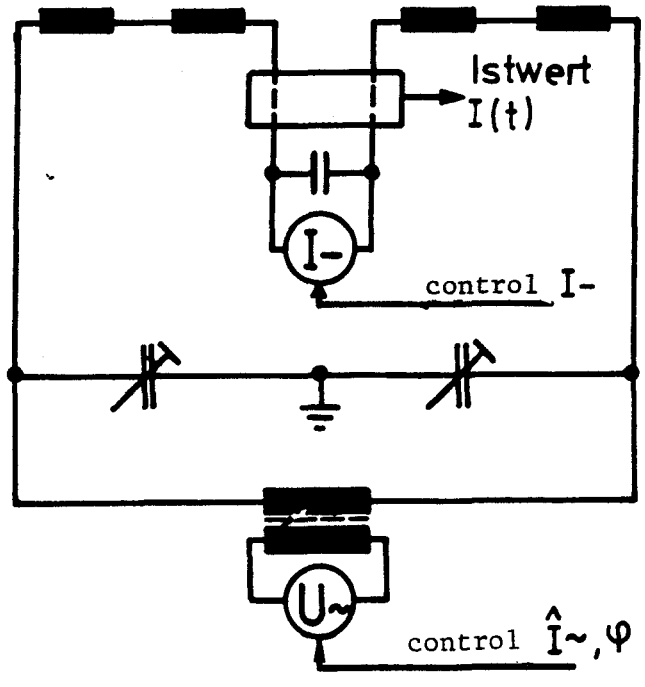

quadrupole winding

bypass capacitor

DC generator

resonant circuit capacitance (adjustable)

transformer with air gap

AC generator

Fig. D2.3-3. AC and DC excitation scheme for quadrupole lenses and injection magnets.

Injection magnets and correction elements

The four injection magnets situated in the IKOR injection section (see fig. D2.2-8) are to be designed for a fast varying field (between 0.6 T and zero) with a useful aperture of 100 mm height and 200 mm width. Their magnetic length is 0.6 m. The required amount of ampère turns for 0.6 T is 48000 A, the inductance per turn is about 1.5 μH. From this follows a maximum stored energy of 360 J, an imaginary power requirement of 180 kW for resonant operation at (e.g.) 500 Hz and a few kW power losses per magnet with a favourable design of the coils. These magnets are operated in a vacuum tank. Their operating voltage is near or below 10 kV.

The layout of the correction elements is roughly sketched in sub-section 2.2.3. The cross section of a correction element is schematically shown in fig. D2.3-4, in analogy to a design at CERN /2/.

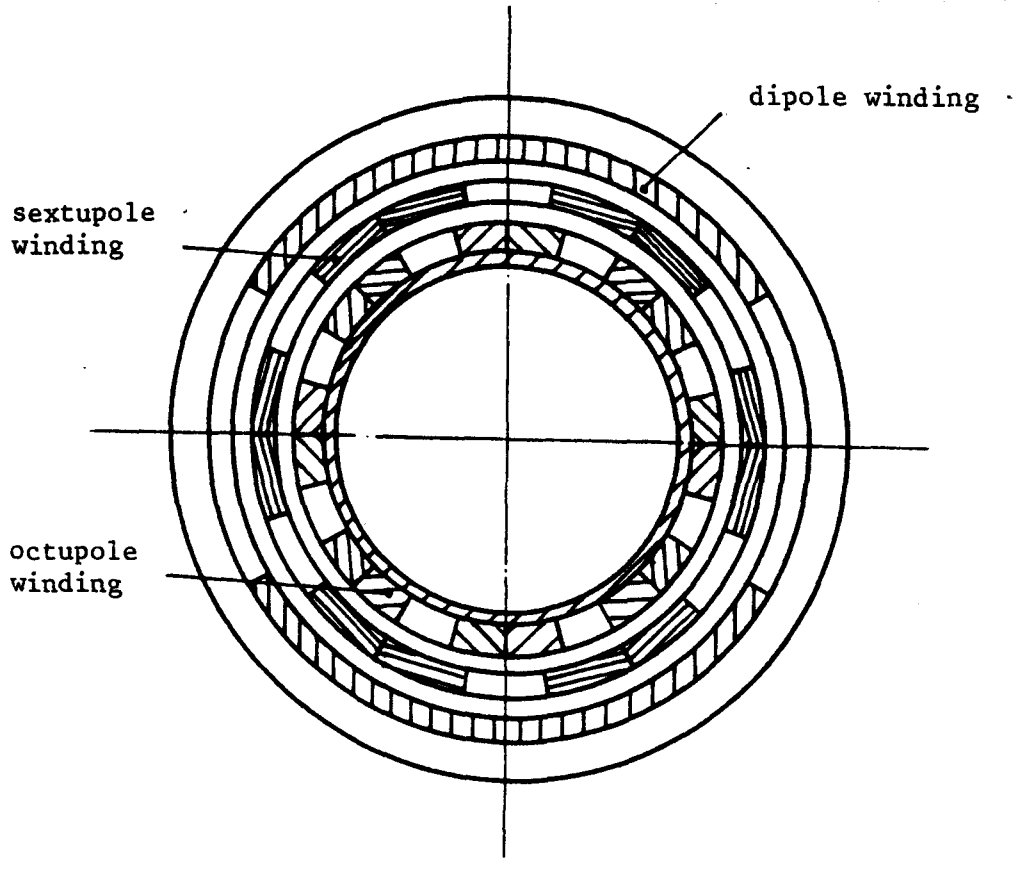

Fig. D2.3-4. Cross section of correction element, schematically

2.3.2 Ejection kicker and septum magnets

Particular priority is assigned to operational reliability and radiation safety with the technical design of the IKOR ejection equipment. Under this aspect an early beginning of prototype work seems convenient.

Ejection kicker magnet

The kick κ which puts the circulating beam into the ejection channel of the septum magnet can be generated, as is known /3,4/, by a kicker magnet carrying a single winding. The minimum product current intensity × length ($I\ell$) for a kicker magnet (with negligible stray field) must be

$$(I\ell)_{min} = \frac{h\kappa}{\mu_o e} p_p \approx 4.3 \text{ kAm}$$

for κ = 10 mrad as example and reference value,

h = vertical kicker aperture = 90 mm, and

p_p = particle momentum = 1.8 GeV/c.

The inductance of the kicker magnet per unit length, $L/\ell = L^*$ is equal to the permeability of free space, $\mu_o = 0.4\ \pi\ \mu H/m$, multiplied by the aperture factor width b over height h, thus $L^* = \mu_o\ b/h$. From the so determined product $LI = b\kappa p_p/e$ (which is 10.8 mVs for b = 180 mm) and the rise time τ_κ of 50 ns a minimum voltage can be derived which must act on the inductance: its value is LI/τ_κ which would be about 200 kV (independent of the total length ℓ). Practically, this value is inconveniently high and can be reduced to a reasonable operational value by subdividing the kicker magnet into several short modules. With the choice of 8 modules proposed as a reference layout, each having 1/8 of the total inductance the individual modules can be operated in the range 25 to 30 kV /5,6/.

The discharge of high-voltage L/C-pulse forming networks is a proven method for generating kicker pulses of constant current (low ripple and overshoot, etc.), the L/C-circuits representing sections of lines or being built according to the principle of lines /7/. In simplified form such a system is shown in fig. D2.3-5. With the current I a voltage U = IZ appears on a module. The characteristic impedance Z of the system has to be chosen so low that the loading voltage of the network (2U) lies within safe operational limits of the applied switch. Low characteristic impedances in the range 10 to 50 Ohms are achieved only by an artificial increase of the capacitance per unit length, C^*, on the kicker magnet (condenser plates arranged in cells, their own inductance does also play a role /8/) and, thus, by a reduction of the wave propagation speed. The required capacitance C^* increases proportionally, to the square of 1/Z, the propagation speed decreases linearly with smaller Z.

For the choice taken as reference /6/: 2U = 60 kV, Z = 25 Ω, I = 1200 A, one needs an effective total length of the kicker magnet of 3.6 m or 450 mm per module (with 8 modules).

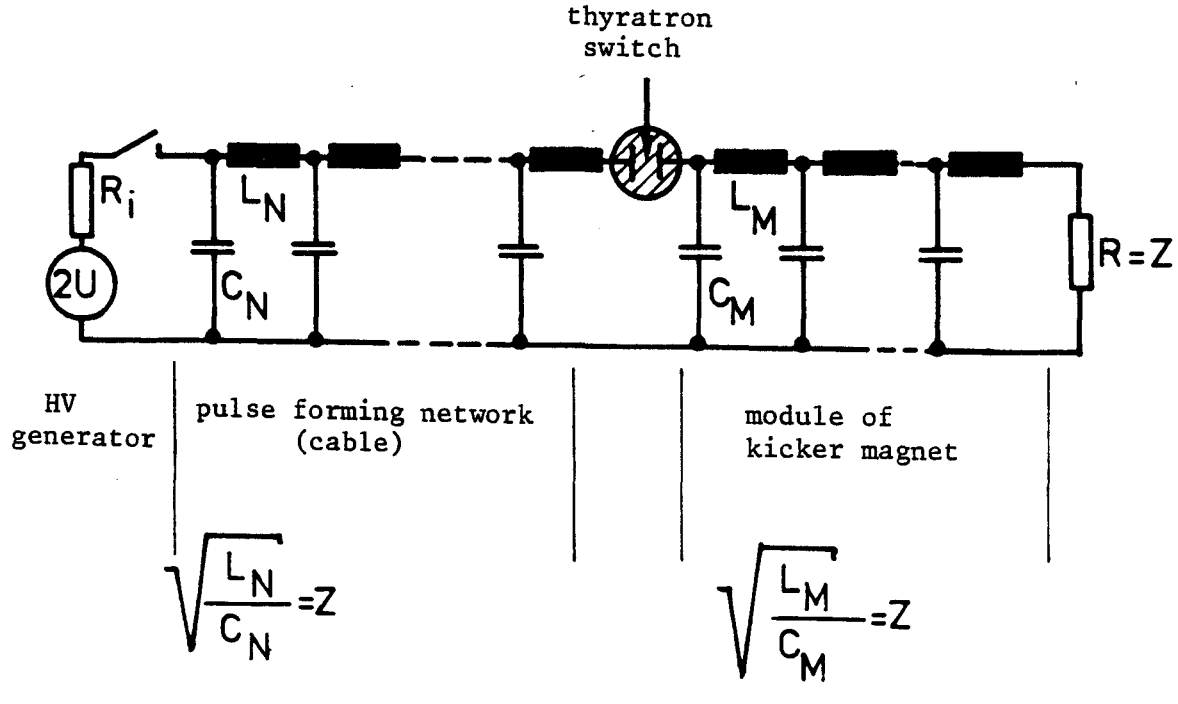

Fig. D2.3-5. Generation of kicker pulses for beam ejection, schematically.

The magnetic field would be at 16.7 mT. With the aperture dependent value $L^* = L/\ell = 25$ nH/cm one arrives at $C^* = 1/25$ nF/cm for Z = 25 Ohm or 1.8 nF per module, wave propagation speed 1 cm/ns, filling time of a module 45 ns. Filling a module upstream or downstream with respect to the beam introduces an increase or a decrease of the kick, respectively, by the electric field /6/, here a few percent. The available filling time variies in the opposite sense.

Hydrogen or deuterium filled thyratrons can be used as high voltage switches between the individual PFN's and their kicker modules. A duty cycle of 10^{-3} and a pulse length of 0.8 µs are common thyratron rates. A critical parameter may be the rate of current rise which typically is at 100 kA/µs /9/. Triggering the thyratrons of individual modules at slightly different times, i.e. with systematic deviation from the regular program, can be applied if necessary, in order to generate kicks of varying strength with time, e.g. for head and tail of a skewed beam bunch (see sub-section 2.2.5). For the same purpose, as a refinement, individually differing loading voltages can be selected. Less attractive, but also possible, are differing lengths of modules within the frame of limited filling time and of the total investment for the stabilization of the beam.

The geometrical dimensions will be large when considering the pulse forming network and the number of equal units (see fig. D2.5-2 on cross section of building). The total volume would correspond to the installation at the CERN antiproton accumulator, this system operates at 80 kV loading voltage and using SF6 filled coaxial cables. The length of an unwound kicker cable of IKOR lies at about 100 m. The electrical length including the connecting section of the thyratron switch will be adjusted to half the beam revolution period $T_{rev} = 0.76$ µs.

Evacuated sections of coaxial lines will connect the thyratrons with the kicker modules which are enclosed inside a tank of about 0.8 m diameter and 5 m length. This tank is designed for remotely handled installation and removal, with appropriate design of vacuum, current, signal, and cooling water connections, for installation in a narrow

specially radiation shielded area, similar to the CERN SPS target beam and beam dump magnets /10/. Much care must be devoted to this engineering task.

The kicker modules themselves (see fig. D2.3-6) may be designed as symmetric double C-shaped ferrite magnets with radially oriented condenser plates, or as asymmetric C-shaped ferrite magnets. Subdivision into about 10 L/C-cells per module is convenient at high capacitive loading for a sufficiently flat pulse shape. Cooling water channels are enclosed in the condenser plates in order to keep the inserted ferrite pieces below their Curie temperature. The ferrite material should be specified for a cutoff frequency around 20 MHz such that undesired higher modes of beam oscillations are attenuated /11/. The terminating resistors of the kicker modules can be mounted on the outer surface of the tank or may be connected, by additional connecting lines, to the equipment tunnel. In case of symmetric magnets 16 thyratrons and 16 feeding lines are required as a miniumum.

The design of a kicker magnet without ferrite may also be worthwile considering. In this case, about twice the amount of current and comblike conductors are required for a sufficiently good dipole field /12/. Furthermore, modifications of the reference layout are possible such that the kicker modules are operated with short-circuited output, thus offering twice the current with a double filling time.

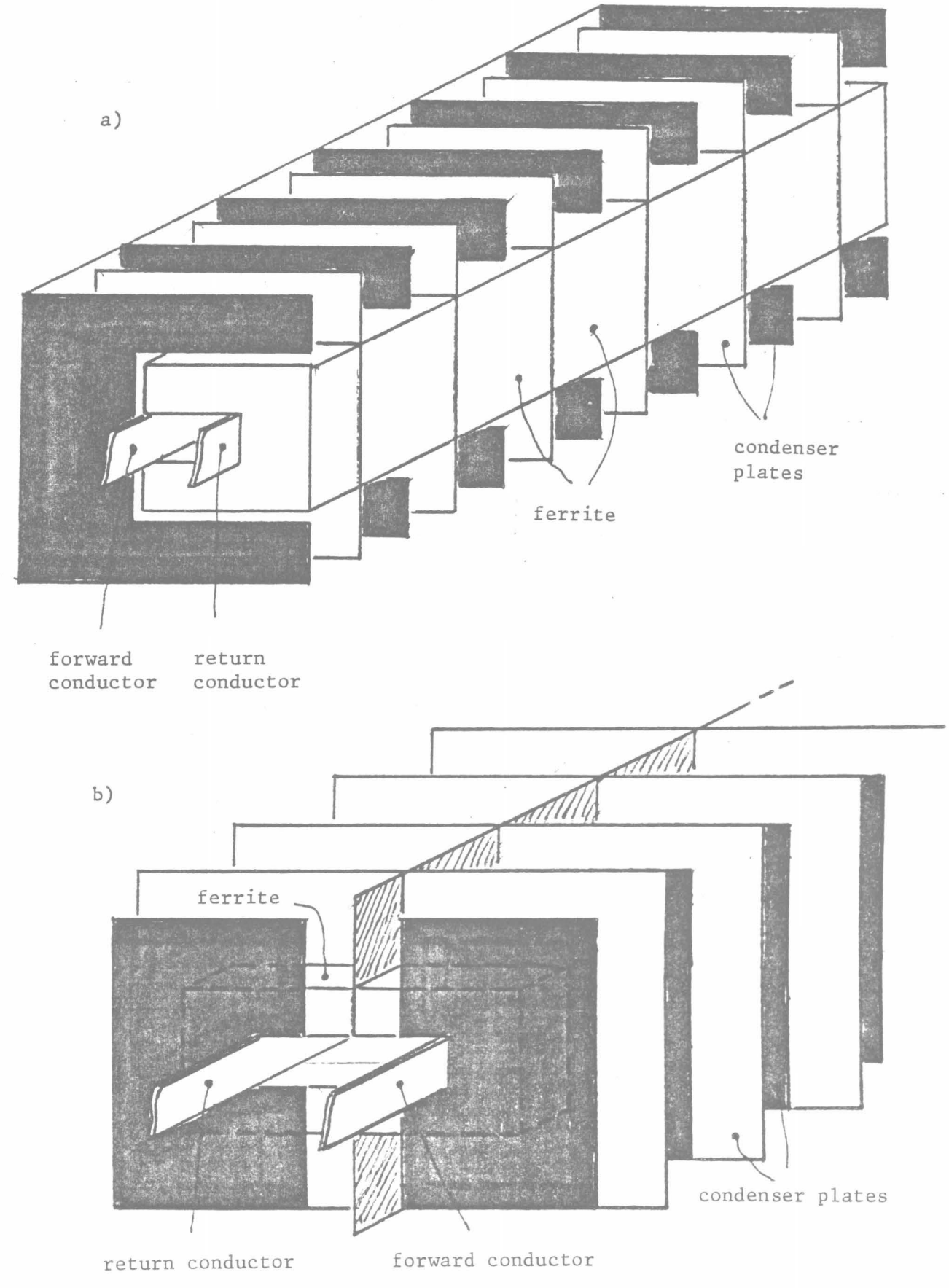

Fig. D2.3-6. Typical structure of a kicker module
a) asymmetric C-shaped magnet (6 cells)
b) symmetric (double C) magnet with metallic separation

Septum magnet

The septum magnet of IKOR (see fig. D2.3-7) has a C-shaped iron yoke of 0.8 m length. A thin water-cooled copper bar, the septum, acts as separation between the strong magnetic bending field in the gap and the field-free (better nearly field-free) region at the other side, where the proton beam circulates. The septum should be as thin as possible and must therefore tolerate a high current density and withstand strong deforming forces. At the beam entrance it is 22 mm thick. Downstream the thickness may increase to the triple value.

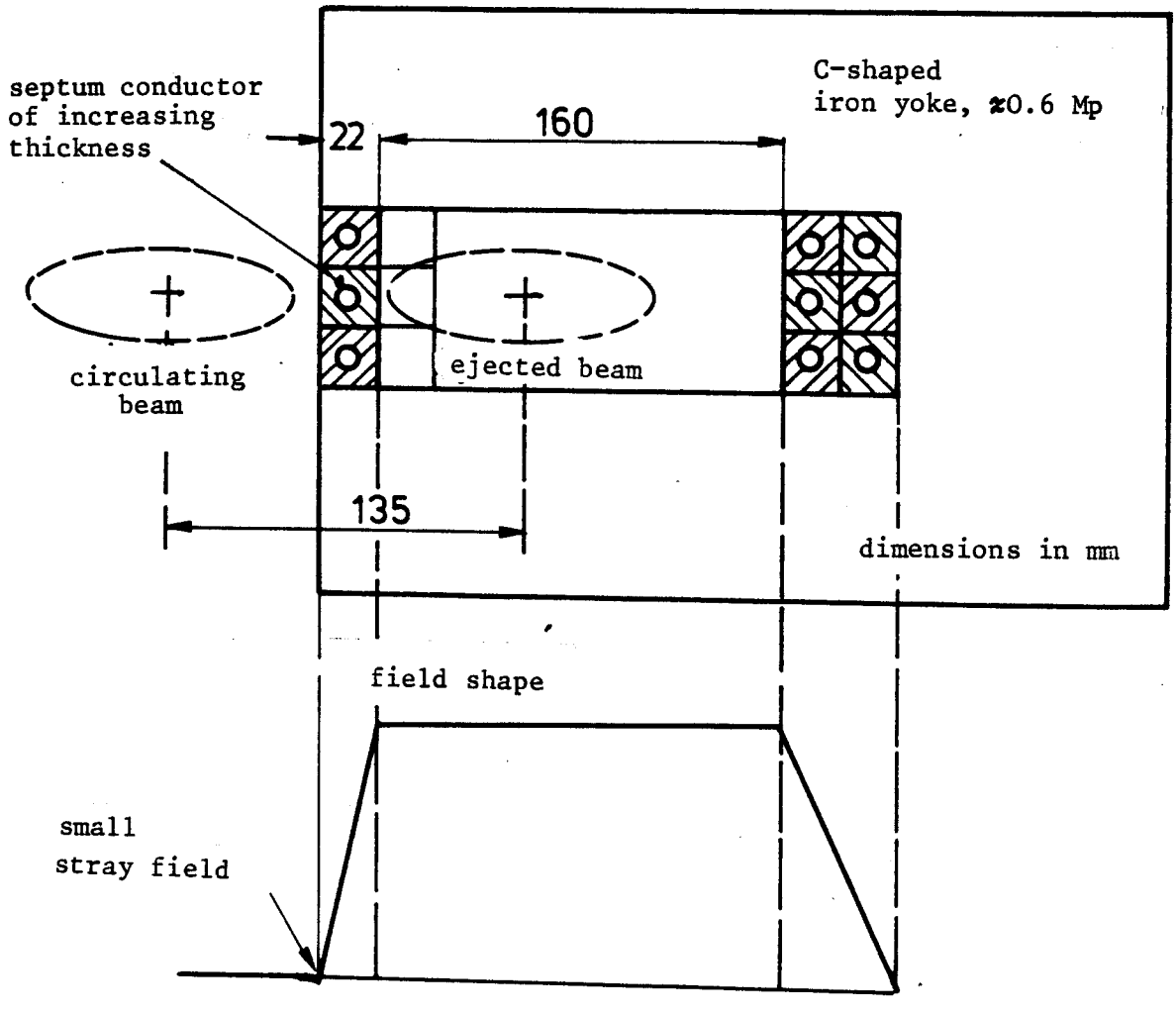

Fig. D2.3-7. IKOR septum magnet, schematically.

For a gap of 70 mm average height and a magnetic field of 1 T the septum must have a current of 67 kA. A small correction arises for the precise value which is influenced by the desired radial focussing gradient of 0.5 T/m in the ejection channel over its useful width of 160 mm (variation of the gap height by about 13 mm). On the circulating beam side, the magnetic field will be about 5 mT with additional shielding.

The current density of the septum is 70 A/mm^2 at the entrance, the power requirement is of the order of 160 kW. For the engineering design /13/, there are a few practical examples /14,15/.

2.3.3 Vacuum System

The basic requirements of the ring vacuum environment are:

1. the vacuum causes no significant disturbances to the proton beam
2. the vacuum chamber provides the appropriate impedance and image current stability to the proton beam
3. the chamber must be radiation resistant and the vacuum system must be serviceable in spite of high radiation levels expected near the beam in several sectors of the ring.

Multiple scattering of the beam by the residual gas must be negligible. The following comparison provides a maximum allowable value of the vacuum pressure: the initially injected beam will make 658 revolutions through the residual gas and about 5 traversals of the stripping foil (800 $\mu g/cm^2$). The scattering mass presented to the beam by the gas will be less than 1% of the foil if the operating gas pressure is less than 1.8×10^{-6} Torr of mass 28 molecules.

An analysis for the SNQ Ring shows that the beam-gas-wall desorption which is dangerous with long time storage rings (e.g. CERN-ISR) will not be a problem /16,17/.

Throughout most of the ring circumference, the vacuum chamber will be round stainless steel tube with remotely operable flanged joints. To be radiation resistant, no elastomets will be used. A pressure of 10^{-7} Torr or less will be achieved by an ion-pump and turbo-pump system /16/. In the final design, cryopumping will be considered as a substitute for ion and turbo-pumps. Cryopumping is now economically competetive and has the advantages of being inherently fail-safe and of requiring only passive elements in the high radiation region.

The detailed shape of the vacuum chamber with respect to requirement 2 depends on the results of the beam dynamics studies.

The chamber within the fast-tuned quadrupoles must allow the changing magnetic field to pass through the chamber while presenting a conducting surface to the beam to carry the beam image currents. Because of the large frequency difference between the image currents of 600 kHz minimum and the magnetic field of 500 Hz, a thin metallic coating on the inside of the ceramic chamber through the quadrupole may accomplish both functions. In addition, the neighbouring metal chambers must be connected to the magnet pole pieces by low inductance capacitors in order to attenuate sufficiently the radiation of rf fields by the circulating beam /1/.

References on section D2.3 (*) this study, annex D

/1/ G. Schaffer, AC and DC for pulsed magnets of IKOR, KFA Jülich 3.1.GS.1 (*)

/2/ G. Bariboud et al., The new PSB multipole magnet system, CERN/PS/BR 77-42

/3/ see for instance:
P.E. Faugeras et al., The SPS fast pulsed magnet systems, CERN/SPS/BT/76-1

/4/ D. Fiander et al., The injection kicker of the CERN antiproton accumulator, IEEE Trans. Nucl. Sci. 28, June 1981

/5/ H. Kuhn, G.H. Schröder, High power pulse generators for fast pulsed magnets, developments and operational experience, CERN-SPS/80-06/ABT, June 1980

/6/ see ref. /47/ on section D2.2

/7/ H. Kuhn, W.C. Middelkoop, J. O'Hanlon, The design of the ISR inflector, IEEE Trans.Nucl.Sci. 16, No 3, June 1969, p. 738

/8/ G. Nassibian, Travelling wave kicker magnets with sharp rise and less overshoot, IEEE Trans.Nucl.Sci. 26, June 1979, p. 4018

/9/ English Electric Valve Co, Hydrogen Thyratrons, Product Data

/10/ M. Ellefsplass and E. Weisse, CERN, private communications

/11/ G. Schaffer, V. Vaccaro, G. Wüstefeld, Ferrite losses and implications to beam stability in IKOR, KFA Jülich 2.3GS/VV/GW.1 (*)

/12/ G. Stange, A new type of pulsed air-core multipoles of extremely simple construction, IEEE Trans.Nucl.Sci., June 1981
and Interner DESY-Bericht M-80/07, August 1980

/13/ R.C. Wolgast, Septum magnet of IKOR, KFA Jülich 3.2.RCW.1 (*)

/14/ R. Bertolotto, Septum magnet for fast ejection, CERN/MPS/SR 70-3

/15/ H. Weisberg, E. Rodger, An improved copper septum magnet design, IEEE Trans.Nucl.Sci. 28, June 1981

/16/ J. Ahlbäck, Vacuum summary by Scanditronix, KFA Jülich 3.3.JA.1 (*)

/17/ O. Gröbner, CERN, private communication

D2.4 Beam transport system

The general layout of the beam transfer channels Linac-IKOR and IKOR-Target is schematically drawn in Fig. D2.4-O (see also Fig. A1.6-6). The following sub-sections contain the results of a detailed study.

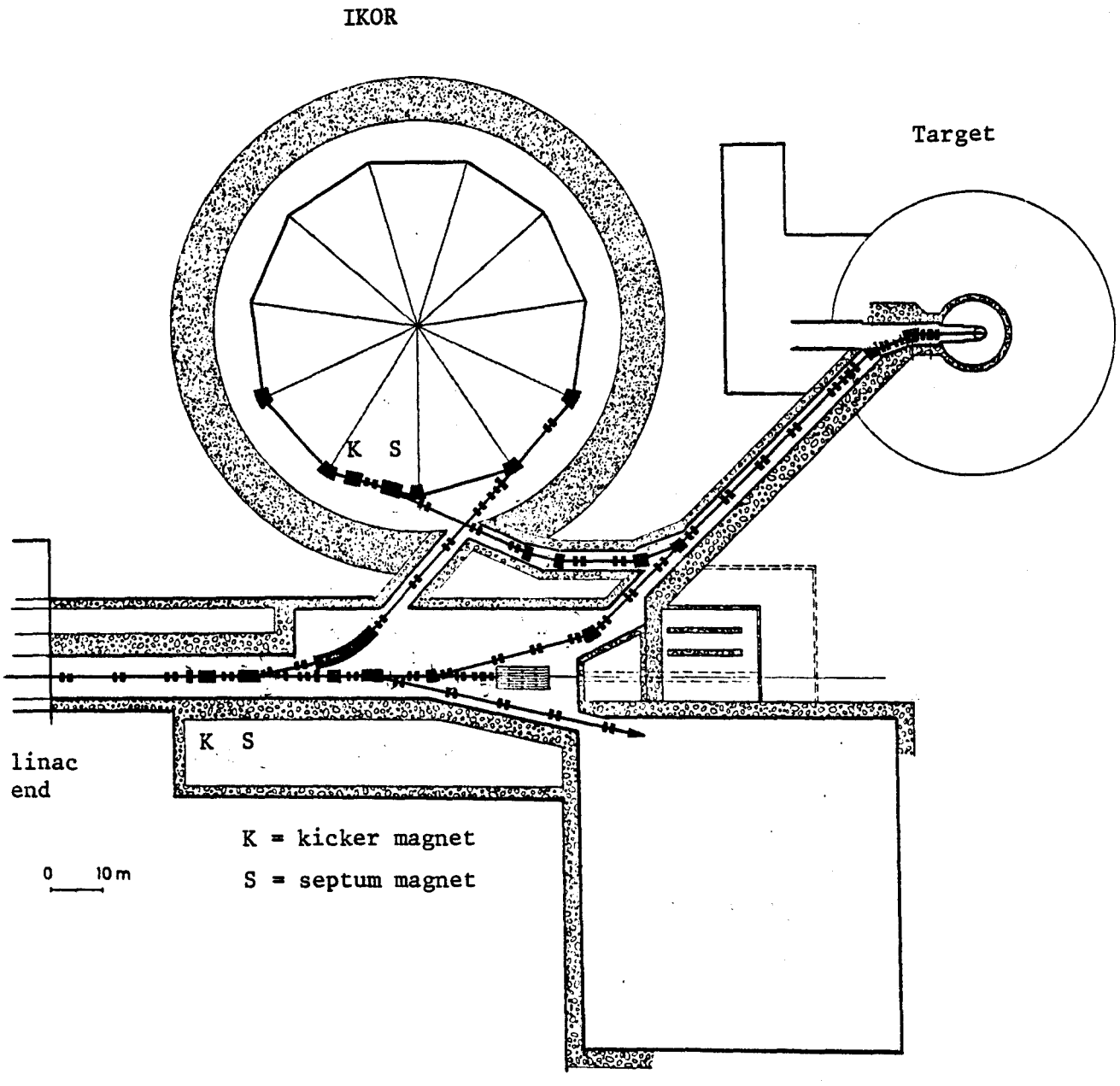

Fig. D2.4-O. IKOR beam transport, general layout

2.4.1 Beam transport Linac-IKOR

The purpose of the injection beam line (see fig. D2.4-1) is to transport the H^- beam from the linac to the stripper foil at the compressor ring and, if necessary, debunch it.

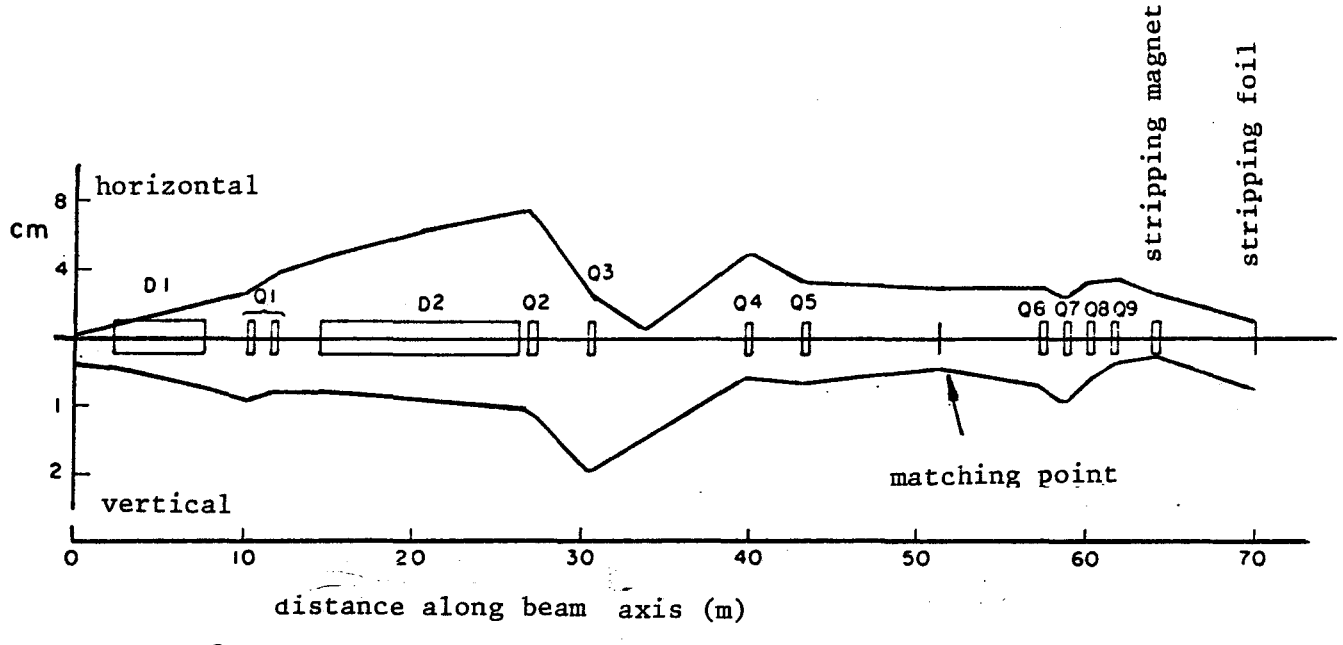

D1 = 15° septum magnet

D2 = 33.46° bending magnet

Fig. D2.4-1. Beam transport Linac-IKOR, horizontal and vertical beam envelopes. The envelopes are for 2σ (i.e. they contain 95% of the beam). It is assumed that the beam halo is removed by an annular stripping foil in front of Q1. The emittance (2σ) is assumed to be 3.3 π mm mrad in the horizontal plane as well as in the vertical plane. The beam microbunch has a length of about 12 cm at the stripping foil in the ring.

The origin is taken to be at the center of the stripper magnet, 2.36 m upstream of the 15° septum magnet. An astigmatic double waist with 1.5 mm horizontal and 5 mm vertical half width is assumed. The beam emittances in both planes are 5 mm mrad (3σ phase space) and the bunch length is assumed to be 2.6 cm. (Possibly the linac will produce a longer bunch.)

At the end of the injection beam line, at the stripper foil, an elliptical beam spot is desirable /1/ with half widths (2σ phase space) of 5 mm and 7 mm, respectively, in the horizontal and vertical planes. The exact shape of the beam spot is not critical, but it must not occupy a smaller area at the foil than is implied by the above in order to minimize the power density. The bunch length should be 10 - 12 cm in order to reduce the space charge effects in the ring.

In the transport system the field in the active regions of the bending magnets and quadrupole lenses must not exceed 0.3 T in order to keep the electro-magnetic stripping probability below 10^{-5}. This requires magnets with a minimum bending radius of 20 m.

The injection beam line consists of a 15° septum magnet and a 33.46° inflection magnet, both operating at 0.3 T (ρ = 20.07 m), and 8 - 10 quadrupole lenses. It is 69.86 m long. Between the two bending magnets there is a quadrupole doublet. Its function is to adjust the dispersion of the system so as to achieve the desired debunching as well as to provide adequate vertical focussing. Solutions ranging from four fold debunching to approximately a dispersion free system can be achieved. For the dispersion free system, the geometry has to be slightly changed in order to keep the quadrupole field low enough.

The growth in effective phase space is approximately proportional to the debunching factor. For a 10 cm long bunch, the effective horizontal phase space is 48 π mm mrad, roughly 10 times the initial value. If the linac produces a beam bunch longer than 2.6 cm, a setting which gives a smaller debunching effect is used.

Four quadrupole singlets are used to transport the beam from the end of the 33.46° magnet to a "matching point" 25 m away, and a quadrupole "quartett" is used to achieve the required conditions at the stripper foil 18.73 m downstream from the "matching point". If a single, predetermined, condition is chosen at the stripper foil, the "quartett" can probably be replaced by a doublet.

If a four fold debunching factor is used, for a given spot size at the stripper foil, the angle will be 10 timer larger than for an achromatic system. Consequently, one should always produce a horizontal waist at the foil as this minimizes the divergence angle for a given spot size. If the beam is clipped to the 2σ phase space, a spot of half width 10 mm and 4 mrad (waist) horizontally and 7.6 mm and 1.2 mrad (correlation coefficient is close to 1, e.g. rotated phase space ellipse) has been provided for the four fold debunching (bunch length 10 cm). The vertical beam size in the stripper magnet 5.95 m upstream from the stripper foil is 3 mm half height.

Finally, an annular stripper foil can be placed in front of the doublet between the bending magnets, to remove the tails of the beam. Both horizontally and vertically the correlation coefficients are close to 1 (e.g. rotated phase space ellipses), an ideal condition for this purpose. The quadrupole lens is weakly focussing for the stripped particles, which will reduce beam blow-up on the way to the beam dump located part away along the 33.46° bending magnet.

2.4.2 Beam transport IKOR-Target

This beam transport line (ejection beam line, see fig. D2.4-2) will transport the compressed proton beam from the ring to the target 124.93 m away. As the momentum spread is approximately 0.4% an achromatic system is highly desirable. There should be no sharp focua anywhere in the beam line thus reducing the effects of space charge.

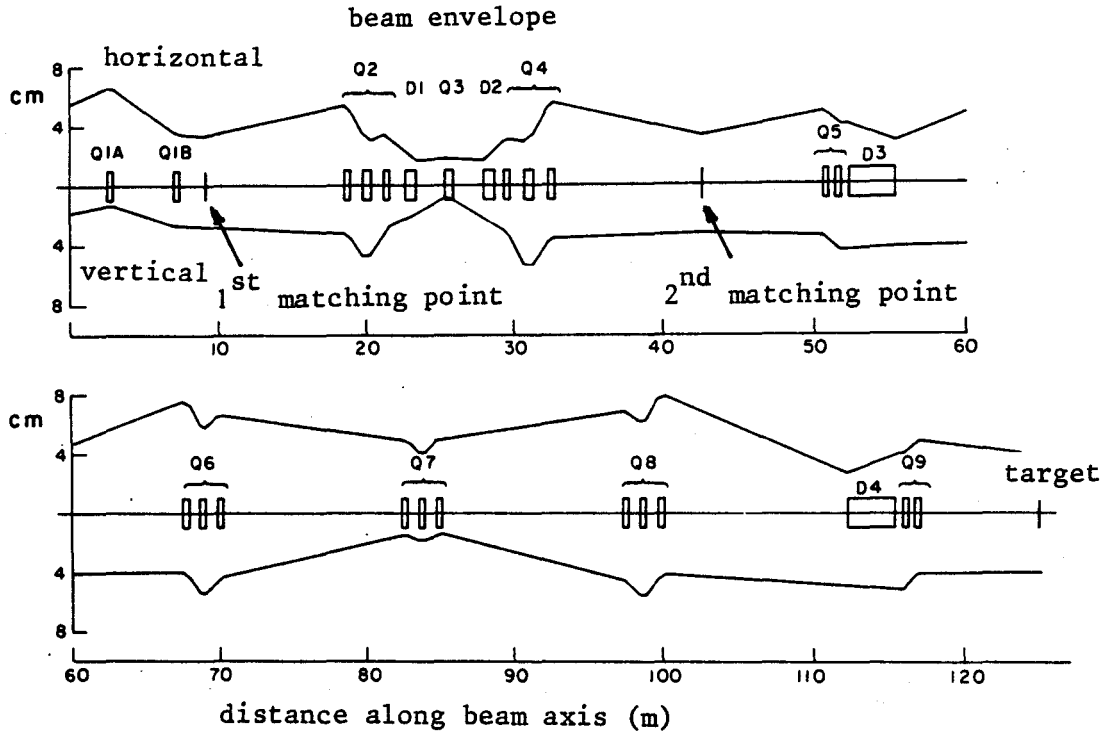

Fig. D2.4-2. Beam transport IKOR-Target. Horizontal and vertical beam envelopes for 150 π mm mrad horizontal and 50 π mm mrad vertical emittance.

The beam transport system IKOR-target consists of two 11° and two 45° bending magnets, and 22 quadrupole lenses, and is designed in a modular fashion with three major sections:

1) a ring matching system that produces a double waist at the "first matching point"
2) an achromatic and telescopic center section with 22° of bend, which transforms the waist in the "first matching point" to a waist in the "second matching point"
3) an achromatic final section which produces an 80 mm diameter double waist at the center of the target and also allows some adjustment of the beam.

The starting point is at the entrance edge of the ring magnet just

following the extraction cell. The septum magnet situated 1 m upstream the starting point has a radially focussing field gradient of 0.5 T/m. The emittances and initial half widths are assumed to be 150 π mm mrad, x = 55 mm and x' = 4.9 mrad and 50 π mm mrad, y = 18 mm and y' = 3.9 mrad, respectively, in the horizontal and vertical planes (values are taken from /2/ (see also sub-section 2.2.6).

Two quadrupole singlets are used to produce a double waist 9.2 m downstream the starting point with half widths of 34 mm and 27 mm, respectively in the horizontal and vertical planes. The strengths and positions of these singlets depend critically on the details of the phase space ellipses. If those turn out to be quite different, more elements would have to be added and/or the positions of the present elements would have to be changed.

The center section consists of two 11° bending magnets with reflection symmetry, with a quadrupole singlet centered on the symmetry plane and adjusted to produce an achromatic condition. Two quadrupole triplets, one immediately before, and one immediately after the achromat produce a double telescopic system, that is the transfer matrices are diagonal, horizontally and vertically the magnifications are 1 and 1.2 respectively. The beam spot at this point is nearly circular with a diameter of 66 mm. The length of this section is 33.41 m.

The final section consists of two 45° bending magnets separated by a drift of 56.88 m. The two bends have antireflection symmetry /3/ and are connected by 3 triplet lenses operated in a symmetric manner. The triplets are adjusted to give an achromatic solution with unity magnification in both planes; the focal length is also infinite for both planes. Immediately proceeding and following this achromatic section is a quadrupole doublet. The doublets are adjusted to transform the 66 mm diameter waist at the "second matching point" to a double waist of diameter 80 mm at the target center, 7.9 m downstream. The total length of this section is 82.4 m.

Throughout the system, the beam is kept large, the only exception is at the middle of the center section where the horizontal diameter is 16 mm. However, the vertical is 37 mm, which is large enough to avoid space charge blow-up. Throughout most of the system, the beam diameter is in the range 60 to 150 mm, which should make space charge effects negligible.

References on secion D2.4

/1/ P.F. Meads, Transformations re'beam distribution on foil, KFA Jülich, 2.4.PFM.7, this study, annex D

/2/ see ref. /57/ of section D2.2

/3/ J.C. Herrera and E.E. Bliomptis, Rev.Sci.Instr. 37 (1966) 783

D2.5 Operational means

2.5.1 Beam observation and controls

Beam observation

The beam diagnostic requires possibilities of control and measurement on beam shaping, beam losses, beam position and on other beam properties. Due to the high beam intensity and possible activation of components the beam will be formed essentially in the low-energy part of the Linac-IKOR system. Only a reduced amount of beam current is to be scraped-off or dumped in the compressor system (e.g. removing of tails).

For monitoring beam losses, ionisation chambers and scintillation counters have shown good reliability and ease of maintenance. They will be installed in appropriate quantities around the ring and permit the determination of azimuthal distribution of beam loss. An evaluation of these results is needed for beam correction and for access controls.

Capacitive probes are proposed as essential elements for measuring the beam properties as they have been in reliable service on other accelerator installations /1/. They permit the determination of horizontal and vertical beam position coordinates as well as the observation of the time structure of the circulating particle bunch. Betatron frequencies in the ring can be measured by means of Q-diagram measurement through beam excitation (e.g. according to /2/) and by observation of the beam noise /1,3/.

The methods cited can be applied with advantage if the monitoring systems are equipped with local intelligence by analytical data treatment. The results can directly be inserted into the control loops. Only relevant physical results have to be transmitted to the operator via the computer system.

Control system

The idea seems applicable that the whole complex linac, compressor ring and targets will be set up in several stages and that there will be future extensions. It is therefore required that the control system be designed flexible, extendable, and transportable to allow for the addition of new subsystems. IKOR being a part of the overall installation, it is also assumed that the control system for this ring /4/ is an integral part of the overall control facilities. No singular solution must be searched in order to avoid losses of operational usefulness.

The following major requirements have to be met /4/:

- ease of use for machine development, running in, routine operation, and later extensions,
- availability of any information concerning the state of hardware and beams as well as access to any parameter requiring control,
- formation of repetitive procedures into appropriate (autonomous) subprocesses for better transparency and control,
- reliability and security (of the control system), as well as
- extensive maintenance and diagnostic facilities.

A computer control system is required for the operation of the linear accelerator (see chapter B2, section B2.5). A compatible supplementary computer system has to be provided for the operation of IKOR. The overall system must have a hierarchical structure with computer-controlled subsystems in which data monitoring and processing is done as close as possible to the level where these data are available /1,3,5/. This will limit the propagation of information and design changes outside the originating subsystem. Moreover, the operational safety is essentially improved. Within this structure, subsystems are autonomous systems which can independently be developed, tested, operated, and maintained.

From the above it follows that at least one powerful and adequately equipped processor has to be dedicated to the autonomous control of IKOR. Elements of apparatus and instrumentation must be interfaced to this processor(s) by the interface which is standard for the rest of the SNQ-facility. The equipment will be supervised by local controllers. Such controllers (processors) may also be dedicated to closed loop controls such as orbit corrections, beam-loss-monitoring within the radiation safety interlock or device-setting and pulse-to-pulse programming during injection, ejection or acceleration if it applies.

Access to the control system: All normal operation and much of the machine physics should be done in one main control room for the entire SNQ-complex. If several consoles are provided in the central control station they should have equal capabilities for application to the overall system. It must also always be possible to operate equipment from remote consoles. These may be somewhat simpler than those in the main control room. They should, however, have full capabilities of monitoring and control when authorized. It should be possible to interconnect remote consoles at any level of the network or hierarchy respectively. It must be stressed that this capability is essential as a machine development, running-in and maintenance tool /4/.

Timing system: A high precision timing system will certainly be implemented centrally, e.g. to control the phasing of RF generators. This system should also provide signals to the accumulator ring for equipment which relates to the passage of individuanl bunches /6/. Signals with lower resolution will be derived for synchronisation of control actions. An event-based technique may be used where the items involved have access to a centrally generated and coded event stream and where instrumentation is able to react on its particular event-codes /7,8/.

2.5.2 Radiation protection and shielding

Beam losses

According to the IKOR concept (2.1.2) the ring is designed for minimum beam losses, its purpose is only to compress the beam pulses of the linear accelerator. In contrast to particle accelerators, beam loss at injection is as aggravating as at ejection since there is no difference in particle energy.

The losses in the compressor ring are difficult to assess, hence a beam loss concept has to be introduced for all radiation shielding considerations. Following this, the maximum beam losses have to be fixed, which appear tolerable for shielding, induced radioactivity and radiation doses of components. When exceeding these maximum loss limits the intensity at injection must be reduced.

For the following considerations, we assume that losses over long time at no location of the compressor ring will be more than half a percent of the basic nominal intensity of 2.7×10^{16} p/s, i.e. about 1×10^{14} p/s. Thus the maximum lost beam power is limited to ~ 25 kW.

Exceeding these values for short time during commissioning of the compressor ring can be tolerated. If higher instantaneous beam losses cannot be reduced within one hour, care is to be taken that no person outside the shielding, in the free access area, may be exposed to more than 0.5 mrem/h. In order to avoid gamma-radiation levels from the induced radioactivity, and doses for the components which would be too high, the mean value of beam losses during one month must stay below the limit values.

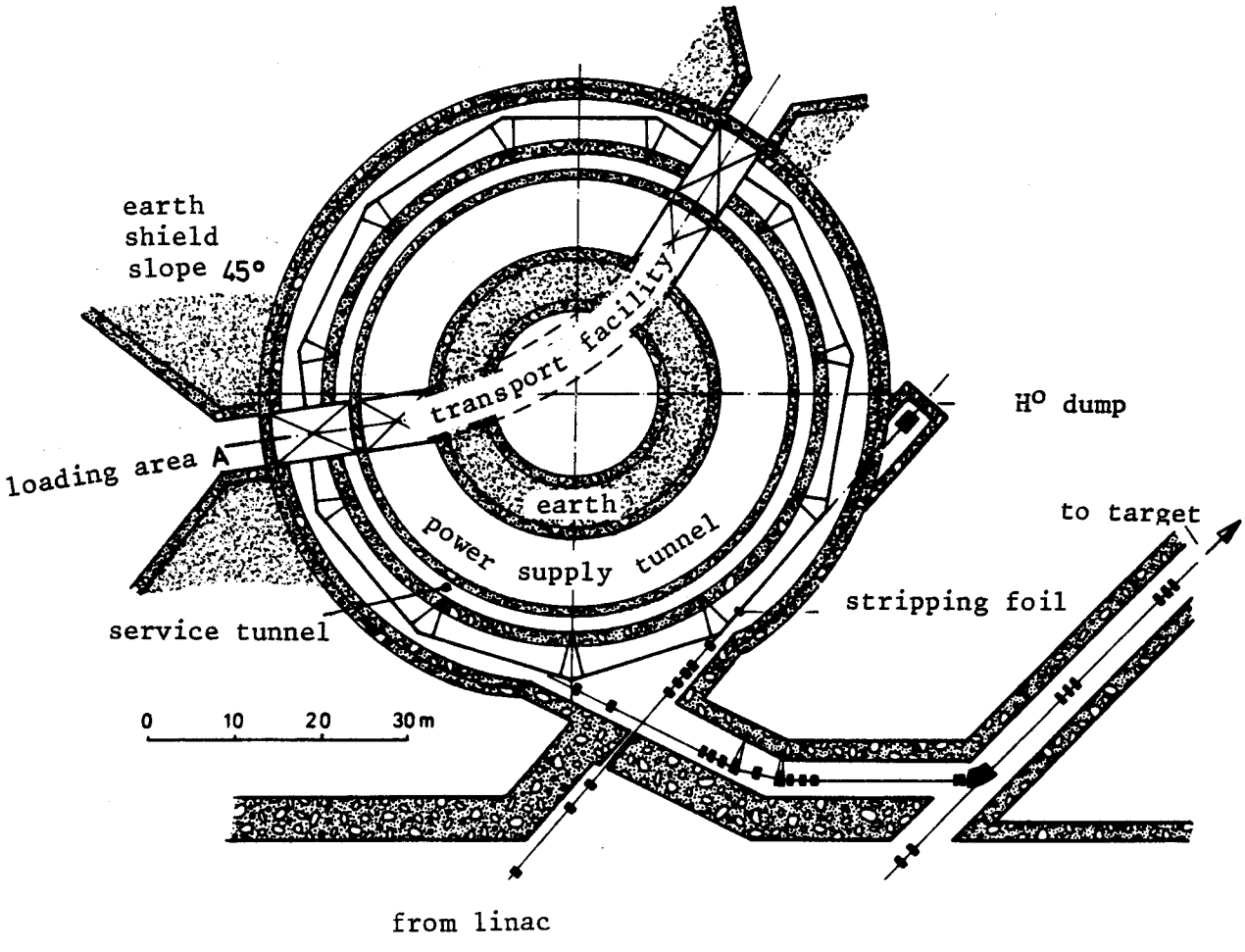

Fig. D2.5-1. Section through the compressor ring in beam height (schematically), with positions of crane ports. The transport facility connects ring, equipment channel, and loading areas.

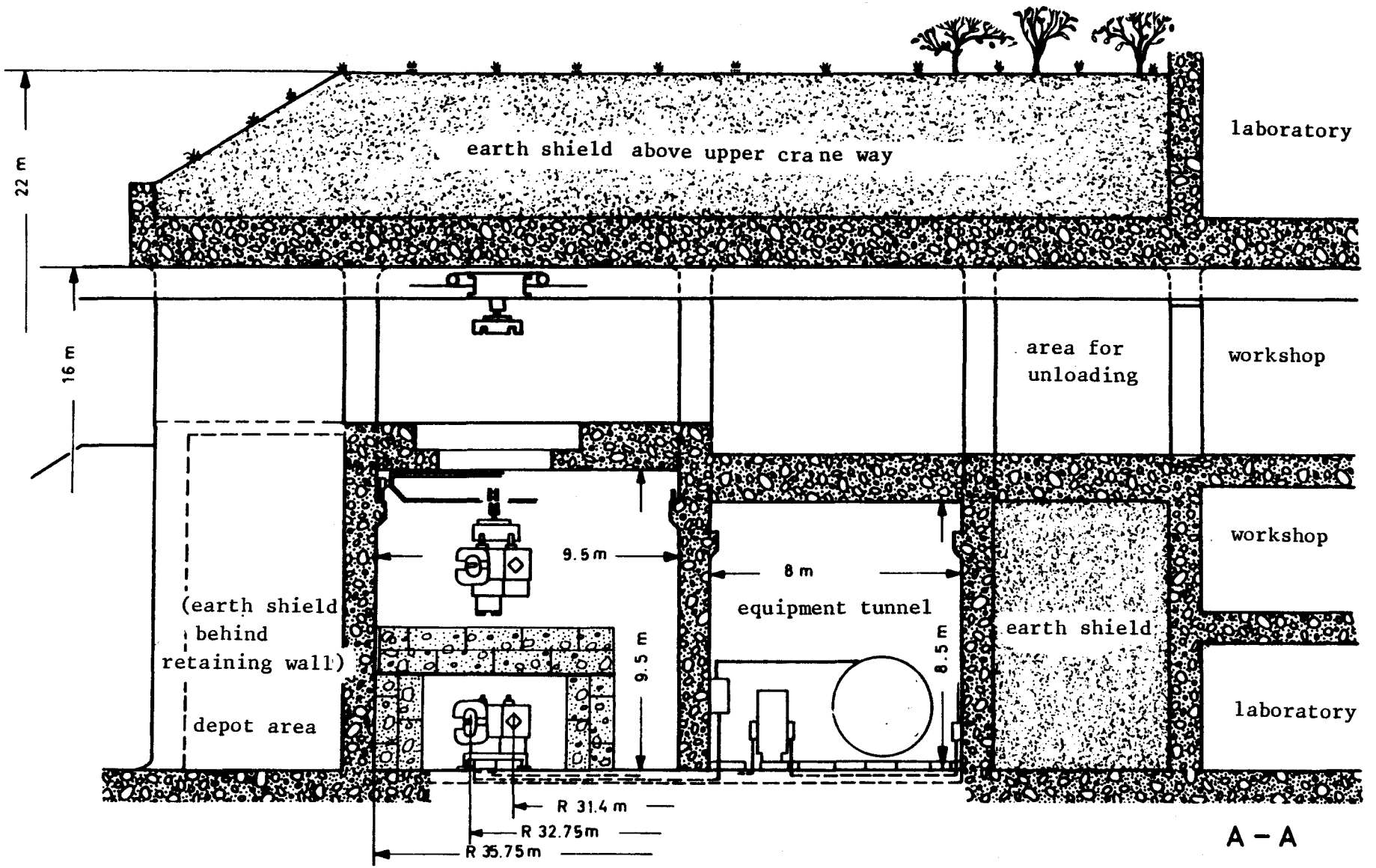

Fig. D2.5-2. Section through the IKOR ring tunnel and equipment tunnel with shielding. Upper crane way = transport facility for taking ring components in and out.

Shielding against secondary radiation

Since 0.5% beam losses may arise at any place of the compressor ring, the required shielding thickness is everywhere the same. The maximum average dose rate outside the shielding is 0.5 mrem/h (§29 Str.Sch.V.). The distance from source to shielding surface is important for the assessment of the required shielding. Assuming this distance to be above 10 m the necessary shielding thickness for concrete or earth is 1600 g/cm^2 /9/. The proposal as sketched in one of the figures D2.5-1 to D2.5-3 indicates a possibility to shield the compressor ring and the equipment tunnel correspondingly. An optimization is only possible within the frame of a final design of the compressor ring and of the auxiliary equipment (see also sub-section 2.5.3).

The proposed shielding concept also provides the possibility to reinforce the local shielding in regions where beam losses occur and to reduce the outer shielding correspondingly.

The necessary shielding for short distances is at the same time sufficient for the reduction of the radiation outside the operationally controlled area. The basic concept which we use provides a dose rate < 0.5 mrem/h above the tunnel shielding. Even if these radiation levels were reached everywhere, one would have to expect < 2 µrem/h at 100 m distance or < 10 mrem/a.

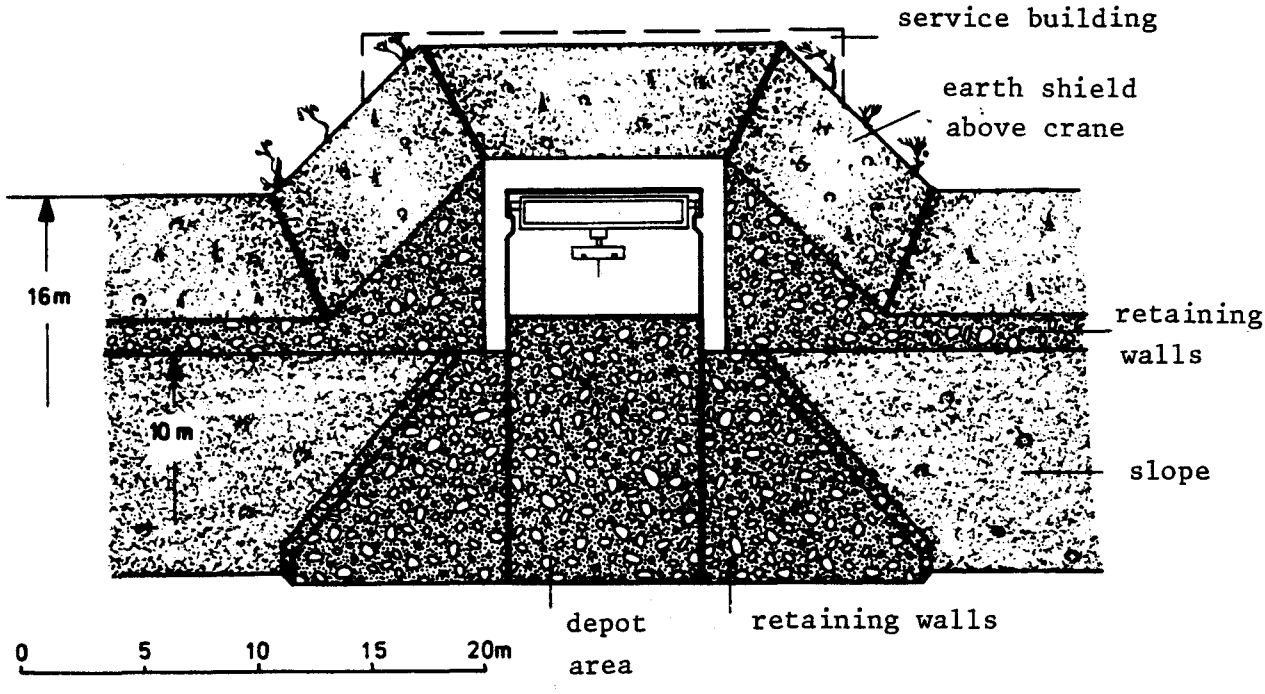

Fig. D2.5-3. Partial view of transport facility from the loading area, schematically.

Induced radioactivity

A beam loss of 10^{14} p/s (1.1 GeV) generates gamma-dose rates of 10^{1} to 10^{2} rem/h in contact with directly irradiated components ~50 cm remote from the beam axis /10/. The radiation levels to be expected at a working distance from such components vary strongly with the geometry and mass of the irradiated material and with the existing shielding (also self-shielding of the components). However, we must start from the possibility that 24 hours after switchoff dose rates of more than 300 mrem/h will exist and that for this reason a highly restricted area in the neighbourhood of these components must be established. Since the conditions for all ring components are the same, remote handling must be possible for all of them. The construction of the ring and of the components takes these requirements into account. Besides the components inside the tunnel also the air of the tunnel and the cooling

water is activated. The same precautions as on the linear accelerator are sufficient to exclude danger for the operations crews and for the environment: Ventilation of circulating air during operation and closed circuits of cooling water for the ring elements /10/.

Radiation damage

Organic insulating material is heavily damaged in the range 10^8 to 10^{10} rad. Even the best known epoxy resins cannot be used anymore with $> 10^{10}$ rad. But greater doses have to be taken into account, on the most exposed coils, after 10 years operation /9/. Therefore we intend to equip bending magnets and quadrupole lenses with anorganic coil insulation. Electronic components cannot be used in the ring tunnel, electric components and cables only after appropriate selection of material and location in the tunnel.

Radiation damages are not only a financial problem, they also reduce the personal radiation protection since work on components damaged by radiation means work on most activated components. A radiation resistent compressor ring according to the present concept permits maintenance programs to be carried out under good radiation protection. Components destroyed by radiation also would increase the mass of radioactive material which must be disposed off. Hence it is required that all ring components must withstand 10 years beam operation at 0.5% continuous loss. Coil insulations are layed out for $> 10^{10}$ rad, cables for $> 10^9$ rad, drive and control elements for $> 10^8$ rad. Nothing will be installed in the ring which does not withstand a radiation load of 10^8 rad without damage.

2.5.3 Remote handling and servicing

Access to the ring

The beam losses assumed in this study lead to high activation of the ring components and of the building structures. The gamma (beta) level in the ring even after a relaxation time of 24 hours is so high that

one has to expect > 300 mrem/h for full-body exposure at working distance. In regions where beam losses of the order of 10^{-3} have occurred, the compressor tunnel can only be entered after long waiting time. Therefore, exchange of IKOR components by means of a remotely controlled crane is foreseen.

Generally, access to the ring after switchoff is restricted until the activation of air is reduced to a level where switchover to fresh air ventilation is possible (1 to 4 hours waiting time).

Access to low acticated zones of the ring is possible, if the monitoring system for remanent gamma dose rate indicates acceptable radiation levels. The total dose during a maintenance period should for no person exceed 100 mrem, whereby one assumes that 8 short and one long maintenance periods in a year are necessary.

Requirements to remote handling

All elements of the ring are designed such that they can be exchanged by a remotely controlled crane. Appropriate connections for vacuum, power supply, signals and cooling water are foreseen similar to those which have been used with the CERN SPS target magnet /11/. All control elements and auxiliary equipment subject to repair are mounted in a fashion that they can be exchanged remotely together with the compressor ring component. In the tunnel proper only 'passive' radiation resistant components are fixed which do not require maintenance. Also, provisions are made in order to design all conventional installations such that they either can be exchanged via remote control or that they need no maintenance.

The assembly of all elements inside the ring, i.e. of components of the compressor ring, auxiliary equipment or conventional installations is planned such that a manipulator mounted on a crane or on a mobile lafette can perform all necessary jobs (ref. "Mantis" CERN /12/).

The figures D2.5-1 to D2.5-4 show two possibilities for remote exchange: handling of connections from a shielded service tunnel and exchange only by the crane. Which of these possibilities can be used more economically will be subject to detailed engineering. With existing accelerators, there are practically proven solutions which fulfil the discussed requirements.

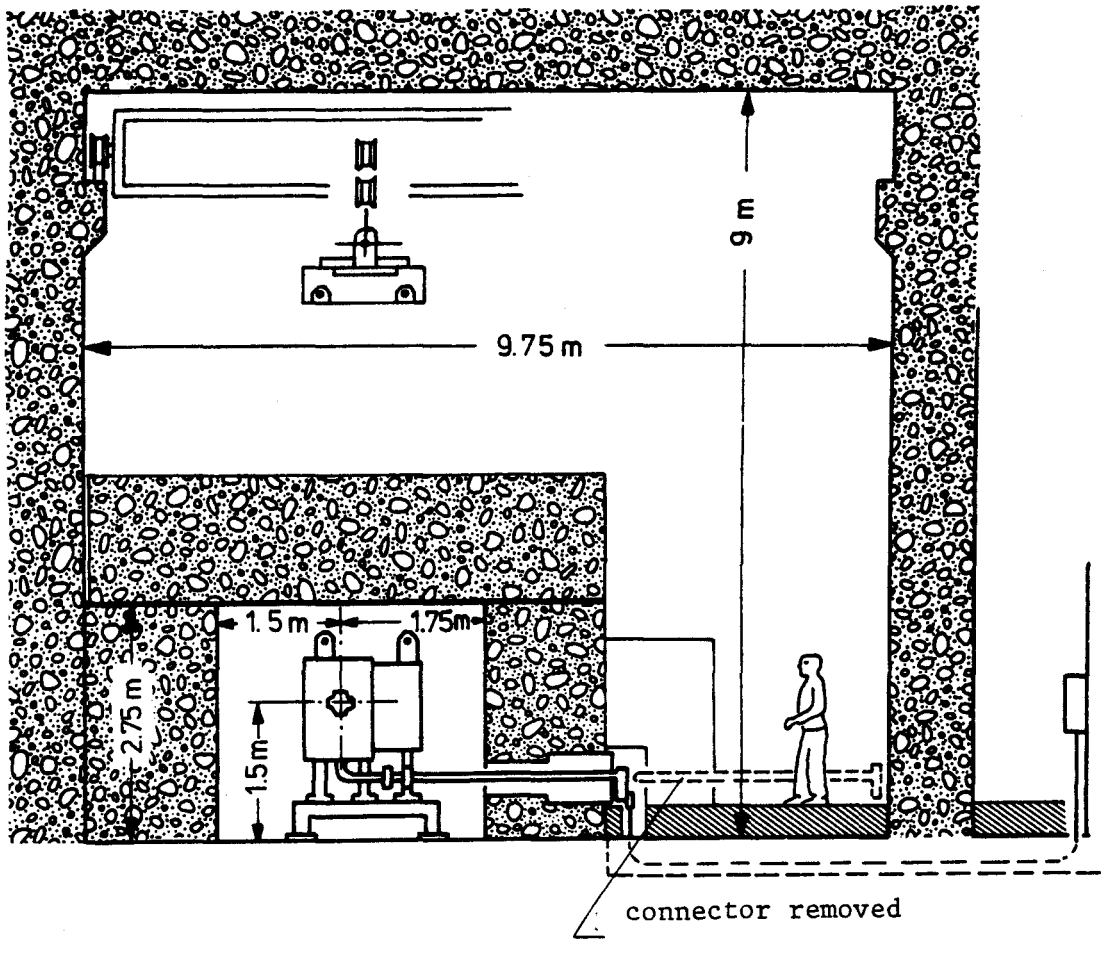

Fig. D2.5-4. Alternative solution to semi-remotely handled installation and removal. IKOR ring elements can be decoupled from a service path. From top, access by crane mounted auxiliary tools.

Transport of radioactive components

Remote exchange of highly radioactive components has to be completed by a transportation system which allows activated components to be brought out of the ring and to be deposited on a safe place without undue radiation exposition.

The proposed solution is shown by Fig. D2.5-1 and Fig. D2.5-2. The ring crane brings the components to the exit gate. A transport crane takes the load over and puts it into a depot and repair hall adjacent to the ring. The load is automatically fixed to the crane. Also as an option, the possibility is considered to put the load onto a railway vehicle or to put it on a shielded mobile platform for transportation (SPS magnet vehicle /13/). The final choice of means for transportation is determined by the rule that the collective dose per person, related to transportation should be no more than 10% of the total dose for handling. Experience shows that a substantially lower fraction of 'transportation dose' can be expected if appropriate care is taken. Provisions are made to interconnect intermediate depot, hot cells and final depot by the transportation facility.

References on section D2.5 (*) this study, annex D

/1/ The LEP Design Study, CERN/ISR-LEP/78-17 and 79-33 (1978/79)

/2/ B. Autin et al., IEEE Trans.Nucl.Sci. NS-20, p. 802 (1973)

/3/ ISABELLE Proposal, BNL 50519 (1976)

/4/ W. Busse, Requirements for a SNQ control system, KFA Jülich, 5.1.WB.1 (*)

/5/ M.C. Crowly-Milling, The design of the control system for the SPS, CERN 75-20 (1975)

/6/ H. Fischer, Synchronisierungssystem für die Spallationsneutronenquelle, KFA Jülich, 5.1.HF.1 (*)

/7/ C.G. Beetham et al., The SPS timing system proposal, CERN/LAB II-CO/Int/CC/74-2 (1974)

/8/ G. Daems et al., The timing and the program-line-sequencer for the new PS control system, CERN (to be published)

/9/ M. Höfert, Estimations of radiation problems for the compressor ring operated in conjunction with the German neutron spallation source, CERN Internal Report HS-RP/IR/80-80, 18/12/80

K. Goebel, Strahlenschutzprobleme beim Betrieb eines Hochstrom-Linearbeschleunigers, III. Abschirmung des Beschleunigertunnels, KfK Primärbericht 11.04.02.P.12J, April 1980

/10/ K. Goebel, Strahlenschutzprobleme beim Betrieb eines Hochstrom-Linearbeschleunigers, II. Aktivierung der Beschleunigerstruktur, KfK Primärbericht 11.04.02.P12.F, March 1980

/11/ M. Goujon, M. Mathieu, Raccord à vide Télécommandé, Note technique SPS/SME/78-240, 20/3/78

M. Ellefsplass, Some details on the handling of plug-in magnets, SPS/RA/TM/76-6, 25/3/76

/12/ R.A. Horne, General purpose remote handling proposal for the construction of Mantis 2, CERN/PS/0050H/RAH/mk, November 21, 1980

G.W. Köhler, Manipuliersysteme für Beschleunigertunnel, Konzepte, KfK Primärbericht 11.04.03 P 11A, Dec. 1979

/13/ SPS magnet vehicle, CERN-SPS Specification, drawing No. 8014/5160/1

D2.6 Time schedule and cost

2.6.1 Time schedule

Fig. D2.6-1 gives a rough survey concerning the eventual process of realization of the compressor ring. The construction phase proper is about 6 years. The commissioning period with beam is estimated to need 6 to 12 months.

An optimisation and prototype program (see also part I, chapter 8) should provide the basis for a swift development of the construction program. The following activities should mainly be included:

- a more profound study of beam dynamics, in particular collective effects
- optimization of the ejection system with due regard to the influence on beam stability by the kicker magnets during filling, technical details on the layout of the septum magnet, furthermore modifications aiming at double pulse ejection for neutrino experiments
- investigations concerning lifetime and production of stripping foils used for injection
- technical questions concerning pulsed magnet powering (quadrupole field in ring, dipole fields of injection magnets)
- detailed studies on remotely handled installation of ring components
- technical layout of the negative feedback system for damping transverse beam oscillations
- studies on new principles of pulse compression.

Also, the development of beam monitors and further studies on the computerized control system should preceed the construction phase.

For the project realization under broad participation of industry the organization of working teams with expert knowledge will be required.

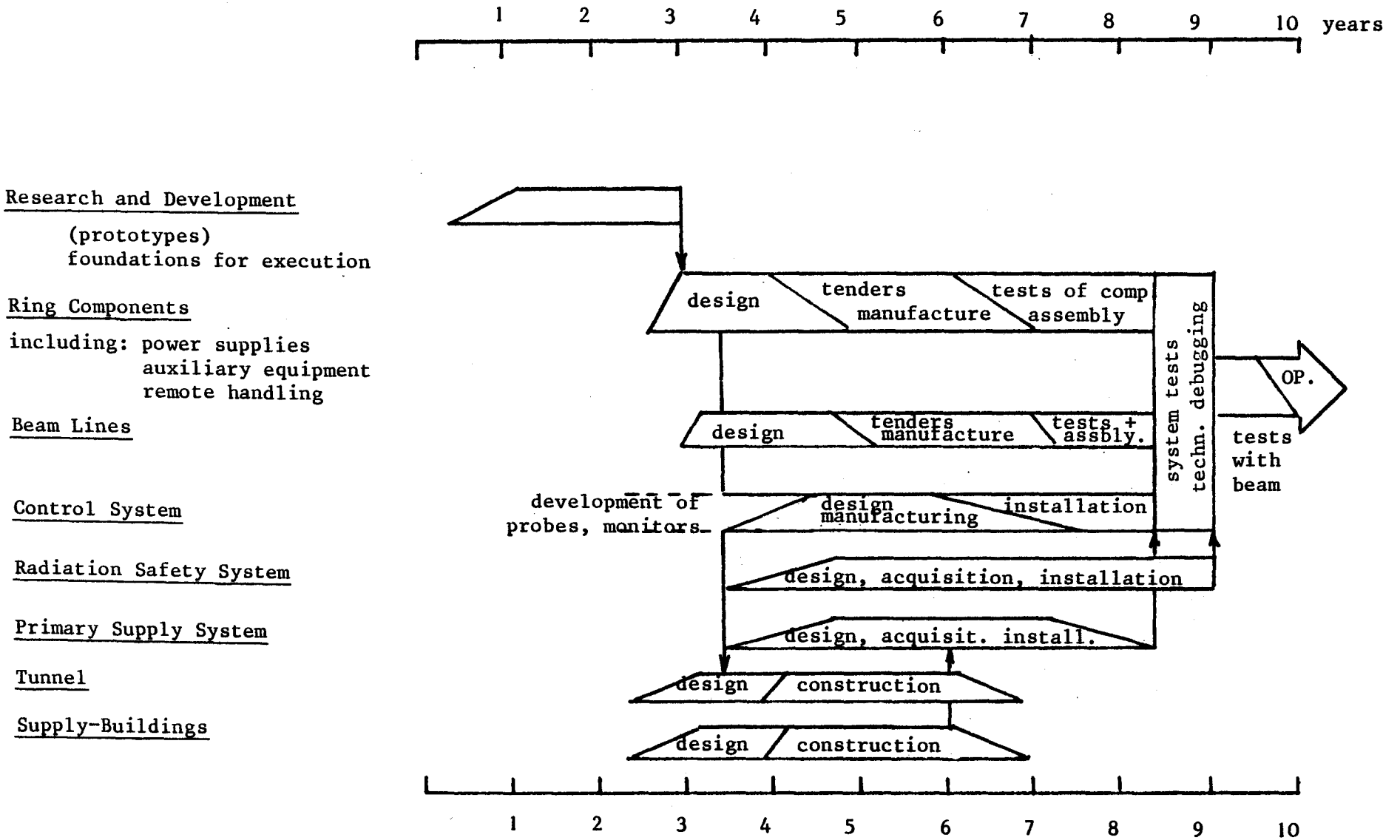

Fig. D2.6-1. Time schedule for an IKOR R & D and construction program.

2.6.2 Costs

The rough cost figures enumerated in the following have been estimated to within ± 20%. A higher precision can only be reached after further engineering studies and call for tenders.

Compressor ring

			cost in MDM
Magnet system including power supplies			
consisting of:	bending magnets (11)	6,5	
	quadrupole lenses (33)	4,8	
	correction elements	1,2	
	installation	2,0	
	various costs	0,5	15,0
vacuum system			5,0
injection system			6,9
ejection system			9,1
beam stabilization			6,6
beam instrumentation			4,5
beam transport to ring			5,0
beam transport ring - target			10,0
special cooling circuits and safety equipment			5,0
control system (computerized)			8,0
facilities for remote handling			5,0
laboratory equipment			3,0
electricity supply and other equipment			4,0
ring, total			87,1
unforeseen			8,9
			96,0

Building:

ring tunnel and beam transport channels	20,0
main equipment building	10,0
	30,0

D2.7 Additional considerations

2.7.1 Alternative backup solutions

Should some problems arise in the future that precludes operation at isochronism, there are several options available. The ring may be operated with the transition energy substantially above 1100 MeV (sub-section 2.2.2), i.e. non isochronous. One of the ejection schemes mentioned in the following will then be applied.

Hole-Keeper

To keep particles out of the azimuthal void, one can consider a pulsed cavity that operates at the same frequency as the ring but is excited only during the passage of the azimuthal void. This "hole keeper" would accelerate (slow) particles at the leading edge of the void to keep them from falling further behind and would decelerate (fast) particles near the trailing edge of the void that would otherwise enter the void /1/.

Azimuthally-uniform beam

Ejection with electrostatic septum: Another possibility is to fill the ring uniformly, leaving no azimuthal void whatsoever. This is highly preferable with regard to instabilities as the azimuthal gradient in charge density would be eliminated (sub-section 2.2.5). Ejection could still be accomplished by means of moving the beam with a fast kicker such that it passes across a thin electrostatic septum /2-4/.

Beam is lost on the septum only during the kicker rise time which may be as short as 50 ns and then roughly only in the proportion that the septum width bears to the beam width. It is conceivable that such a mode of operation would result in a loss to the septum of only 0.01% of the accumulated beam /5/. Under these assumptions, the leading electrode of the septum would run at a nearly constant temperature of $628^{o}C$ with a fluctuation of about 3^{o}. This mode of operation is compa-

rable to that of a beam splitter for a 500 μA cw accelerator. It should be noted, however, that losses in actual ejection systems generally far exceed the theoretical losses.

Resonant ejection: In deviation from the known method of "fast ejection", resonant ejection can be considered. A smaller but faster kicker magnet (risetime 10 ns) would be used in order to determine only phase and shape of the initial amplitude of the oscillation wanted, the existing broadband negative feedback equipment would be used in order to excite the beam in few turns to very large oscillation amplitudes by transverse positive feadback. If a coherent betatron oscillation is excited then ejection can be performed in a single turn. One has to aim at keeping the losses at about one promille. The costs lie in a larger vacuum chamber according to the oscillation. A detailed study of this proposal is pending.

2.7.2 Proton injection

Because of the very high beam power, the direct injection of protons without charge exchange ist most critical. It will be necessary to drastically trim the tails of the lateral distributions in order to reduce the emittance that must be handled by a factor of 10 in each plane. One half of the beam (~ 2.5 MW average power) would have to be removed, if this part can be used for other purposes. Normal multiturn injection methods (see further below) obtain optimal beam brightness at the expense of relatively high losses (55 to 80%). Stacking into synchrotron space as practiced, for example, at the CERN ISR is not possible within the 500 μsec cycle. Because of the limited number of turns that could be injected within the aperture using proven methods, it would be unrealistic to expect to inject much more than 2×10^{13} protons into the ring. A reduction of the linac beam emittance would help but to a limited extend since the beam diameter should be at least of the order of magnitude of the septum thickness.

Tail stripping

The tails may be removed from the beam by using electrostatic beam splitters of small wires or foils such as is done at SIN. The location of these splitters must be an optical image of the injection inflector. Heating and radiation damage to the splitters appear to present no difficulties.

Multiturn injection

Unlike the charge exchange method described above with protons, each injected turn must occupy a separate volume of phase space. For the radically trimmed beam, the available betatron volume exceeds that needed by over a factor of four, but no one has ever demonstrated simultaneous injection into more than one phase plane. In the course of the BNL AGS improvement project, a highly efficient method was proposed whereby the machine is run at a radial half-integral resonance, and successive turns are stacked like a closely spaced picket fence /6/. The method was dropped because a slight shift (0.02) in the tune reduces the efficiency from over 90% to less than 70%. However, applied to the SNQ ring the method provides for the injection of approximately 100 turns of the bright portion of the beam. By injecting above the median plane with an appropriate vertical tune, it is reasonable to double the number of turns, using the vertical plane to miss the inflector on the second turn after injection.

Spiral injection: This method, originally conceived as a means of injecting protons with high efficiency is expected to provide comparable efficiencies without the danger of operating on the half-integral resonance /7/. To accept the full 658 turns of even the radically-trimmed beam would require doubling the aperture.

Injection by rf kicker-septum: Because of the tight bunch structure, it is conceivable that 20 or more turns could occupy the same betatron phase space were there a method to inflect a bunch entering the ring without disturbing previously injected bunches. Were this possible,

the number of turns to be accomodated in betatron space is reduced to around 30.

Using a coupling resonance: If the ring is run very close to a difference resonance during injection, and the beam is injected onto the median plane, a skew quadrupole will couple horizontal betatron oscillations into vertical betatron oscillations. The sum of the squares of the amplitudes in the two planes is constant and is equal to the square of the equilibrium orbit displacement /8/. The period of oscillation and the ratio of the peak amplitudes depend upon the distance from the resonance and the strength of the skew quadrupole. By appropriately setting the period of the exchange of amplitude, the rate of shift of the equilibrium orbit may be reduced with the consequent enhancement of the filling efficiency.

A modification of this method is to inject with the equilibrium orbit not perturbed in which case the entire beam is injected onto the hypershell

$$x^2 + (\beta_x x')^2 + z^2 + (\beta_z z')^2 = a^2$$

where a is the distance of the septum from the closed orbit.

2.7.3 Conclusion

Because the successful injection of protons would require a reduction of beam losses from about 50% to about 0.5% for full intensity, and even with such improvements, only the bright half of the beam could be injected, direct injection of protons is not recommended.

References on section D2.7 (*) this study, annex D

/1/ see ref. /9/ on section D2.1

/2/ J. Walton et al., An improved design of Fermilab septa, FNAL report

/3/ Y. Baconnier et al., High-voltage aspects of the electrostatic septa for the CERN-SPS/ABT/78-113

/4/ M. Olivo, High-voltage electrostatic splitter (EHT) for the 590 MeV proton beam line, SIN-Jahresbericht 1979, p. A11

/5/ see ref. /59/ on section D2.2

/6/ Brookhaven National Laboratory, Proposal to increase the AGS intensity, BNL report 7956 (1964)

/7/ P.F. Meads jun., Proton injection, some thoughts, KFA Jülich, 7.2.PFM.1 (*)

/8/ G. Guignard, A general treatment of resonances in accelerators, CERN 78-11, p. 64-70 (1978)